Design and Characterization of a Novel Mechanical Surrogate Neck Model for Use in Head Impact Applications

by

Samantha R. MacGillivray

A thesis submitted in partial fulfillment of the requirements for the degree of

Master of Science

Department of Mechanical Engineering
University of Alberta

Abstract

Head and brain injuries are commonly caused by head impacts in sport and recreational activities. Despite attempts to decrease head impact injury risk through mandated helmet use, mild brain injuries are still prevalent. Brain injury research and helmet assessment methods use surrogate models to acquire representative impact biomechanics. Current standardized mechanical surrogate neck models were developed for non-direct head impact applications and are too stiff in bending to produce realistic head rotations during direct-head impacts. Misrepresentation of head impact response behaviour restricts injury assessment effectiveness. To improve injury assessment capabilities and decrease the risk of mild brain injuries, new mechanical surrogate neck models must offer a more realistic head impact response.

The objective of this study was to refine the design and characterize the head impact response of a novel mechanical neck model. Design refinement methods addressed limitations of an existing mechanical neck prototype (the Phase I neck). Response during head impact experiments characterized the refined prototype (the Phase II neck) to evaluate repeatability, tunability, durability, and biofidelity. The overarching goal was to develop a neck model for use in head impact applications that exhibits humanlike responses.

The Phase II neck replicated the anthropometry of the 50th percentile male neck. The internal structure was composed of alternating rubber and aluminum elements, and three

longitudinal steel cables to provide stabilization. Silicone rubber encased the internal structure to approximate viscoelastic tissue. A silicone flange at the base prevented neck hyperextension during head impact experiments. Compression springs were placed along the steel cables to tune head mechanics during head impact experiments.

The study used an instrumented head surrogate fixed to the neck prototype to acquire head mechanics. Head mechanics during head impact experiments at low (2 m/s) and high (6 m/s) impacts speeds, and at three locations (crown, back, and oblique-facemask) characterized the Phase II neck response. Quantified measures of neck response evaluated design refinements against the Phase I prototype, efficacy as a standardized model, and offered insight for future design iterations. The Phase II neck response compared to volunteer data available in literature provided a preliminary evaluation of its ability to produce humanlike head kinematics.

Overall, repeatability of impact mechanics exhibited an average coefficient of variation of 11%, which was an improvement compared to Phase I neck repeatability and satisfied requirements for standardized mechanical surrogates. By using different compression springs, the ability to tune head mechanics was demonstrated for back impacts. The ability to tune head mechanics during back impacts, but not during crown or facemask impacts, was explained by the cable and spring geometry. Minor design changes could produce tunable head mechanics for all impact directions. With the capacity to tune head mechanics, the Phase II neck can achieve a humanlike head impact response. A

quantitative long-term repeatability study and a qualitative inspection demonstrated excellent durability compared to the Phase I prototype, as there were consistent response measures and no observed damage. Biofidelity of the Phase II neck was demonstrated by correlating time series head kinematics to those from human volunteer head impact experiments, with resulting CORAplus ratings greater than 0.75 (good curve correlation).

In summary, the Phase II neck was an improved model over the previous prototype regarding inter-test variance, durability, ability to tune head mechanics, and humanlike responses. Results suggest Phase II neck efficacy as a standardized model for use in head impact applications and the capability to replicate humanlike responses. A neck model that is repeatable, durable, and can be tuned to match the human head impact response could improve accuracy in acquiring mechanics associated with mild traumatic brain injuries.

Preface

This thesis is an original work by Samantha MacGillivray. Contents of this thesis have been previously published (below) and presented at the 2019 International Research Council on Biomechanics of Injury Conference held in Florence, Italy.

> Samantha R. MacGillivray (presenter), Jason P. Carey, and Christopher R. Dennison. "Repeatability of a Mechanical Surrogate Neck for Low Speed Impact Testing: A Preliminary Assessment." *International Research Council on Biomechanics of Injury* (2019).

The volunteer study was conducted by Kristen Reynier et al. (2019) at the University of Virginia, USA. The volunteer comparison data used in this work was obtained from literature (Reynier et al. 2019) with the authors' permission.

The Cone Beam Computed Tomography (CBCT) machine was available from the Faculty of Medicine and Dentistry, at the University of Alberta.

Acknowledgements

Firstly, I would like to thank my supervisor, Dr. Christopher Dennison, for providing guidance and support. I am grateful for the countless hours he spent throughout the completion of my thesis, from approving spring purchases and assisting with experiments, to reviewing my written documents and advising on my overall professional development.

I would also like to thank past and present members of the Biomedical Instrumentation Lab for creating a positive and collaborative environment and assisting with experiments. Special thank you to Megan Ogle for developing the Phase I neck and sharing your extensive neck knowledge.

Thank you to Dr. Dan Romanyk for connecting me with individuals in the Faculty of Medicine and Dentistry for use of the Cone Beam CT scanner and to Carla Clarke for conducting the scans.

I would like to thank Kristen Reynier and Dr. Matthew Panzer for sharing information on their volunteer experiments.

To my family and friends, thank you for your endless support and encouragement throughout my schooling. Special thanks to Sam Anderson for his genuine comradery and for being my data clustering mentor. To Chance, thank you for being my critic, catalyst, and haven; this thesis would not have been possible without your unwavering support, patience, and love.

Table of Contents

List of Tables

List of Figures

List of Nomenclature and Acronyms

PII Neck	Phase II Neck
LS	Low speed impact
HS	High speed impact
CR	Crown impact location
BK	Back impact location
FM	Oblique facemask impact location
SD	Side impact location
NC	Neck compression
NC1	Neck compression case 1
NC2	Neck compression case 2
v	Resultant impact speed (m/s)
a	Linear acceleration (g)
α	Angular acceleration
ω	Angular velocity (rad/s)
$\Delta t\omega$	Angular velocity duration (ms)
F	Force (N)
M	Moment (Nm)
Peak X	Maximum mechanic within 200 ms (X = a, α, ω, F, and M)
Impact F, impact M	Force and moment at time of maximum acceleration
SD	Standard deviation
CV	Coefficient of variation
r_x and r_y	Residuals defined as the deviation of NC2 v. NC1 data from the line y = x ($r_y = -r_x$)

1 Introduction

This chapter introduces the role of surrogate models in injury biomechanics, highlights the importance of a mechanical neck model that can replicate human head motion during head impacts, reviews the mechanics of traumatic brain injury and how the neck influences head motion, and outlines common surrogate neck requirements. The thesis objectives and structure are then summarized.

1.1 Motivation

Traumatic brain injury (TBI) is a significant cause of disability and death worldwide. Based on a survey conducted by the Centers for Disease Control and Prevention, TBI accounted for approximately 2.87 million emergency department visits, hospitalizations, and deaths in the United States (2014) [1]. TBI is caused by an external force or an abrupt high-energy head movement. These causal mechanics can occur during vehicle collisions, sports-related impacts, and mundane falls. TBI can result in long term physical and cognitive impairments that disrupt normal brain function and degrade quality of life [2].

To decrease the prevalence of TBI, researchers are working towards defining injury tolerances by quantifying impact biomechanics [3]. Biomechanics refer to the mechanics of an impacted body, which is subject to injury. To measure these mechanics, laboratory studies commonly employ human models such as post-mortem human subjects (PMHS),

animal models, anthropometric test devices (ATDs), and human volunteers. ATDs are most commonly used as they are an easily accessible human surrogate capable of repeatable use and can be standardized for laboratory comparisons [4].

ATD head and neck models are commonly used in head injury research for passenger and pedestrian automotive safety studies as well as sport and military protective equipment development. To accurately acquire head and neck injury mechanics, neck models must approximate neck anthropometry, produce humanlike impact responses, provide repeatable results, and have sufficient durability [4]. Most current ATD neck models are accepted as repeatable and durable; however, in head impact applications, many are thought to be too stiff in bending to create realistic head rotations. As angular velocity is an essential predictor of brain injury [5], inaccurate representation of head rotation can generate inaccurate impact mechanics and limit biomechanical assessment.

A repeatable and durable surrogate neck model is necessary for head impact injury research; however, accurate representation of live human responses (biofidelity) is essential to acquire injury mechanics. There is a need for an ATD neck model that can produce accurate head impact injury measures to advance the knowledge of injury biomechanics, improve safety equipment and regulations, and ultimately decrease the prevalence of TBI.

1.2 Mechanics of Traumatic Brain Injury

Head biomechanics greatly influence the type and severity of TBI. These injuries generally result from high energy trauma that disrupts normal brain physiology. As described by Melvin and Lighthall, brain injuries have been clinically categorized as either focal or diffuse [6]. Focal injuries, including hematomas and contusions, occur in localized areas and are generally considered more severe compared to diffuse injuries [6]. Diffuse injuries occur in widespread areas and include mild TBI, such as concussion and diffuse axonal injury [6]. In terms of causal mechanics, linear and rotational head motion are present for

both focal and diffuse injuries; however, linear kinematics correlate better to focal injuries [7], and rotational kinematics correlate better to diffuse injuries [8], [9].

While it is not entirely understood how the neck response governs head biomechanics in TBI, it is hypothesized that the neck tethers the head and transforms linear kinematics to rotational kinematics. Eckersley et al. utilized finite element models and demonstrated that head impacts to a headform attached to a neck produced greater angular acceleration compared to a neckless headform [10]. While linear kinematics are less effected by neck response [10], angular kinematics are governed by the neck. Inaccurate angular kinematics greatly limits the assessment of diffuse TBIs. Injury assessment surrogate necks must be validated in head impact conditions to produce humanlike responses.

1.3 Design Practices & Performance Requirements of ATD Necks

ATDs must satisfy specified performance requirements before being implemented into standardized injury assessment. This section discusses common design practices and performance requirements followed in the development and validation of a neck model. Organizational groups generate and maintain ATD design and performance specifications. Examples of such groups are the International Organization for Standardization (ISO) TC 22/SC 12/WG 5 (Anthropomorphic Test Devices group) and United States Code of Federal Regulations (CFR) Title 49 Part 572 (Anthropomorphic Test Devices group).

1.3.1 Common Design Practices

During the design and development of an ATD neck, several common practices are followed such as the representation of human neck anthropometry (shape, size, and mass distribution) [11]. Low dimensional tolerances are generally required, and strong materials that are similar to the anatomical neck material are often used. Geometry and material decisions often aim to reduce fabrication and development costs. A physical appearance

similar to that of the human neck is important; however, for injury assessment, accurate representation of the human neck response is the design priority.

1.3.2 Performance Requirements

Performance requirements define the head and neck response to a simulated impact condition and include repeatability, reproducibility, durability, and biofidelity requirements [11]. These specifications aim to produce reusable mechanical devices that accurately and consistently simulate human behaviour. Neck performance requirements are evaluated by measuring impact mechanics, including head kinematics and neck kinetics. Design iterations are often required to satisfy these performance requirements.

Repeatability pertains to low variations between duplicate measurements from the same condition. Repeatability of ATD neck responses is often assessed quantitatively using standard deviations (SD) and coefficients of variation (CV) between tests, where CV is defined by the percent ratio of the SD to the mean. Maximum allowable CV values are used to categorize ATD response repeatability as acceptable or unacceptable [11].

Reproducibility refers to the similarity between results from the same measurements conducted by different individuals and equipment at different locations. ATD neck reproducibility pertains to consistent mechanical responses from two different models, manufactured by different people and tested with different equipment. Multiple neck models are required to assess reproducibility.

Durability refers to the ability to resist wear and damage during multiple impacts at greater loading conditions than those used in standard practice. The durability of neck components is often assessed qualitatively following at least ten impacts at 150% of the standard highest loading condition [11]. Design choices based on durability requirements often contradict those required for an accurate humanlike response.

Biofidelity pertains to the ability to replicate human behaviour or impact mechanics during similar loading conditions. This performance requirement is arguably the most difficult to achieve and continues to motivate ATD development. To assess neck model biofidelity, several recommendations on performance requirements [12], [13] and standardized performance ratings [11], [14] have been established for automotive collision conditions. Standardized and certified ATD necks are validated for biofidelity of neck responses using methods and data specific for the intended use (for example, automotive injury assessment ATDs are assessed in simulated automotive collision conditions).

1.3.3 Validation of Current ATD Necks

Current standardized ATD neck models were designed and developed for the automotive industry to be repeatable, reproducible, and durable, while giving humanlike responses in collision conditions. Each ATD model was designed and evaluated for a specific collision directionality, limiting their use in oblique testing with multi-directional loading. These necks were designed against sled test data that simulate torso loading in an automotive collision; however, this is mechanically different than head loading in a head impact event. No standardized neck model has been designed for direct head impact loading, but several have been used in head loading applications. However, in head loading events most available standardized neck models have been criticized for being too mechanically stiff [15]–[17]. Head impact applications must use neck models that were developed and validated against head impact data to acquire accurate response measures.

1.4 Statement of Objectives and Contributions

The objective of this research is to develop a repeatable and durable neck model that, when connected to a head model, will produce a mechanically realistic head response in a head impact event relative to the human. Head mechanics are the bases for realism in this work. Specifically, this work advances an initial prototype, referred to as the Phase I neck

[18], through design changes to develop a second prototype, referred to as the Phase II (PII) neck. Additionally, this study characterizes the PII neck response from head impact experiments to assess repeatability, durability, and biofidelity of impact mechanics. The PII neck is designed with the ability to vary compression force along the vertebral column (tunability), allowing adjustments to be made to the neck bending stiffness in order to tune the head mechanics to achieve accurate mechanical realism.

The objectives of this thesis are to (1) advance the design of the Phase I neck to address its limitations and (2) quantify performance characteristics during direct head impacts. The objectives aim to contribute a neck model that is suitable for head impact research.

(1) Objectives for the mechanical design advancements:

- Prevent hyperextension of the neck in impact events.
- Reduce cable tension variation in the internal structure.
- Introduce the capability to tune impact mechanics.
- Improve neck neutral position stability such that it can support a helmeted surrogate headform in an upright position.

(2) Objectives to quantify performance characteristics:

- Repeatability: quantify the variability of impact mechanics between trials.
- Tunability: evaluate differences of impact mechanics between compression cases.
- Durability: evaluate through a quantitative long-term repeatability assessment and qualitative inspections.
    - Long-term repeatability: assess the systematic trend of impact mechanics over multiple impact trials, to determine if impact mechanics are consistent or systematically increase/decrease.
    - Inspections: visually assess mechanical components after impact tests for indications of damage or component failure.
- Biofidelity: correlate mechanics against head impact human volunteer data.

1.5 Thesis Organization

The Background chapter reviews ATD necks in head injury biomechanics research. Relevant human neck anatomy is outlined. Current standardized ATD necks used in injury biomechanics are reviewed, including design approaches, performance evaluation methods, and limitations of responses to direct head impacts. Finally, the Phase I neck is summarized, including the limitations which this thesis aims to eliminate.

The Methods chapter summarizes the design approaches used to address previous limitations, and the experimental methods used to quantify characteristics across two neck compression force cases, three impact locations, and two impacts speeds.

The Results chapter outlines critical findings for the characterization objectives, including model repeatability, tunability, durability, and biofidelity.

The Discussion chapter explores implications from the design changes and characterization analyses, highlighting advances of the PII neck prototype in comparison to the Phase I neck and standard model requirements. Limitations of the PII neck will also be explored.

Finally, the Conclusion outlines the thesis contributions and recommendations for future work to improve model repeatability, tunability, durability, and biofidelity.

2 Background

This chapter provides an overview of the human neck anatomy, the role of ATDs, and current standardized ATD neck design, performance requirements, and limitations in head impact applications. A summary is given of the previous novel neck prototype, on which this work is based.

2.1 Human Neck Anatomy

The following section discusses human neck anatomy to gain an understanding of relevant neck structural components. The human neck supports the head, connects it to the torso, and governs head mobility and movement range [19]. Structural components of the neck consist of muscles, ligaments, tendons, and the central skeletal cervical spine. The cervical spine consists of seven vertebral segments (Figure 2.1).

The occipital condyles (OC) at the skull base connect to the superior cervical vertebrae, the atlas (C1) and axis (C2) [20]. The junction between the OC and atlas is called the atlanto-occipital (AO) joint. The most inferior cervical vertebrae (C7) interacts with the first thoracic vertebrae (T1). Although the atlas and axis have a distinct structure, cervical vertebrae C3 to C7 have consistent structural components with increasing size moving inferiorly. These consistent structural components include the body, vertebral foramen, spinous process, and transverse processes [20] (Figure 2.2). The body forms the

anterior load-bearing section, and vertebral foramen provides a posterior space for the spinal cord to travel through [20]. Spinous processes are posterior projections, which fuse to achieve the lordotic curvature. Transverse processes are lateral muscle attachment projections [20].

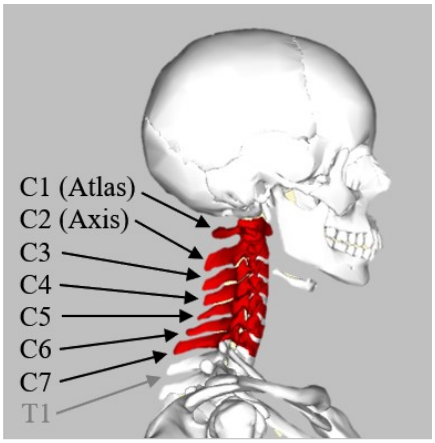

Figure 2.1: Seven vertebral bodies of the cervical column.

Image modified from Wikimedia Commons: Cervical Vertebrae Lateral provided by Body Parts 3D – Anatomography (The Database Center for Life Science).
https://commons.wikimedia.org/wiki/File:Cervical_vertebrae_lateral.png
Image licensed under the Creative Commons Attribution-Share Alike 2.1 Japan license.

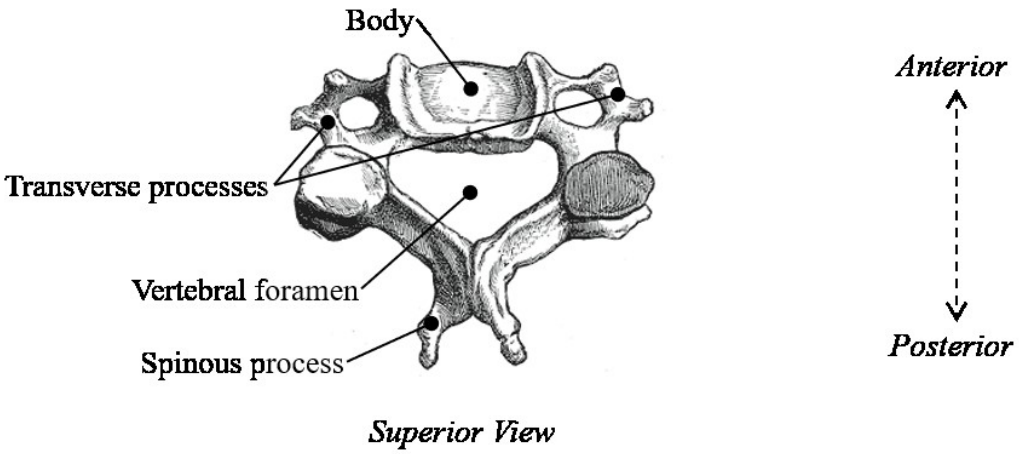

Figure 2.2: Superior view of a cervical vertebra with the distinct structural components: body, vertebral foramen, spinous process, and transverse processes.

Image modified from Wikimedia Commons: Gray84 clean.png
https://commons.wikimedia.org/wiki/File:Gray84_clean.png
Image licensed under the Creative Commons CC0 1.0 Universal Public Domain Dedication

Intervertebral discs are fibrocartilage pads that separate each vertebral body and enable mechanically coupled vertebral movements [20]. In addition to vertebral recruitment, intervertebral discs provide energy absorption for the column. Structurally, intervertebral discs consist of three components, including the nucleus pulposus, anulus fibrosus, and vertebral end plates (Figure 2.3). Nucleus pulposus is a soft and gelatinous core surrounded by a tougher fibrocartilage layer (anulus fibrosus) [20]. Vertebral end plates form a thin superior and inferior surface and fuse to adjacent vertebral bodies

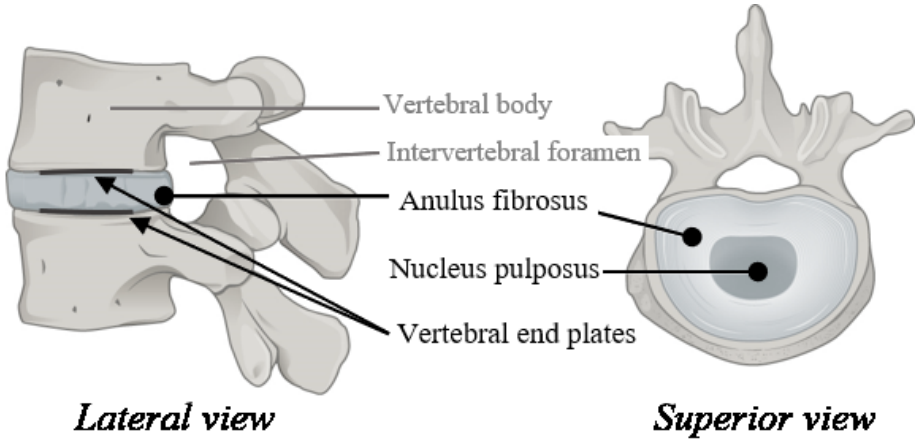

Figure 2.3: Lateral and superior view of an intervertebral disc, highlighting the main structural components: nucleus pulposus, anulus fibrosus, and vertebral end plates.

Image modified from Wikimedia Commons: 716 Intervertebral Disk.jpg
https://commons.wikimedia.org/wiki/File:716_Intervertebral_Disk.jpg
Image licensed under the Creative Commons Attribution 3.0 Unported license.

The cervical column forms the main skeletal structure of the neck, while the complex viscoelastic surrounding structures (musculature, ligaments, tendons, and skin) provide stability, controlled movement, and partially govern head motion.

2.2 Surrogate ATDs in Injury Biomechanics

ATDs were developed for injury risk assessment in an impact environment, where they must replicate live human behaviour to accurately acquire repeatable and reproducible measures of impact mechanics. The difficulty of creating a durable ATD (typically made

of metals, composites, rubbers, and foams) that accurately reflects the impact response behaviour of a live human has driven the continuous evolution of ATD surrogate models.

The first ATD, named Sierra Sam, was developed in 1949 for the aviation industry. In the 1960s, the Sierra Family and Very Important People ATDs were developed for the aviation and automotive industry [21]. These initial ATDs were designed to be durable and represent human weight and shape; however, they lacked humanlike stiffness and sufficient design specifications, resulting in inconsistent responses between dummies [21]. Although these ATDs had several deficiencies, they served as the initial prototype for later ATD model design. In 1972, General Motors developed a frontal impact ATD for assessing seat belt systems (Hybrid II) [22]. This model was durable and produced repeatable responses, but still lacked a humanlike response stiffness [21]. In the pursuit to achieve a repeatable and durable surrogate, which reflects live human response in impact, ATDs have evolved into complex and highly engineered models. Over the years, several standardized ATDs have been developed, including Hybrid III, THOR, ES-2re, BioSID, SID-IIs, WorldSID, and BioRID.

2.3 Standardized ATD Necks Currently Available

2.3.1 Hybrid III Neck

The Hybrid III neck (Figure 2.4) was designed for the automotive industry to reflect humanlike head flexion and extension in high-speed rear-end and frontal vehicle collisions [23]. The neck is composed of five aluminum elements and four rubber discs. Three aluminum elements approximate vertebral neck structures and two aluminum elements, at the superior and inferior ends, function as attachment surfaces [23]. Five aluminum elements are connected by four moulded butyl elastomer discs (75-durometer shore hardness) [23]. Rubber disc design is asymmetrical with anterior horizontal slits for less resistive neck extension compared to flexion [23]. A steel cable positioned through the

neck centre provides axial strength [23]. Brackets are secured to the superior and inferior aluminum elements to connect to the head and thorax. A pin joint on the superior bracket connects the head, and stiff rubber blocks (nodding blocks) limit head extension and flexion. A fixed connection to the thorax restricts relative translation and rotation between the neck base and thorax. Neck kinetics are measured through an upper and lower neck load cell located at the OC/C1 and C7/T1 vertebrae, respectively.

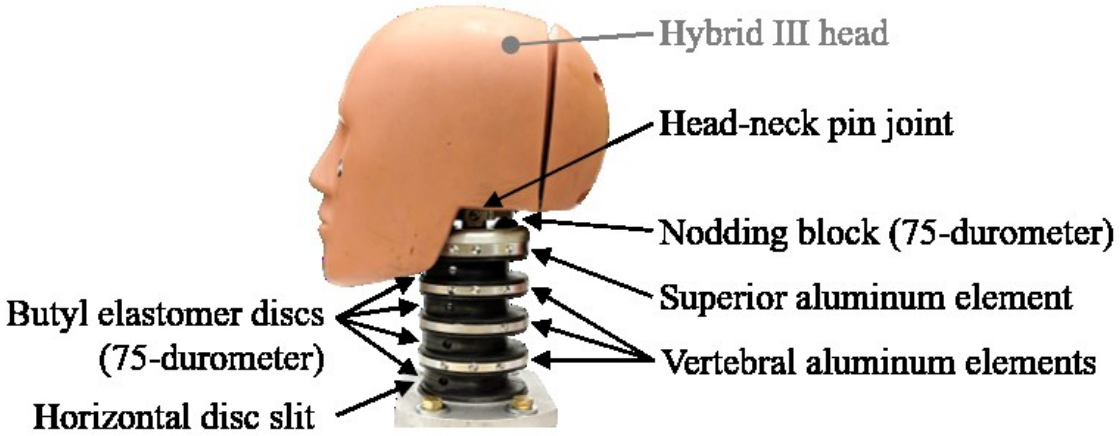

Figure 2.4: An annotated image of Hybrid III head-neck complex, highlighting neck components (base aluminum element, centre steel cable, and load cells not shown).

Hybrid III neck response was evaluated through performance requirements outlined by Mertz et al., which detail dynamic flexion/extension loading corridors [12]. Loading corridors [12] were established for head rotation and upper neck moment from data of human volunteers at non-injurious loading conditions and PMHS at injurious loading conditions during dynamic sled tests [24]. During Hybrid III neck development, Foster et al. [23] performed biomechanical response assessments by replicating the dynamic sled tests to generate neck flexion and extension. Generally, neck performance satisfied the flexion and extension requirements but had small deviations [23]. Although the Hybrid III neck response did not entirely satisfy performance requirements, it was considered a significant improvement in neck biofidelity, compared to previous prototypes [23].

Although the Hybrid III neck was designed and evaluated for automotive collision injury assessment, it is widely used for applications with multi-directional direct head impacts. Often in head and neck injury studies and helmet certification methods, only the head-neck assembly is used [25]–[27]. Contradictory to its extensive use, the Hybrid III neck is not without criticism. The Hybrid III neck was shown to have greater compressive stiffness than that of human cadaver tissue [15], [16], and greater flexion bending stiffness than pre-tensed human volunteers [17]. As neck bending stiffness influences head motion, inaccurate TBI risk assessments may result from the use of a neck, which exhibits stiffness properties greater than the live human. Despite these limitations, the Hybrid III neck is widely used in studying TBI mechanics and is considered a repeatable and durable surrogate model [28].

2.3.2 THOR Neck

In the 1990s, a new ATD, named THOR (Test device for Human Occupant Restraint), was developed by the National Highway Traffic Safety Administration (NHTSA). In 2013, following many revisions, the most recent THOR design was released [29]. The aim was to improve ATD response compared to Hybrid III performance in frontal and lateral automotive collisions [30]. It was hypothesized that a multidirectional neck design, including simulated passive muscle force using a spring-cable system, would produce humanlike head-kinematics in automotive collisions [31], [32].

The THOR neck was constructed from six alternating aluminum and rubber plates (three each) and with spring-cable systems along the anterior and posterior sides [32], [33]. Each cable ran parallel along the neck length and was rigidly connected within the thorax and upper head region. Within the head, a coil spring, rubber tube, and cable load cell were positioned along the cables [33]. The anterior and posterior systems used springs with different stiffness to achieve distinct head flexion and extension capabilities. Neck response was tuned by adjusting the rubber tube length on each cable [32]. An additional slack

cable was positioned through the neck centre to prevent neck hyperextension. A superior pin connection to the head allows for a greater rotational range of motion compared to the Hybrid III head-neck connection [31]. The THOR neck was instrumented with four load cells: an upper and lower neck load cell, and an anterior and posterior cable load cell. Head-neck rotation was measured by a rotary potentiometer located at the head-neck pin joint [31]. To improve response accuracy, the THOR neck was designed and developed to satisfy human volunteer corridors for flexion acceleration sled tests [13].

The THOR certification manual [34] and response guidelines [35] outline assessment methods and requirements for dynamic neck response, as per 49 CFR, Part 572, Subpart E [14]. THOR and Hybrid III necks are subject to the same flexion/extension certification methods and performance specifications from indirect head loading.

Studies evaluating THOR neck performance, in various impact conditions, have shown differing head-neck response compared to the Hybrid III [31], [36]. Using NHTSA's Biofidelity Ranking System [37], the THOR neck was shown to demonstrate greater biofidelity compared to the Hybrid III neck [17]. Another study showed that THOR head response more closely reflects PMHS response during sled acceleration tests, compared to Hybrid III-PMHS comparison [38]. These improved responses were thought to result from the THOR neck design [38], which satisfies human volunteer corridors [13].

Although improved humanlike responses have been shown in sled acceleration tests, limitations of the THOR neck have also been identified. At high impact speeds, the spring-cable system has been speculated to reach its compressive boundary case, resulting in abnormal head response [31]. Model reproducibility and ease of use have been criticized because of assembly and instrumentation complexity [17].

2.3.3 Side Collison ATDs – ES-2re, BioSID, SID-IIs, and WorldSID

Several ATDs have been developed for side vehicle collision injury assessment, including the ES-2re, BioSID, SID-IIs, and WorldSID [21].

In 1986, European researchers developed a side impact ATD prototype (EUROSID). Following international efforts and prototype revisions (EUROSID-1, ES-2 [39], [40]), ES-2re was available for commercial use in the 2000's [41]. Documentation of the ES-2re neck composition is sparse. Based on the Humanetics Innovative Solutions Inc. (Farmington Hills, MI) ES-2re Male Side Impact Dummy Parts Catalog [42], the main neck component is a single moulded rubber column with superior and inferior plates for connecting to the head and thorax. The head and neck are connected through a pin joint, which allows for lateral head motion. Upper and lower neck load cells are used to measure neck kinetics.

BioSID (Biofidelic Side Impact Dummy) was developed in 1989 and became available for commercial use in 1990 [21], [43]. BioSID uses a Hybrid III neck. This neck choice was based on comparisons to human volunteer response during sled tests, which suggested the Hybrid III head-neck had humanlike lateral responses [44]. Although BioSID is considered repeatable, reproducible, and durable in side-impact assessment, it was never implemented into regulation and is not widely used [21].

The SID-IIs was based on the first SID (Side Impact Dummy) ATD. SID-IIs is a second-generation (II), small (s) SID ATD and represents the anthropometry of a small female adult. The design was based on the BioSID model and also uses a Hybrid III neck. In 2007, SID-IIs was implemented into regulation under 49 CFR, Part 572, Subpart V [14].

In 2001, the WorldSID prototype was developed [45]. Following performance evaluations and design revisions, WorldSID was available for commercial testing in 2011. WorldSID uses ES-2 neck components consisting primarily of a rubber column. Through an

evaluation by Been et al. (2004) [46], WorldSID neck performance was shown to be repeatable and humanlike against ISO performance standards [11].

2.3.4 BioRID II

BioRID II was developed in the early 2000s for rear vehicle collision injury assessment. The neck was designed to restrict head motion to the sagittal plane and exhibits an initial postural curvature. BioRID II neck was composed of seven asymmetrical acetal plastic vertebrae alternating with polyurethane rubber blocks (shore A hardness 40). Four steel cables were passed through the vertebral elements and attached to a superior aluminum plate and T1 vertebral element. The cables were passed along lower spinal segments and exit the body at the spine base. Outside the body, four cables were attached to a spring-damper system to control head-neck flexion/extension motion [47]. An upper neck load cell was used to measure neck kinetics. Human volunteer corridors of head mechanics during sled tests were used by Linder et al. to validate the neck for repeatability and humanlike response [47]. Although BioRID II was used for rear impact injury assessment, repeatability and reproducibility concerns have been identified for low-severity tests [48].

2.4 Standardized ATD Neck Evaluations

Standardized rules and regulations for dynamic neck performance (CFR Title 49, Part 572, Anthropomorphic Test Devices) [14] were chartered using the Hybrid III assessment methodology and now act to certify all ATD models in the automotive industry, including the THOR neck [34]. This legislation details the equipment, test procedure, and required response metrics. CFR neck validation procedure for flexion/extension is outlined as follows [14]:

- Mount the head-neck to the end of a rigid pendulum arm with the midsagittal plane parallel to the pendulum plane of motion.

- Raise and release the pendulum arm from a height to generate an impact velocity of 6.89 to 7.13 m/s and 5.95 to 6.19 m/s for neck flexion and extension, respectively.
- Pendulum deceleration is achieved by the rigid pendulum arm impacting a damping block (honeycomb material); neither the head nor neck impacts any object.

As no direct impact occurs to the head nor neck, neck response specifications only apply to torso loading applications [14].

CFR 49 Part 572 also outlines performance requirements for side-impact ATDs [14], with the same pendulum configuration and procedure as above. However, the head-neck is mounted with the midsagittal plane perpendicular to the pendulum plane of motion [14]. Again, neck response biofidelity is assessed for torso loading.

An objective Biofidelity Ranking System (BioRank) was developed by NHTSA to assess neck response biofidelity [37]. This method used a mathematical equation to quantitatively evaluate ATD response and was initially developed to compare against PMHS response corridors from sled tests [49]. The BioRank equation can be adopted to evaluate response against any time series data. THOR neck flexion/extension was evaluated [17] through BioRank and against human volunteer data obtained from sled acceleration tests [13]. BioRank assessment method was adopted into regulation (ISO/TR 9790) and was used to assess WorldSID neck biofidelity in lateral inertial loading [11].

A database of human neck responses to inertial loading was developed from volunteer sled acceleration tests conducted at the Naval Biodynamics Research Laboratory (NBDL) and included responses from various acceleration and directional conditions. This data was used to assess responses of ATD necks [17], [50] and to develop performance requirements [51]. Although the database is widely used for neck performance evaluation, experimental replication is difficult as information on subject stature is not well documented.

While many regulations detail biofidelity requirements for automotive collision conditions, neck performance requirements are not defined for impact loading directly to the head. To the author's knowledge, there are currently no neck performance requirements for direct head loading. However, recent studies aim to characterize volunteer head mechanics from direct head impacts [52]–[54], which can contribute to future regulation of neck performance during direct head impacts.

2.5 Head Impact Applications

While standardized ATD necks were designed and validated for use in automotive collision injury assessment, several have been used in direct head impact applications where they may not accurately represent live human responses. These applications aim to study linear and angular head kinematics. This section outlines direct head impact applications and the importance of accurate head mechanics.

Laboratory studies use ATD neck models to characterize impact biomechanics and infer injury risk, with the Hybrid III neck being the most common model. These studies tend to focus on sports, such as football and hockey, as many athletes experience injury from head impacts. The National Football League (NFL) has reconstructed injurious head-to-head impacts using ATD head-neck models to acquire impact mechanics [55]. Injury data and corresponding ATD kinematic measures are used to estimate injury risk levels [55], design better equipment, and improve game regulations.

Helmet certification standards also employ ATD necks to assess energy attenuation as all helmets aim to reduce energy transfer to the head and brain. The National Operating Committee on Standards for Athletic Equipment (NOCSAE) football helmet standard [56] and Hockey STAR rating system [25] assess helmet performance from linear and rotational head kinematics obtained during impacts directly onto a helmeted Hybrid III head and neck. NOCSAE football helmet certification methods use a pneumatic linear

impactor to obtain peak acceleration values and authorize certification based on thresholds levels [56]. The Hockey STAR rating system evaluates helmet performance from acceleration measures obtained during pendulum impacts [25].

Contradictory to its extensive use in injury studies and helmet assessment methods, the Hybrid III neck is commonly criticized for being too stiff in bending during direct head impact conditions. Considerable differences between peak linear and angular acceleration measures between a Hybrid III and PMHS have been identified during impacts to the forehead and occipital bone [57].

Many academic researchers and industry corporations have worked towards developing a mechanically realistic neck model [18], [30], [50], [58], [59]. However, there is still a need for an ATD neck that is capable of producing accurate injury measures from head impact loading while satisfying repeatability and durability requirements.

2.6 Phase I Neck Prototype

A novel mechanical surrogate neck, referred to as the Phase I neck (Figure 2.5), was designed and developed in 2018 by Ogle (Biomedical Instrumentation Lab, University of Alberta) [18]. The overarching goal was to develop a laboratory ATD neck model capable of humanlike dynamic responses during direct head impacts. To achieve this goal, prototype iteration is required to test, refine, and perfect the neck. Therefore, the Phase I neck served as the initial prototype to test design concepts. This section outlines the Phase I neck design, response assessment methods, and prototype limitations.

The Phase I neck was designed to represent the anthropometry of a 50^{th} percentile male neck, including overall length, diameter, and cervical spine components [18]. Cervical vertebral bodies and intervertebral discs were approximated by seven aluminum (6061-T6) elements and eight 3D printed rubber (TangoBlack – FullCure ® 970, 3D Printers Canada, Vaughan, On) elements, respectively. The size and shape of each aluminum

element represented a simplified vertebral structure, including a body and transverse processes [18]. The size of the aluminum and rubber elements increased inferiorly through the cervical levels to reflect anatomical size increases. The rubber discs were designed with additional material on the anterior side to create a lordotic curvature [18]. Three steel cables were passed through each cervical level, one through the aluminum and rubber element centres, and two through the simplified aluminum transverse processes. Clamping collars at the base of the neck were used to tension the three cervical cables. To approximate muscle tissue, the vertebral column was encased in silicone rubber (Ecoflex ® 00-30, Smooth-on Inc., Macungie, PA) [18].

Figure 2.5: Phase I neck developed by Ogle (2018) [18].

The neck bending stiffness was found to be much less stiff than that of a Hybrid III neck model [18]. The Phase I neck was characterized in quasi-static flexion/extension bending and dynamic direct head impacts and compared to PMHS data to evaluate mechanical realism. Component durability was considered acceptable [18].

Consistent cases of hyperextension were observed during impact tests due to high neck compliance to bending and separation of silicone from the base plate [18]. The cervical cable clamping collars would slip during impact tests, which resulted in a large variance of impact measures and poor repeatability [18]. While using the prototype, extremely high neck compliance to bending was observed, such that the Phase I neck was unable to support an ATD headform upright [18]. Neck response in quasi-static and dynamic impact evaluations differed from that of PMHS data. A method to control neck response to satisfy human behaviour was not presented [18].

The Phase I neck tested initial concepts towards a laboratory neck model for use in direct head impact applications. The overall objective of this thesis is to address limitations of Phase I neck, refine the design to produce a Phase II model, and characterize its response from direct head impact tests.

3 Methods

This chapter describes the design methods used to develop the PII neck, highlighting refinements compared to the Phase I neck. Also outlined are the experimental techniques used to achieve direct head impacts and obtain impact metrics for assessment of the PII neck response.

3.1 Mechanical Design of the PII neck

The PII neck was developed based on the Phase I neck created by Ogle in 2018 [18]. The goal of this second prototype was to address limitations through design refinements and to assess model response behaviour during direct head impacts. This section describes the foundational design methods used to replicate the Phase I neck and the approaches used to improve the design.

3.1.1 Design Aspects Consistent with the Phase I Neck

This section outlines the foundational design of the PII neck, which partially replicates the previous Phase I neck prototype. This design aimed to create mechanically durable and repeatable neck components that resembled human anatomy. These components included vertebral bodies, intervertebral discs, and soft tissue surrounding the cervical spine. The Phase I neck design resembled the anthropometry of the 50^{th} percentile male

neck [60]. The overall dimensions of the PII neck were kept consistent with this design, as shown in Table 3.1. Neck width is measured along the coronal plane, and neck depth is measured along the sagittal plane.

Table 3.1: External anthropometry of 50th percentile male neck, Phase I neck prototype, and PII neck prototype.

External Measurements	50^{th} Percentile Male	Phase I neck	PII neck
Neck Length	108 mm [60]	115 mm [18]	115 mm
Neck Depth	123 mm [60]	100 mm [18]	100 mm
Neck Width	117 mm [60]	100 mm [18]	100 mm
Neck Circumference	394 mm [60]	314 mm [18]	314 mm
Neck Mass	1100 gm [61]	-	1960 gm *

** Mass is calculated from a CAD model due to 2020 laboratory restrictions.*

Design of the internal structural components replicated that of the Phase I neck [18] except for slight enlargements to accommodate cable design changes. The internal structural components approximate simplified cervical elements. Seven vertebrae were waterjet cut from 6061-T6 aluminum (¼ in thick), and eight intervertebral discs were 3D printed from TangoBlack rubber (TangoBlack–FullCure® 970, 3D Printers Canada, Vaughan, On). Annotated CAD examples are shown in Figure 3.1. Dimensions of the vertebrae were based on anatomical measurements observed by Panjabi et al. [62]. Measurements of vertebral body width (w), body depth (d), pedicle length (l), and transverse process angles (α) are shown in Table 3.2. Measurements of rubber disc width (w) and depth (d), were consistent with the inferiorly adjacent aluminum vertebrae. A rubber disc height (h) of 4.5 mm was chosen to achieve the appropriate neck length [18]. Additional material on the rubber disc anterior side, defined by inclination angles (ϑ), was based on anatomical measures [62] to achieve the lordotic neck curvature, also shown in Table 3.2. A constant hole diameter of 6.8 mm was used for all cervical elements.

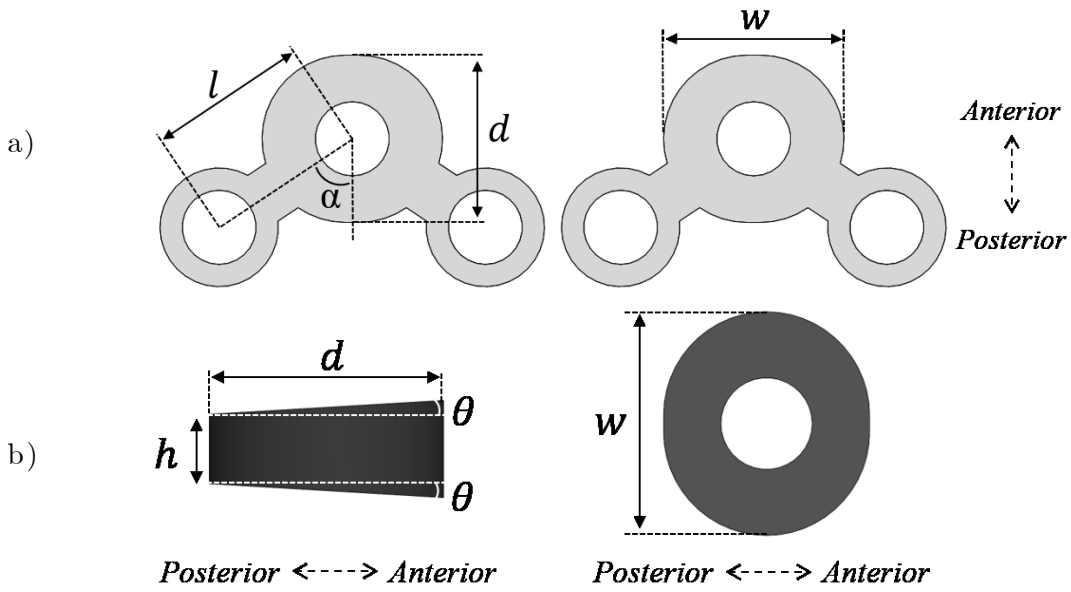

Figure 3.1: Annotated CAD models of internal structural components, including a) aluminum vertebra and b) rubber intervertebral disc.

Table 3.2: Measures of PII neck internal structural components: aluminum vertebra and rubber intervertebral discs.

Aluminum Vertebrae Measures					Rubber Disc Measures	
Vertebrae	w (mm)	d (mm)	l (mm)	α (deg)	Intervertebral Disc	ϑ (deg)
C1	16.90	15.45	13.70	57.76	0-C1 & C1-2	0.00
C2	16.90	15.45	13.70	57.76	C2-3	3.38
C3	16.50	15.25	14.60	56.45	C3-4	3.75
C4	17.00	15.50	14.70	57.68	C4-5	3.38
C5	18.50	16.50	15.40	56.58	C5-6	1.91
C6	20.50	17.50	15.70	56.06	C6-7	3.60
C7	22.50	17.50	16.20	54.46	C7-T1	3.27

As in the Phase I neck, the PII neck had three steel cables fed through the alternating cervical elements to achieve mechanical stability and vertebral recruitment. Top and bottom aluminum plates were used to provide column compression surfaces and to attach supplementary brackets. An aluminum bracket was attached to the top plate, which comprised of a pin joint to connect the neck to an ATD headform. The internal structural components are shown in Figure 3.2.

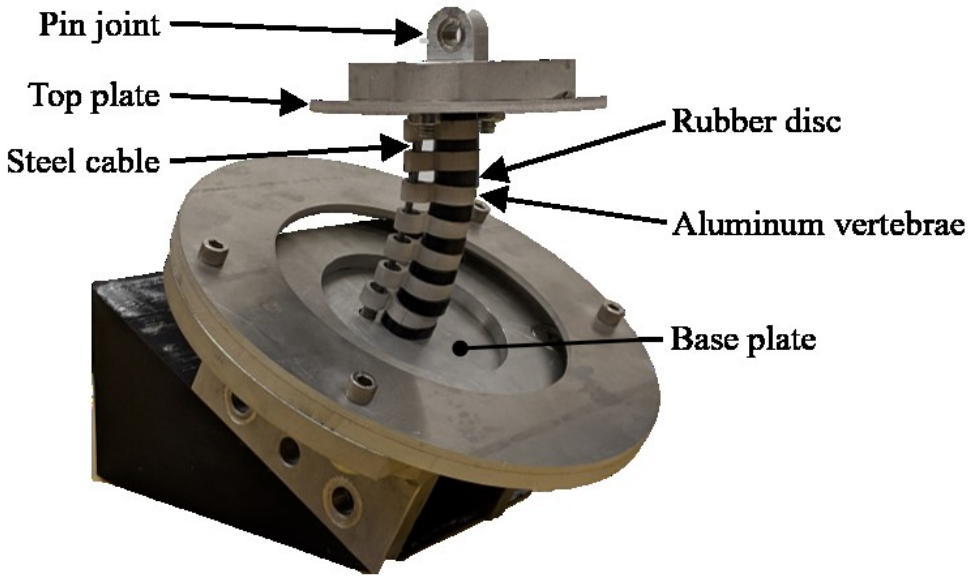

Figure 3.2: PII neck internal structural components: alternating aluminum and rubber elements, steel cable, top and bottom plates, and a pin joint to connect a headform.

The internal structural column was encased in silicone to approximate human neck viscoelastic tissue (Figure 3.3). The type of silicone used for the PII neck differed from the Phase I neck, which will be discussed in the next section. Before casting the silicone, a vacuum chamber was used for degassing the liquid to prevent air bubbles, which can cause high-stress concentrations within the silicone.

Figure 3.3: Final design form of PII neck with an external silicone casing.

The aim was to produce a re-usable model with synthetic properties; therefore, material properties of the Phase I and PII neck components were chosen based on availability, ability to manufacture, and structural durability. Materials were not chosen to approximate tissue properties. Phase I and PII neck material properties were compared (Table 3.3) to corresponding anatomical structure properties, including the vertebrae (aluminum and bone), intervertebral discs (rubber and fibrocartilage), and viscoelastic casing (silicone and muscle tissue) [18]. Specifically, the comparisons include yield strength (σ_y), ultimate tensile strength (σ_u), Young's modulus (E), hardness, elongation at break, and shear modulus (G). Through this comparison, the Phase I neck was considered to be more durable than human tissue [18]. Material properties of the PII neck component were kept consistent with the Phase I neck, except for the silicone.

Table 3.3: PI and PII neck material properties compared to human tissue properties.

Material	σ_y (MPa)	σ_u (MPa)	E (GPa)	Hardness	Elongation at Break (%)	G (GPa)
Aluminum 6061-T6	270	310	69.0	60 (Rockwell)	12.0	26.0
Vertebral bone, cancellous [63]	-	-	0.17	-	-	-
TangoBlack 3D printed rubber	-	2.00	-	61 (Shore A)	48.0	-
Intervertebral disc [64]	-	8.80	3.61E-3	-	-	-
EcoFlex 00-30 silicone (PI neck)	-	1.38	6.9E-5	00-30 (Shore)	900	-
Dragon Skin 20 silicone (PII neck)	-	3.79	3.40E-4	20 (Shore A)	620	-
Relaxed muscle tissue	-	-	2.70E-5 [65]	-	-	4.6E-6 – 23.8E-6 [66]

3.1.2 PII Neck Design Advancements

This section discusses PII neck design changes that addressed limitations of the previous Phase I neck prototype.

During dynamic impact tests, the silicone of the Phase I neck would separate from the base plate and allow the neck to hyperextend beyond human limits [18]. A silicone flange was designed at the base of the PII neck to prevent hyperextension. The silicone flange was compressed between aluminum ring plates and the base plate to prevent separation of the silicone during dynamic impact tests. Figure 3.4 demonstrates the silicone flange and plate design.

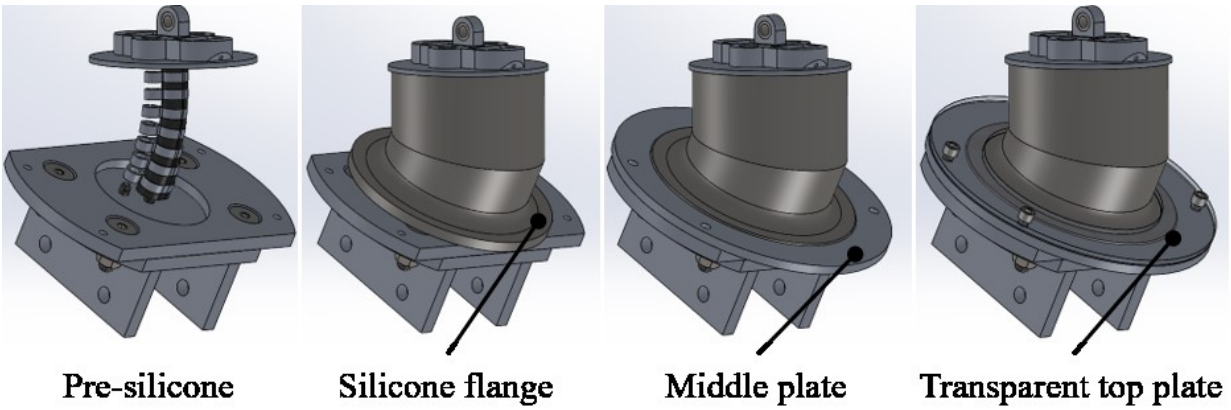

Figure 3.4: A series of annotated CAD models demonstrating PII neck without silicone, silicone base flange, and middle and top (transparent) aluminum ring plate.

The Phase I neck used cable clamping collars at the cervical cable base to secure cable tension; however, the clamping collars were observed to slip during experiments. This slipping of collars was speculated to cause high variation in impact mechanics [18]. To achieve consistent cable tensioning, the cervical cable assembly was redesigned. The redesigned steel cable assembly was composed of three parts welded together: a steel cable (1/8 in diameter, 3450T28 Galvanized Steel Wire Rope, McMaster-Carr, Cleveland, OH), compression ball fitting (3869T63 Ball-with-Shank-End Roller Swage End Fitting, McMaster-Carr, Cleveland, OH), and hollow threaded rod (94624A121 Hollow Threaded

Stud, McMaster-Carr, Cleveland, OH), shown in Figure 3.5. Below the base plate, locknuts were threaded onto the cable assembly to achieve consistent cable tension throughout the column during impact experiments.

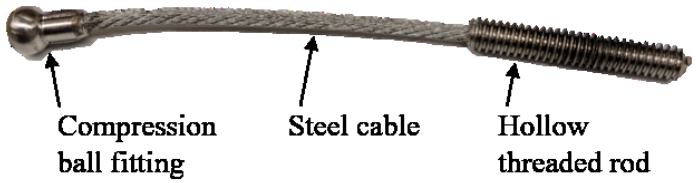

Figure 3.5: PII neck steel cable assembly (compression ball fitting, steel cable, and hollow threaded rod) to achieve consistent cable tension during dynamic impacts.

In efforts to introduce a method to tune impact mechanics, springs were incorporated at the cervical cable base to create passive compression force along the internal column (Figure 3.6). By adjusting the compressive load across the column, neck bending stiffness can be tuned, which was hypothesized to alter the PII neck impact response. By switching between two sets of three springs with different stiffness properties, two passive neck compression (NC) force cases were used to evaluate the ability to tune impact mechanics.

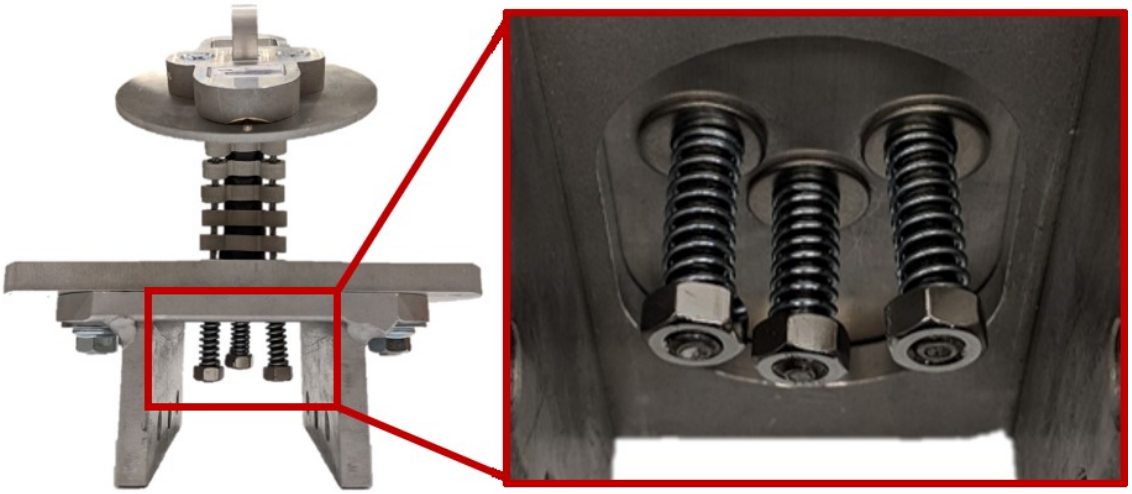

Figure 3.6: A set of three compression springs along the base of the cervical cable assemblies to create a passive net compression load across the internal column.

The Phase I neck silicone rubber (Ecoflex® 00-30, Smooth-On Inc., Macungie, PA) was chosen based on a study assessing the ability of silicone materials to simulate tissue

biomechanics [66]. However, as the Phase I neck could not adequately support an ATD headform in an upright position, Ecoflex® 00-30 was deemed too flexible [18]. Based on this limitation, a silicone with higher shore hardness (Dragon Skin™ 20, Smooth-On Inc., Macungie, PA) was chosen for the PII neck. Dragon Skin™ 20 was also determined to be a material capable of approximating muscle tissue [66]. The PII neck, with Dragon Skin™ 20 silicone, was able to support a helmeted ATD headform in an upright position.

3.2 Experimental Methods

3.2.1 Experimental Equipment

Quantified impact mechanics obtained during upright head impact experiments were used to evaluate the PII neck prototype. A custom pendulum was used to achieve direct head impacts, where an impactor was guided through a frictionless arc and into an ATD headform. The impactor was an ISO headform (medium, mass = 3,366 g, CADEX Inc., Saint-Jean-sur-Richelieu, QC, Canada) fit with a certified football helmet (Schutt F7, NOCSAE certified). The ISO headform was fit with a helmet to prevent damage to it and other test equipment during impact. A rope was fixed to the ISO headform on one end, and the pendulum frame, on the other end, generating an adjustable minimal mass pendulum arm. The pendulum impactor was manually raised and released from a predetermined height to achieve target impact speeds. The impacted equipment consisted of a helmeted (Schutt F7, NOCSAE certified) 50^{th} percentile male Hybrid III headform fixed to the PII neck. The Hybrid III headform was helmeted in anticipation of replicating experiments with volunteers in order to compare the PII neck response to that of living humans. The PII neck base was attached to a rigid support during low-speed impacts and a linear rail during high-speed impacts, shown in Figure 3.7. A rigid support was used during the low impact speed experiments to recreate a human volunteer experiment setup [54]. A linear rail was used during the high impact speed experiments to prevent damage to the impacted Hybrid III headform.

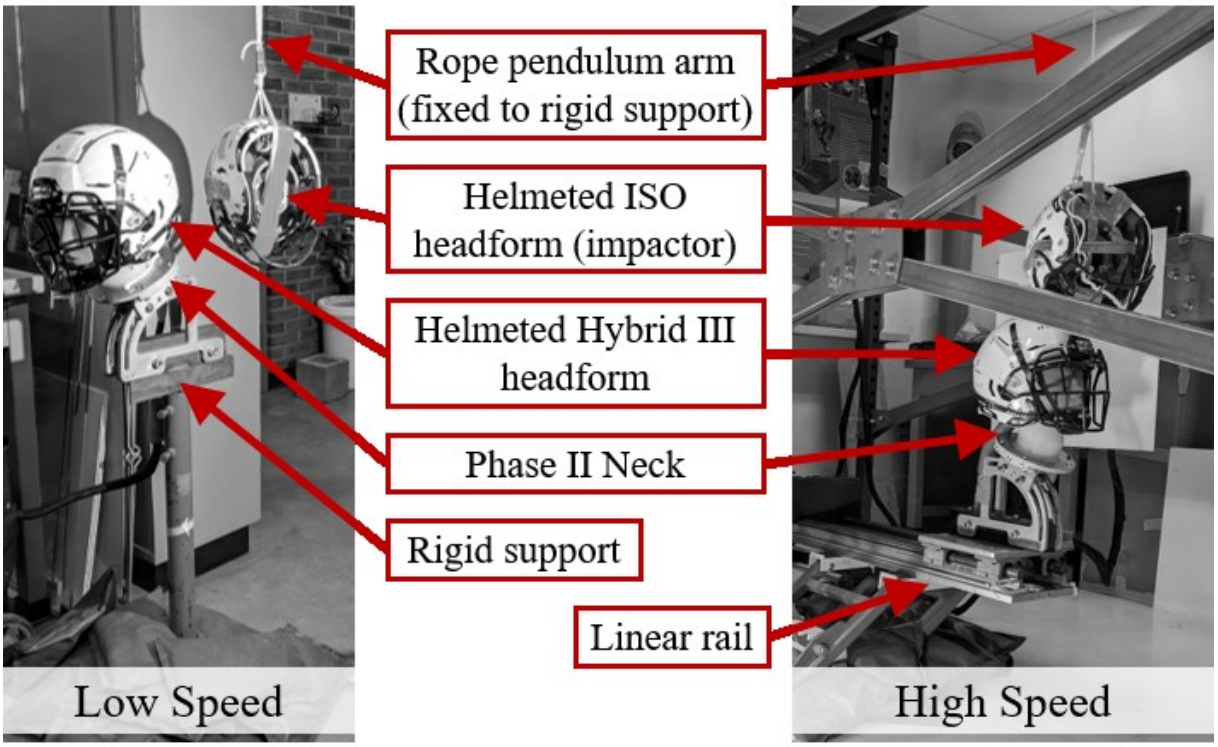

Figure 3.7: Experimental setup with the helmeted ISO headform (pendulum impactor) attached to a rope (fixed to rigid support), and a helmeted 50th percentile Hybrid III headform fixed to the PII neck. For the low and high-speed configurations, the PII neck is mounted to a rigid support and linear rail, respectively.

There were nine uniaxial accelerometers (Measurement Specialties Inc., Hampton VA, model 64C-2000-360), within the Hybrid III headform, arranged in a 3-2-2-2 configuration. Three accelerometers were located at the head centre of gravity (COG), and two accelerometers were each located at the crown, front, and left side of the head using mounting blocks. Through this accelerometer configuration, head COG linear accelerations were directly measured, and angular accelerations were calculated through equations presented by Padgaonkar [67]. A six-axis load cell (mg sensor GmbH, Iffexheim Germany, model N6ALB11A) was located at the base of the Hybrid III headform, to measure upper neck forces and moments. The Hybrid III head with positive coordinate systems for head COG acceleration measures and upper neck kinetic measures (forces and moments), as specified by SAE Standard, J211-1 [68], are shown in Figure 3.8.

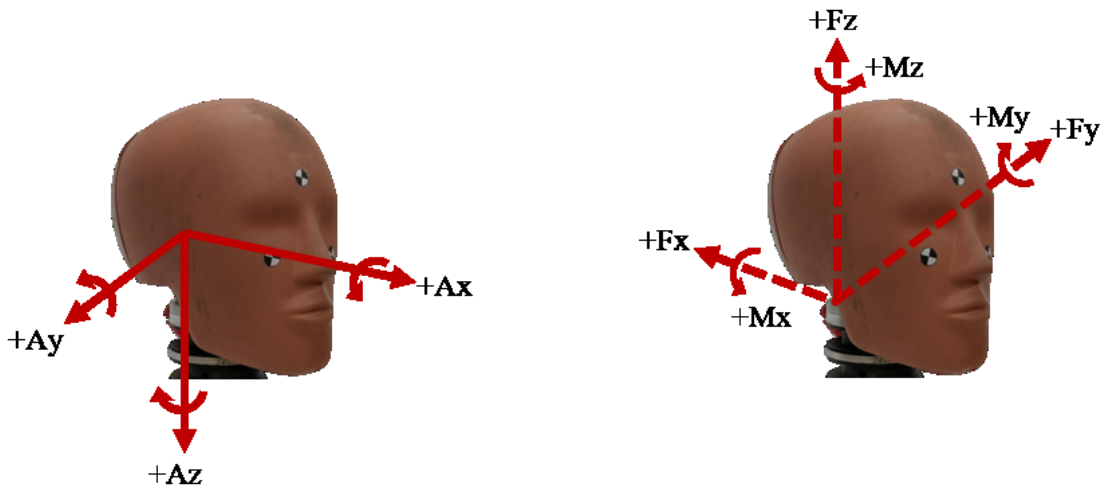

a) b)

Figure 3.8: Positive Hybrid III coordinate directions for the a) head COG acceleration measures and b) upper neck force and moment measures.

Hybrid III data was collected using a National Instruments data acquisition system and software (PXI 6251 and LabVIEW v8.5, Austin TX) at a sampling frequency of 100 kHz. All signals were initially filtered with an anti-aliasing hardware filter, at a 4 kHz cut-off frequency. Acquisition and filtering techniques were in regulation with SAE standard J211-1 (ATD instrumentation in impact event measurements) [68].

Two high-speed cameras (Phantom v611, Vision Research Inc., Wayne NJ) were placed in front of the PII neck-Hybrid III headform assembly to acquire stereoscopic footage of the impact event. This footage was used for post hoc observation and to calculate impact speed. The master and slave cameras were positioned approximately 45° from each other and were each equipped with a Carl Zeiss (Jena, Germany) 50 mm f/1.4 macro lens. Each lens apertures were set at f/4.0 to allow for sufficient depth clarity. Acceptable exposure was provided by lights positioned in front of the cameras. Both cameras were synchronized to record at a sample rate of 3,000 frames per second, with 1280 x 800-pixel resolution and 330 µs exposure time. The high-speed camera placement for the high-speed impact configuration is shown in Figure 3.9.

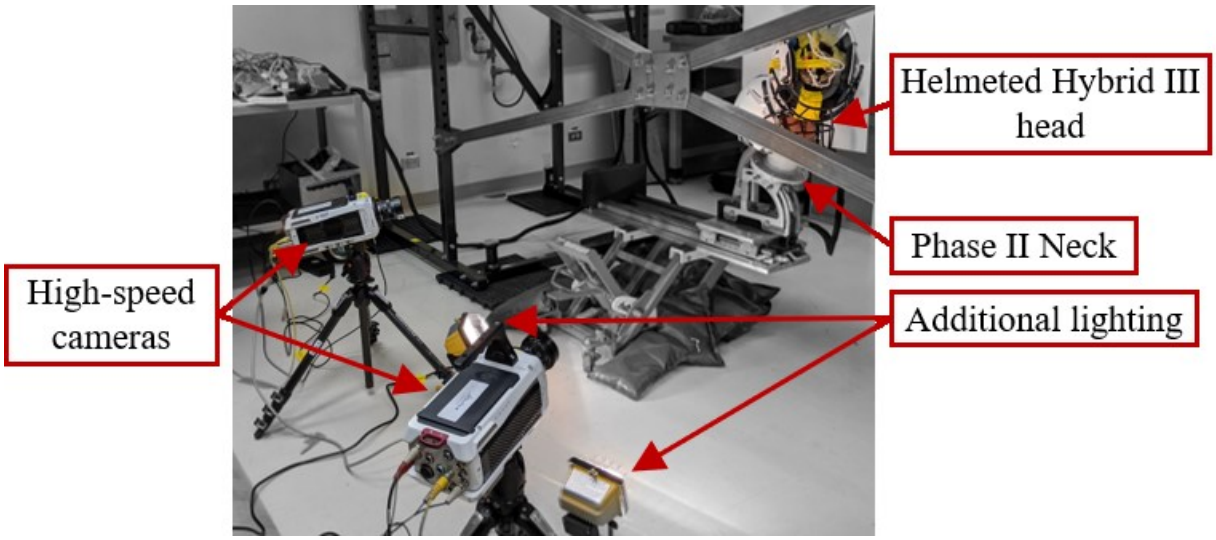

Figure 3.9: Placement of the two high-speed cameras (approximately 45° apart) and additional lighting for the impact experiments.

Impact speed was calculated from three-dimensional (3D) position data and the camera frame rate. The Direct Linear Transformation (DLT) method [69] was used to determine the 3D spatial coordinates from two-dimensional (2D) planar coordinates obtained by the synchronized cameras. The method of applying DLT to calculate 3D displacement was presented initially by Miller et al. [69]. It was later adapted by Yu (2017, Biomedical Instrumentation Lab, University of Alberta) [70], with the use of two synchronized Phantom v611 cameras. The method presented in detail by Yu [70] was replicated in this thesis to calculate 3D position data. In brief, the DLT method with two synchronized cameras required the calibration of the spatial region of interest to determine unique transformation matrices for each camera. Following calibration, the transformation matrices were applied to 2D pixel coordinates from each camera to solve for 3D spatial coordinates. The previously designed calibration apparatus [70] (Figure 3.10) included 17 known 3D spatial coordinate markers, which approximated the impact region of interest. These known markers were used to solve for the two transformation matrices with 11 unknown coefficients. A minimum of six calibration markers was required, as each point generated two equations, but more points were included to improve accuracy.

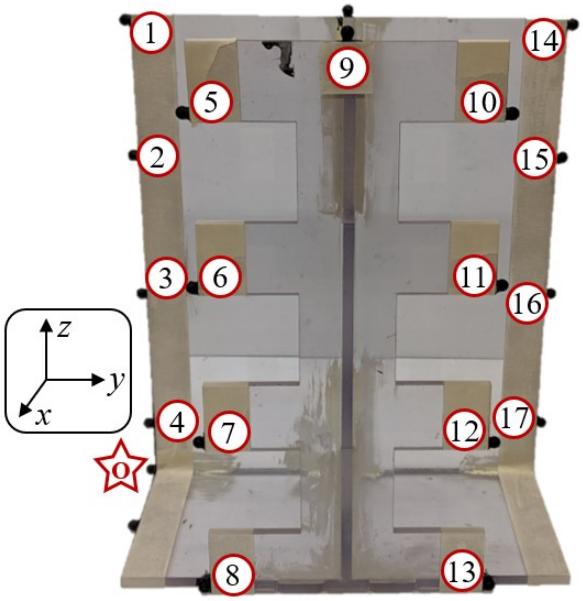

Figure 3.10: Previously designed apparatus [70] used to calibrate the impact volume of interest for applying DLT to calculate impact velocity. The apparatus volume (12 x 10 x 5 in) included 17 known 3D spatial coordinate markers from the origin point, O.

3.2.2 Experimental Protocol

Low and high impact speeds were performed to evaluate the PII neck performance during direct head impacts. The low impact speed of 2 m/s was chosen to allow for comparison with volunteer experiments as it is a non-injurious head impact speed used in ATD evaluation [54]. The high impact speed of 6 m/s was chosen to reflect an upper-speed range used in standard ATD implementation for helmet certification tests [25]. Impact speeds were achieved by raising the pendulum impactor to an appropriate height. Three impact locations were used: crown (CR), back (BK), and oblique facemask (FM), shown in Figure 3.11. These locations are common in helmet certification methods that employ ATD neck models [25]. The ability to tune impact mechanics using the adjustable cervical cable springs was evaluated by using two cases of total neck compression force (NC1 and NC2) across the cervical column ($F_{NC1} = 63$ N and $F_{NC2} = 163$ N). NC cases were achieved by switching between two sets of three compression springs at the base of the cervical cables. The force values of 63 N and 163 N represent the total force created by the three

compression springs, which apply a net compressive load across the base of the cervical column. NC1 (63 N) was achieved using a compression spring with a spring constant, k, of 18.43 lbs/in (9657K105 Compression Spring, McMaster-Carr, Cleveland, OH) and NC2 (163 N) was achieved using a compression spring with a spring constant, k, of 47.75 lbs/in (9657K305 Compression Spring, McMaster-Carr, Cleveland, OH).

Figure 3.11: Impact location definitions for the crown, back, and oblique facemask.

Repeat tests were conducted to evaluate impact response with statistical analyses. Repeatability and tunability of impact response metrics were assessed from three impact locations (CR, BK, and FM) and for two NC cases (63 N and 163 N) with five repeats for the low impact speed (2 m/s) and ten repeats for the high impact speed (6 m/s). Long-term repeatability was assessed from experimental conditions with one impact location (FM) and one NC case (163 N), with 50 repeats at the high (6 m/s) impact speed. Table 3.4 outlines the number of repeats for each analysis. The same two NOCSAE certified football helmets were used for all impact scenarios. The impacted equipment occasionally shifted because of the high impact energy, and therefore minor adjustments were required between repeats to realign the impactor and Hybrid III head.

Table 3.4: Number of repeats for each analysis and experimental impact configuration, including impact location (crown, back, and facemask), neck compression (NC) case (F_{NC1} = 63 N and F_{NC2} = 163 N), and impact speed (low, 2 m/s and high, 6 m/s).

ANALYSIS: Repeatability and Tunability			
		Number of Repeats	
Location	NC Case	Low-Speed	High-Speed
Crown	1	5	10
	2	5	10
Back	1	5	10
	2	5	10
Facemask	1	5	10
	2	5	10
ANALYSIS: Long-Term Repeatability			
		Number of Repeats	
Location	NC Case	Low-Speed	High-Speed
Facemask	2	-	50

The following metrics were used to evaluate PII neck response during head impacts:

- Input metric
    - Resultant impact speed (m/s), v
- Impact metrics
    - Resultant head COG kinematics
        - Linear acceleration (g), a
        - Angular acceleration (rad/s^2), α
        - Angular velocity (rad/s), ω
        - Angular velocity duration (ms), Δt_ω
    - Resultant upper neck kinetics
        - Force (N), F
        - Moment (Nm), M

Before experimental impacts, calibration of the impact region of interest was conducted for the high-speed cameras. Following calibration, the high-speed cameras were required to remain stationary to utilize the transformation matrix determined from the calibration process. High contrast markers were placed on the impacting helmet for consistent 2D pixel coordinate tracking. Post hoc acquisition of 2D pixel coordinates for the calibration and helmet markers, from each camera, was obtained using Phantom Camera Control (PCC) software (Phantom Camera Control 2.6, Vision Research, Wayne NJ). MATLAB software (MathWorks, Natick, MA) was used to implement the DLT method to solve for the 3D spatial coordinates, and then calculate impact speed.

Following impact experiments, the collected Hybrid III data was processed in MATLAB software to apply SAE Standard, J211-1, recommended practice for ATD signals in impact tests [68]. A 4^{th} order low pass Butterworth filter with a 1,650 Hz corner frequency (Channel Class 1000) was applied to head COG linear acceleration and upper neck force signals. Upper neck moment signals were filtered with a 4^{th} order low pass Butterworth filter with a 1,000 Hz corner frequency (Channel Class 600). Angular acceleration of the Hybrid III headform was calculated using the linear acceleration data and equations presented by Padgaonkar [67]. Angular velocity was calculated using angular acceleration and the signal sampling rate. Angular velocity duration was calculated as the time between the signal crossing 10% of the peak before the signal peak, and the most prominent minimum after the signal peak (within 200 ms). Figure 3.12 shows an example of the angular velocity duration calculation. Discrete impact kinetic values were calculated as the upper neck force value at the time of peak head COG linear acceleration, and the upper neck moment value at the time of peak head COG angular acceleration. Figure 3.13 shows an example of how impact force (impact F) and impact moment (impact M) were calculated. Peak values of linear acceleration, angular acceleration, angular velocity, upper neck force, and upper neck moment were determined as the maximum value within a 200 ms time frame.

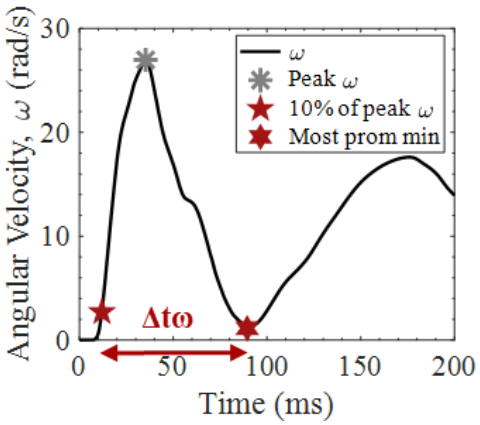

Figure 3.12: Sample plot of angular velocity duration calculation, the time between 10% of peak ω (before the peak) and the most prominent minimum (after the peak).

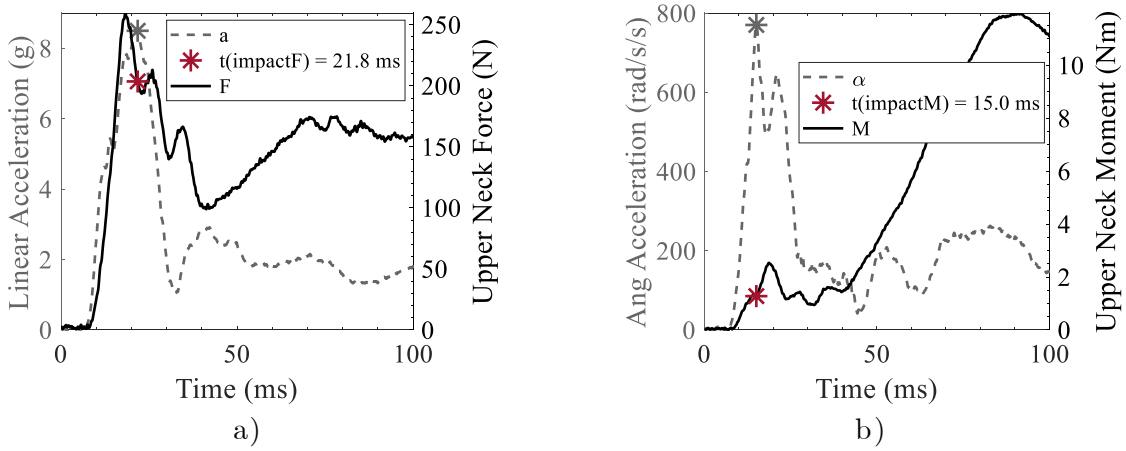

Figure 3.13: Sample plots for determining impact kinetics, where a) impact upper neck force is the value at the time of peak linear acceleration and b) impact upper neck moment is the value at the time of peak angular acceleration

The PII neck response analyses utilized the following time series and discrete values of the impact response metrics listed above:

- Time series metrics: a, α, ω, F, and M
- Discrete value metrics: v, peak a, peak α, peak ω, Δtω, peak F, peak M, impact F, and impact M

Linear acceleration (g = 9.81 m/s^2) is a metric often used in helmet certification standards, which utilize ATD neck models [71]. Studies that also utilize ATDs have shown that

angular kinematics are better predictors of diffuse brain injuries [5], and therefore angular velocity and angular acceleration are included as evaluation metrics. Angular velocity duration indicates the time required for the Hybrid III head to rotate to a maximum range of motion after the impact. Upper neck force and moment data are used in studies that employ ATD head and neck models to assess neck injury [72]. For high-speed facemask impact conditions, the helmet on the headform would interact with the neck base plate after the initial impact time region (but within 200 ms). This interaction between the helmet and plates could result in measures that do not reflect the PII neck performance. While peak head kinematic values occurred during the initial impact time frame (0 – 60 ms), peak upper neck kinetic values under certain conditions occurred after the initial impact time frame and may reflect kinetics during the helmet-plate interaction. Therefore, impact force and moment values were also used to assess neck performance.

3.3 Performance Evaluation Methods

3.3.1 Sample Size

Sample sizes were determined by examining the variance of response metrics from preliminary 3 m/s impact tests with the same experimental methods as outlined in Section 3.2 [73]. The preliminary tests were conducted with a sample size of five repeats. As findings from the preliminary study showed acceptable repeatability of head kinematics and upper neck kinetics [73], a sample size of five was chosen for the low impact speed tests. Based on the minimal difference in response metrics between the two NC cases from the low impact speed tests, a sample size of ten was chosen for the high impact speed tests. For the long-term repeatability analysis, which was conducted last in the sequence of tests, a sample size of 50 was chosen. As the PII neck did not show signs of component deterioration from the previous 90 impacts, 50 consecutive impacts were deemed sufficient to investigate long-term repeatability while managing research time effectively.

3.3.2 Repeatability

Repeatability was assessed by quantifying variability between repeat impacts for all response metrics (listed in Section 3.2.2) and all impact conditions. Percent coefficient of variation (CV), defined as the percent ratio of SD to the mean, as shown in Equation 3.1, was used to quantify metric repeatability. Discrete metric repeatability was categorized as acceptable if CV values were less than 10%, and unacceptable if CV values were greater than 10%, as per ISO 15830-1 standard for ATD performance specifications [11]. Time trace metric repeatability was visually assessed using mean response plots with SD corridors (at each time point, plus and minus one SD) and percent CV plots. Impact speed CV values were also calculated to assess the repeatability of input impact mechanics.

$$CV = \frac{SD}{mean} \times 100\% \tag{3.1}$$

3.3.3 Tunability

The ability to tune impact mechanics during direct head impacts was evaluated using differences in response metrics between the two NC cases. Modifying the cervical cable springs adjusted the passive compression load across the internal structural column, and was hypothesized to adjust the PII neck bending stiffness, and therefore impact behaviour. Independent analyses were conducted for discrete and time series response metrics.

A nonparametric Mann Whitney U-test [74] was used to compare differences in discrete metric medians between the two NC cases ($p < 0.05$) for all impact conditions. A nonparametric test was used because of a small sample size for the low-speed data set. SPSS software (SPSS® Statistics Premium 26, IMB®, Armonk, NY) was used to conduct the statistical analysis.

Impact speed was not considered as a covariate to the impact metrics. Within repeat cases, impact speed varied slightly; however, the range was practically small for injury

assessment applications with a lower and upper bound of 2.03 and 2.46 m/s for the low speed cases, and 5.78 and 6.29 m/s for the high speed cases (presented in Appendix B).

The tunability of time series metrics was evaluated through a visual assessment of NC2 metrics as a function of NC1 metrics at the same time. If the two NC cases resulted in identical responses, the line of y = x would represent the data of NC2 response as a function of NC1 response. However, if the responses differed, the data would deviate from the y = x line. Deviations from the y = x line were referred to as residuals and quantified for all time series samples. Residuals quantified the difference between NC case metrics and indicated the ability to tune impact mechanics; greater residuals indicated greater tunability. Figure 3.14 illustrates the definition of response residuals using example plots. Only one residual measure was used as they are equal and opposite (Equation 3.2). Residuals were plotted with respect to time, along with corresponding time series data, to visually inspect differences between the two NC case impact metrics.

$$r_y = X_{NC2}(i) - X_{NC1}(i) \text{ and } r_x = X_{NC1}(i) - X_{NC2}(i) \tag{3.2}$$

Where, $X \equiv Response\ metric$ and $i \equiv Sample\ number$

$$\therefore r_y = -r_x$$

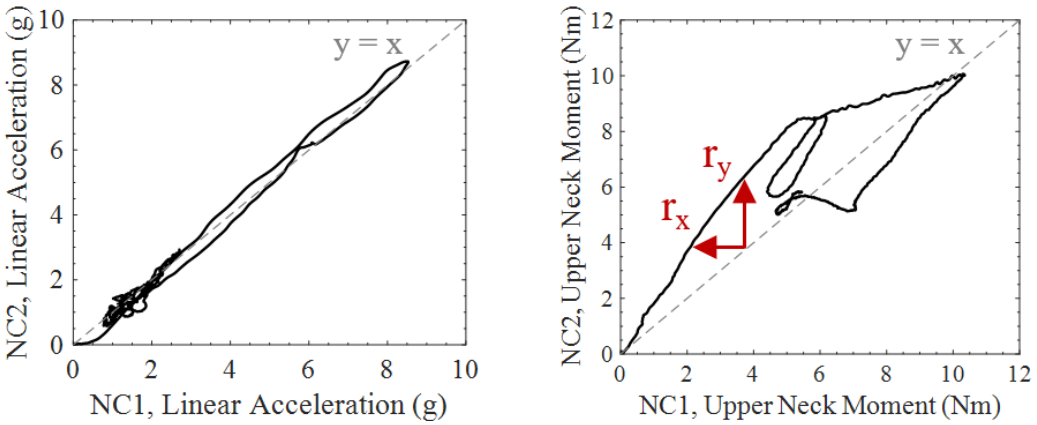

Figure 3.14: Example plots of NC2 v. NC1. (a) Linear acceleration measures are similar and approximately follow y = x. (b) Upper neck moment measures deviate from y = x and deviations are quantified by response residuals (r_y and r_x).

3.3.4 Durability – Long-Term Repeatability

Long-term repeatability refers to the consistency of mechanics over numerous impacts. Long-term repeatability was assessed for all response metrics obtained from the following experimental conditions: 6 m/s impact speed, facemask impact location, NC2 (163 N), and 50 repeats. Facemask and NC2 conditions were used because it was hypothesized to generate the most mechanically demanding impact; facemask impacts produce multidirectional loading and a high compression force case (NC2) produced the least compliant neck response. An analysis was conducted for both discrete and time series mechanics.

Long-term repeatability of discrete response metrics was investigated by characterizing the relationship between the impact metric and experimental repeat number. Discrete metrics were plotted against impact repeat number, and the slope significance of a fit linear regression line was determined ($p < 0.05$). The statistical analysis was conducted in SPSS software (SPSS® Statistics Premium 26, IMB®, Armonk, NY). A statistically significant slope indicated systematically increasing or decreasing mechanics with respect to impact repeat number, and therefore poor long-term repeatability. A statistically insignificant slope indicated consistent mechanics and acceptable long-term repeatability.

Long-term repeatability of time series mechanics was investigated to supplement the discrete metric evaluation through an exploratory clustering analysis. Clustering techniques group large data sets based on a similarity metric to identify the most characteristic patterns within a dataset. This analysis used hierarchical clustering ($k = 2$ clusters) with Ward's method to calculate the distance between all data subgroups using the Euclidean distance as a metric. Ward's method assesses distance between two data sets based on the increase in the total sum of squares (or variance) for the merged cluster [75]. In this analysis, the 50-time series response metrics were clustered based on the least variance increase. A dendrogram (tree diagram) was used to show clustering relationships

between the 50 data sets. The assigned cluster number was plotted against impact repeat number to investigate patterns in time series response over the 50 repeats. MATLAB software was used to conduct the cluster analysis.

Post hoc high-speed video was used to visually investigate the PII neck response differences between the first, twenty-fifth, and fiftieth impacts as a measure of long-term repeatability. Using PCC software, the moment of impact was manually chosen for each repeat and still images were taken at time points throughout the impact.

3.3.5 Durability – Inspection of Mechanical Component Durability

After all impact experiments for this thesis, final qualitative inspections of the PII neck were conducted. No evidence of component damage indicated acceptable durability, and any components which showed signs of structural damage or failed outright indicated unacceptable durability. Inspections included a visual assessment of the exterior parts and imaging using Cone Beam Computed Tomography (CBCT) scans (i-CAT 17-19, CBVT and Panoramic Dental Imaging System, Imaging Sciences International, Brea CA, 5 mA current, 120 kV voltage, 12.5 x 16 cm field of view, and 0.25 Vov.). Imaging software (Avizo 2019.4, ThermoFisher Scientific, Waltham MA) was used to process the CBCT scans.

3.3.6 Biofidelity – Comparison of PII Neck to Volunteer Response

The PII neck biofidelity was assessed by comparing impact mechanics to published volunteer data obtained by Reynier et al. [54]. Reynier et al. performed a non-injurious head impact study with human volunteers at three neck-muscle activation cases: passive (least activated), co-contracted, and unilateral (most activated) [54]. The volunteer study [54] was recreated with the PII neck and the Hybrid III headform to obtain and compare head kinematics. The comparison provided a preliminary validation of the PII neck and identified response limitations to direct future design refinements.

3.3.6.1 Volunteer Comparison – Experimental Methods

The experimental methods were similar to those detailed in Section 3.2, including equipment, instrumentation and data collection and processing methods. Aspects that differed to match the volunteer study methods [54] are outlined below.

The pendulum impactor, the ISO headform encased in foam padding, was manually raised and released to achieve an impact speed of 2 m/s. The Hybrid III headform, fixed to the PII neck, was positioned to achieve impacts to the side of the head. Layers of foam padding, encased in fabric and secured to the Hybrid III headform, cushioned the impact. The PII neck, fixed to a rigid support (see Section 3.2 low-speed experimental equipment), was subject to five impact repeats for each NC case.

Response comparison analyses used peak and time series values of the following metrics:

- Resultant linear acceleration (g), a_R
- X-angular acceleration (rad/s^2), α_x
- X-angular velocity (rad/s), ω_x
- X-angular velocity duration (ms), $\Delta t_{\omega x}$

Kinematic coordinates followed SAE Standard, J211-1 [68] (Figure 3.8). The time between the signal crossing 10% of the maximum before and after the peak defined discrete x-angular velocity duration. Due to laboratory space restrictions, impacts were conducted to the opposite side of the head compared to the volunteer study, resulting in x-angular kinematic measures with opposite signs. The comparison analyses therefore used volunteer x-angular kinematics with a reversed sign.

Discrete comparison methods used mean and SD values of volunteer peak head kinematics [54]. Mean time series head kinematic curves were digitized from published figures [54] and used to calculate volunteer x-angular velocity durations. Time series responses were synchronized by aligning the time of volunteer and PII neck conditions from a 1 g resultant

linear acceleration value. Time series comparison methods used the synchronized kinematic curves. Comparison methods evaluated both PII NC case responses against the three volunteer neck muscle activation cases.

3.3.6.2 Volunteer Comparison – Performance Evaluation Methods

An independent sample, two-tailed t-test for equal means ($p < 0.05$) was used to determine the statistical significance between the PII neck and volunteer peak head kinematic measures. Statistical significance between x-angular velocity duration was not calculated because volunteer x-angular velocity durations were manually calculated from digitized time series plots and had unknown SDs.

Time series response kinematics were compared with an objective rating obtained by using CORrelation and Analysis (CORAplus) software [76]. The CORAplus rating system was developed to compare two complete curves for surrogate model assessment in injury biomechanics research. CORAplus evaluates curve similarity using two independent sub-methods, a corridor and a cross-correlation rating [77]. The corridor method evaluates how well a response curve fits into defined corridors around the reference curve [77]. The cross-correlation method evaluates the response curve compared to the reference curve based on the phase shift, shape, and area [77]. Defined algorithms calculate each rating on a score between 0 (no curve correlation) and 1 (perfect match) [77]. An overall CORAplus rating was determined, from an equal-weighted sum of the three kinematic curve ratings, to evaluate both PII NC case responses against each volunteer muscle-activation condition (reference curve). Default CORAplus settings were used, as suggested by Thunert [76], except for manually defining the evaluation intervals as [5, 30] ms for resultant linear acceleration, [10, 50] ms for x-angular acceleration, and [15, 80] ms for x-angular velocity.

4 Results

This chapter presents results from the assessments of the PII neck biomechanics during head impact experiments. Initial experimental observations are presented, followed by results on repeatability, tunability, durability, and biofidelity of metrics.

4.1 Experimental Observations

For all experimental conditions, the PII neck appeared to experience a similar gross response to head impacts across NC cases.

Figure 4.1 and Figure 4.2 display high-speed images of the head impact response at five-time points for low and high speed impacts, respectively. Each figure contains a series of example images for the three impact locations and two NC cases. The first image of every impact series displays the moment of impact (0 ms time). There was a distinct response difference between NC1 and NC2 for the high-speed back impacts (Figure 4.2 c and d). Between 50 and 100 ms, the NC2 silicone flange shifted out of the clamping plates on the posterior section (Figure 4.2 d), and this was observed for nine of the ten NC2 repeats. No apparent differences were observed between NC cases for the other impact conditions.

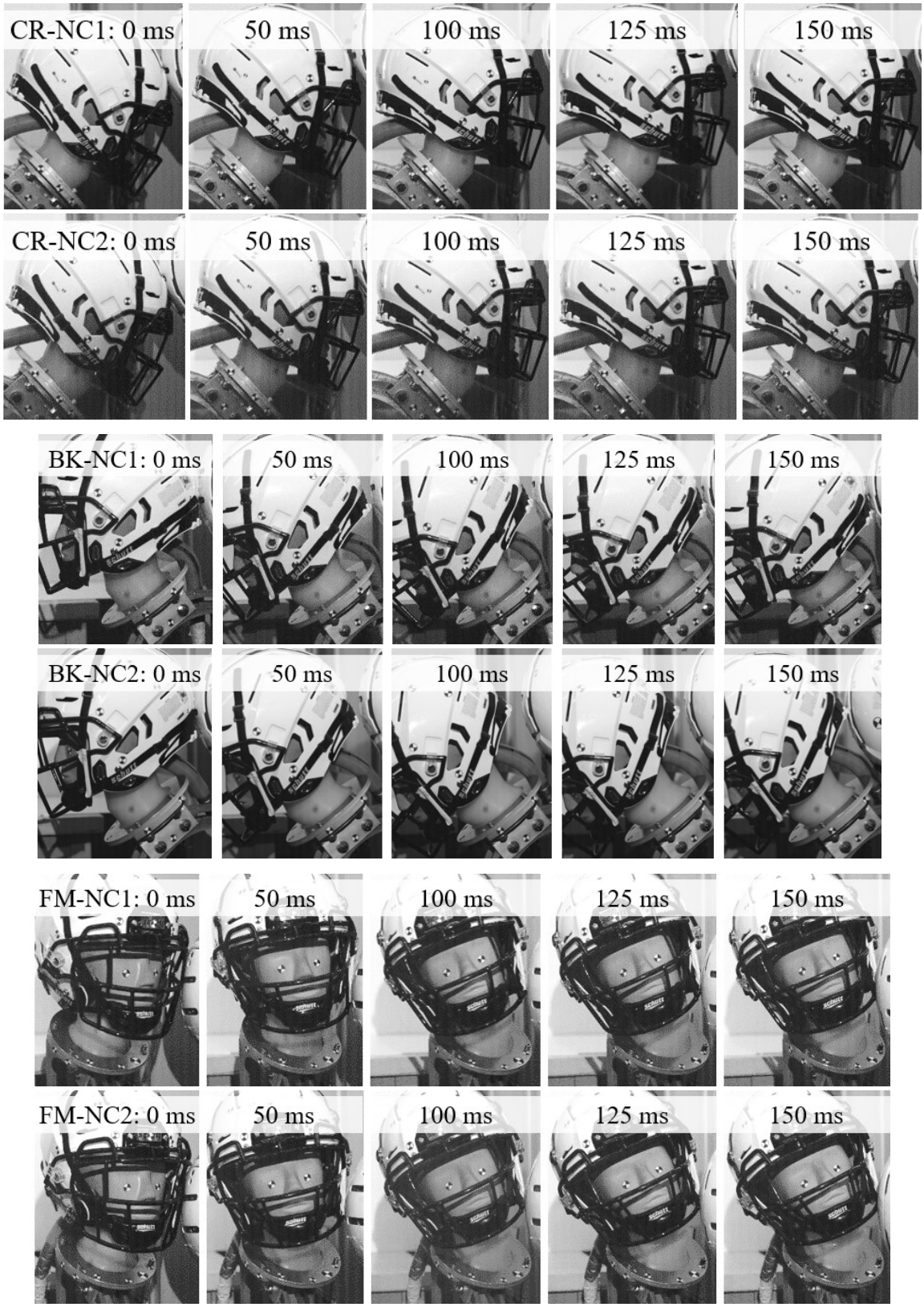

Figure 4.1: Example impact images of PII neck response from low-speed cases: a) CR-NC1, b) CR-NC2, c) BK-NC1, d) BK-NC2, e) FM-NC1, and f) FM-NC2

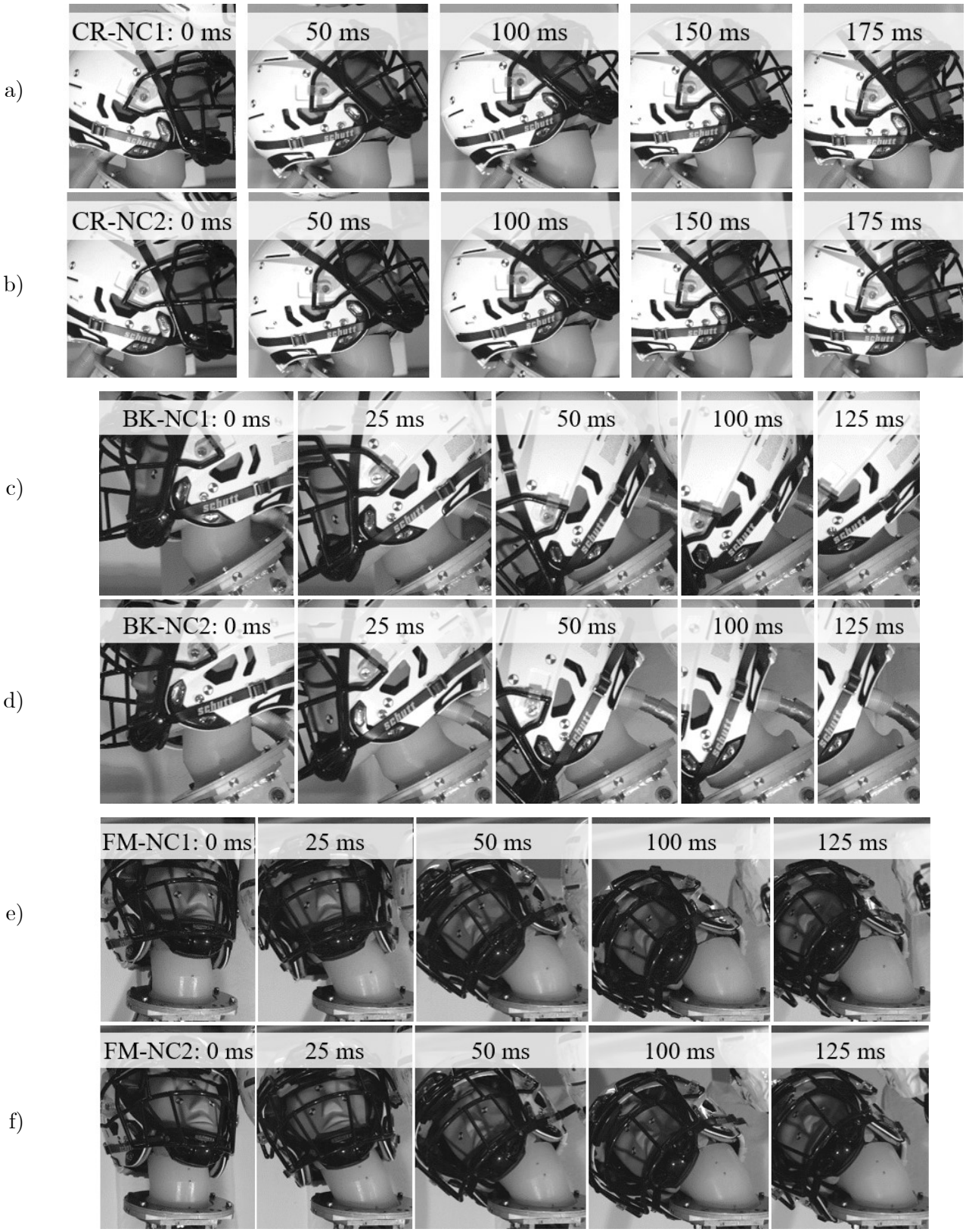

Figure 4.2: Example impact images of PII neck response from high-speed cases: a) CR-NC1, b) CR-NC2, c) BK-NC1, d) BK-NC2, e) FM-NC1, and f) FM-NC2

4.2 Repeatability

The variance of impact mechanics between repeats was investigated to determine PII neck repeatability. Overall, head kinematics exhibited excellent repeatability, and in the small number of cases where repeatability was poor, the variances noted were still within ranges customary of biomechanical testing with ATDs.

4.2.1 Repeatability of Discrete Impact Metrics

From experimental repeats, the mean and SD values of the discrete impact metrics (Table 4.1) were used to calculate percent CVs, illustrated in Figure 4.3. CVs less than 10% indicated acceptable repeatability measures [11]. The case values of percent CVs were summarized in Appendix A. Overall, the results indicated highly repeatable discrete head kinematics and less repeatable discrete upper neck kinetics.

From the 12 experimental conditions, all impact speed CV values were less than 4%, with ten less than 2%.

For low-speed conditions, most CV values were within the acceptability limit (37/48 CVs $< 10\%$). Between low-speed impact locations, back impacts produced the highest number of acceptable CVs (15/16 CVs $< 10\%$). High-speed impacts produced more unacceptable CV values (23/48 CVs $> 10\%$). Between high-speed impact locations, crown impacts produced the highest number of acceptable CVs (10/16 CVs $< 10\%$) and facemask conditions produced the highest number of unacceptable CVs (10/16 CVs $> 10\%$). From all experimental conditions, NC2 produced a higher number of acceptable CVs, compared to NC1. Between all experimental conditions, peak angular velocity and angular velocity duration produced the highest number of acceptable CVs (11/12 case CVs $< 10\%$) and impact moment produced the highest number of unacceptable CVs (11/12 case CVs $> 10\%$).

Table 4.1: Mean and standard deviation (SD) values of discrete input metrics and response impact metrics from case repeats for all experimental impact conditions.

			v (m/s)	Peak a (g)	Peak α (rad/s^2)	Peak ω (rad/s)	Δt_ω (ms)	Peak F (N)	Peak M (Nm)	Impact F (N)	Impact M (Nm)
		*NC	*mean ± SD*	*mean ± SD*	*mean ± SD*	*mean ± SD*	*mean ± SD*	*mean ± SD*	*mean ± SD*	*mean ± SD*	*mean ± SD*
Low speed, n=5	CR	1	2.12 ± 0.04	10.5 ± 1.2	395.5 ± 53.8	5.0 ± 0.9	128.8 ± 3.3	438.9 ± 20.8	9.5 ± 0.9	156.1 ± 78.3	4.9 ± 1.2
		2	2.06 ± 0.02	11.2 ± 0.1	366.1 ± 21.8	4.2 ± 0.4	127.1 ± 2.8	484.5 ± 8.9	9.6 ± 0.2	140.0 ± 9.5	3.9 ± 1.7
	BK	1	2.28 ± 0.03	8.7 ± 0.3	788.3 ± 25.3	8.9 ± 0.2	86.2 ± 1.4	268.2 ± 5.9	12.3 ± 0.2	195.9 ± 8.3	1.8 ± 0.3
		2	2.28 ± 0.03	8.3 ± 0.3	810.6 ± 19.9	9.2 ± 0.2	108.3 ± 3.0	335.4 ± 28.0	11.9 ± 0.5	157.7 ± 6.3	0.64 ± 0.03
	FM	1	2.35 ± 0.04	8.6 ± 0.6	784.7 ± 73.1	8.6 ± 0.7	164.7 ± 12.5	166.7 ± 8.7	10.8 ± 1.3	50.5 ± 4.3	1.1 ± 0.6
		2	2.36 ± 0.08	8.8 ± 0.7	792.4 ± 111.9	8.3 ± 0.5	157.4 ± 11.4	160.4 ± 8.3	10.1 ± 0.7	50.8 ± 4.9	1.8 ± 0.4
High speed, n=10	CR	1	6.03 ± 0.12	31.9 ± 2.7	2051.1 ± 361.6	17.6 ± 0.6	97.0 ± 4.6	943.8 ± 34.8	19.1 ± 7.7	435.6 ± 57.5	9.6 ± 8.9
		2	6.07 ± 0.12	29.5 ± 3.1	2264.5 ± 148.1	17.2 ± 1.2	96.6 ± 0.6	978.1 ± 36.2	15.2 ± 0.8	427.6 ± 31.5	6.7 ± 1.1
	BK	1	6.07 ± 0.08	36.2 ± 1.4	2606.3 ± 314.1	27.4 ± 1.0	70.1 ± 10.6	616.1 ± 118.8	17.8 ± 1.0	483.4 ± 182.5	11.1 ± 1.8
		2	6.13 ± 0.09	36.7 ± 1.8	2286.0 ± 173.9	27.0 ± 0.7	77.5 ± 3.7	797.5 ± 93.1	17.3 ± 0.4	298.2 ± 16.3	8.5 ± 2.2
	FM	1	6.01 ± 0.14	35.0 ± 3.7	3307.9 ± 338.5	21.7 ± 1.4	55.2 ± 2.3	754.4 ± 69.4	28.3 ± 3.3	170.9 ± 33.3	4.7 ± 1.2
		2	5.99 ± 0.10	32.8 ± 4.2	3064.9 ± 341.1	22.7 ± 1.3	56.8 ± 2.4	674.4 ± 81.4	24.2 ± 1.7	172.8 ± 41.2	4.9 ± 1.1

**NC forces: $F_{NC1} = 63$ N, $F_{NC2} = 163$ N*

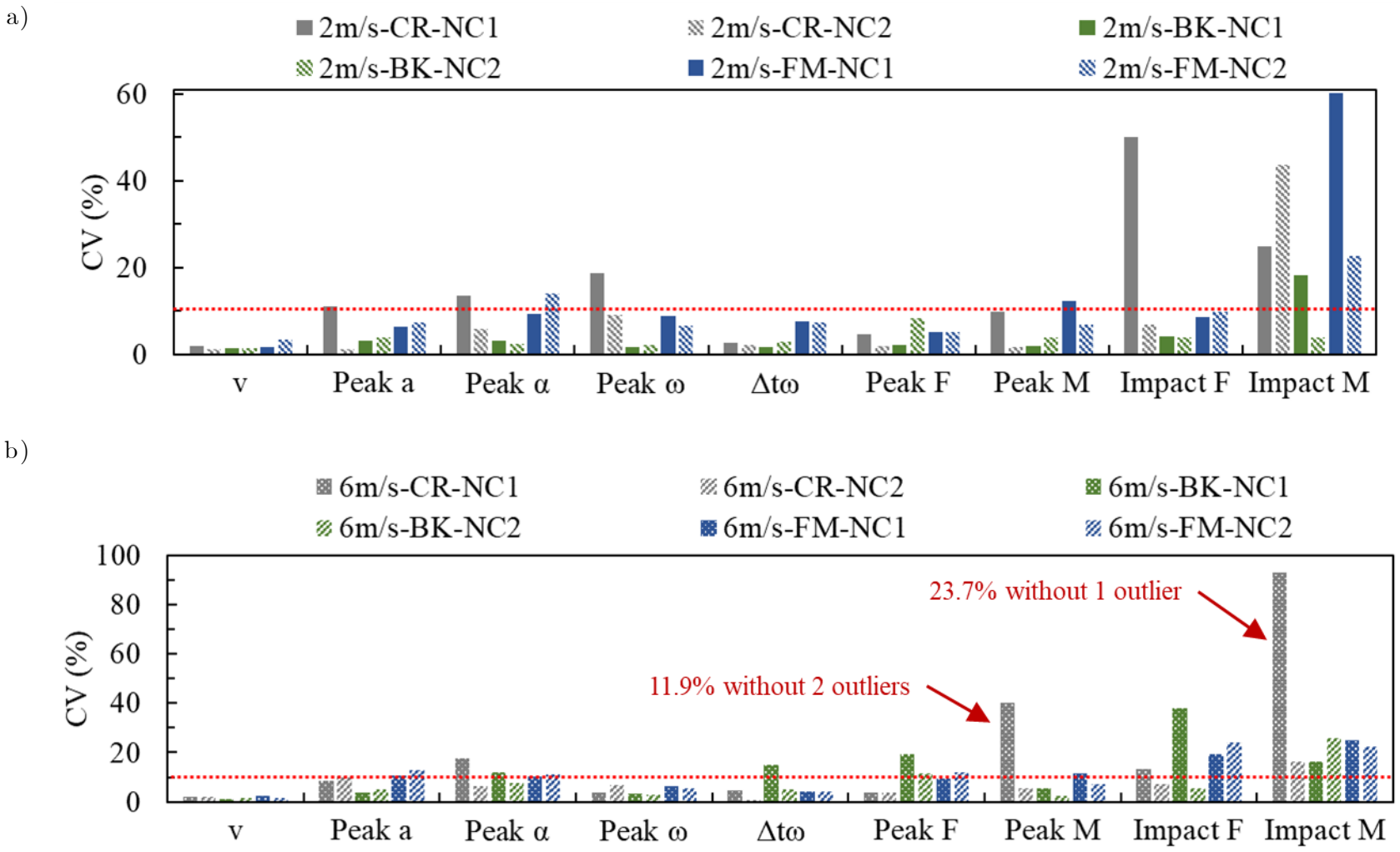

Figure 4.3: Percent CV values of discrete input metrics and impact metrics from case repeats for a) low and b) high-speed conditions. Horizontal dotted lines indicate a 10% acceptable and unacceptable border [11].

4.2.2 Repeatability of Time Series Impact Metrics

Standard deviation corridors about the mean and percent CV values were used to assess time series repeatability visually. Figure 4.4, Figure 4.5, and Figure 4.6 present crown, back, and facemask ensemble averages, respectively. Results were presented (by column) for head linear acceleration, head angular velocity, and upper neck moment for both NC cases obtained from low and high-speeds conditions (presented by row). Angular velocity plots included averaged duration markers with SD error bars. Percent CVs of the time series impact metrics are presented in Figure 4.7 for head linear acceleration, head angular velocity and upper neck moment (presented by column) for both NC cases obtain from the different impact conditions (presented by row). Plots of ensemble averages and percent CVs for head angular acceleration and upper neck force were presented in Appendix A. Overall, the results indicated adequate repeatability of time series metrics.

Low-speed impact metric curves displayed more narrow corridors and smaller CVs than those of high-speed impacts. Head kinematic measures produced more narrow corridors compared to upper neck kinetic curves, but there was no distinct pattern for time series CVs. For all impact conditions, linear accelerations produced the narrowest corridors, while linear and angular accelerations displayed the largest CVs. While facemask conditions produced the widest corridors compared to crown and back conditions, CVs were not more substantial. Between NC cases, NC2 displayed more narrow corridors and smaller CVs. For all case metrics, corridors were most narrow during the initial impact time range and wider later in the time series, while CVs displayed no time dependent pattern. Large CVs between 0 and 10 ms resulted from nearly zero values and were not considered for assessing repeatability.

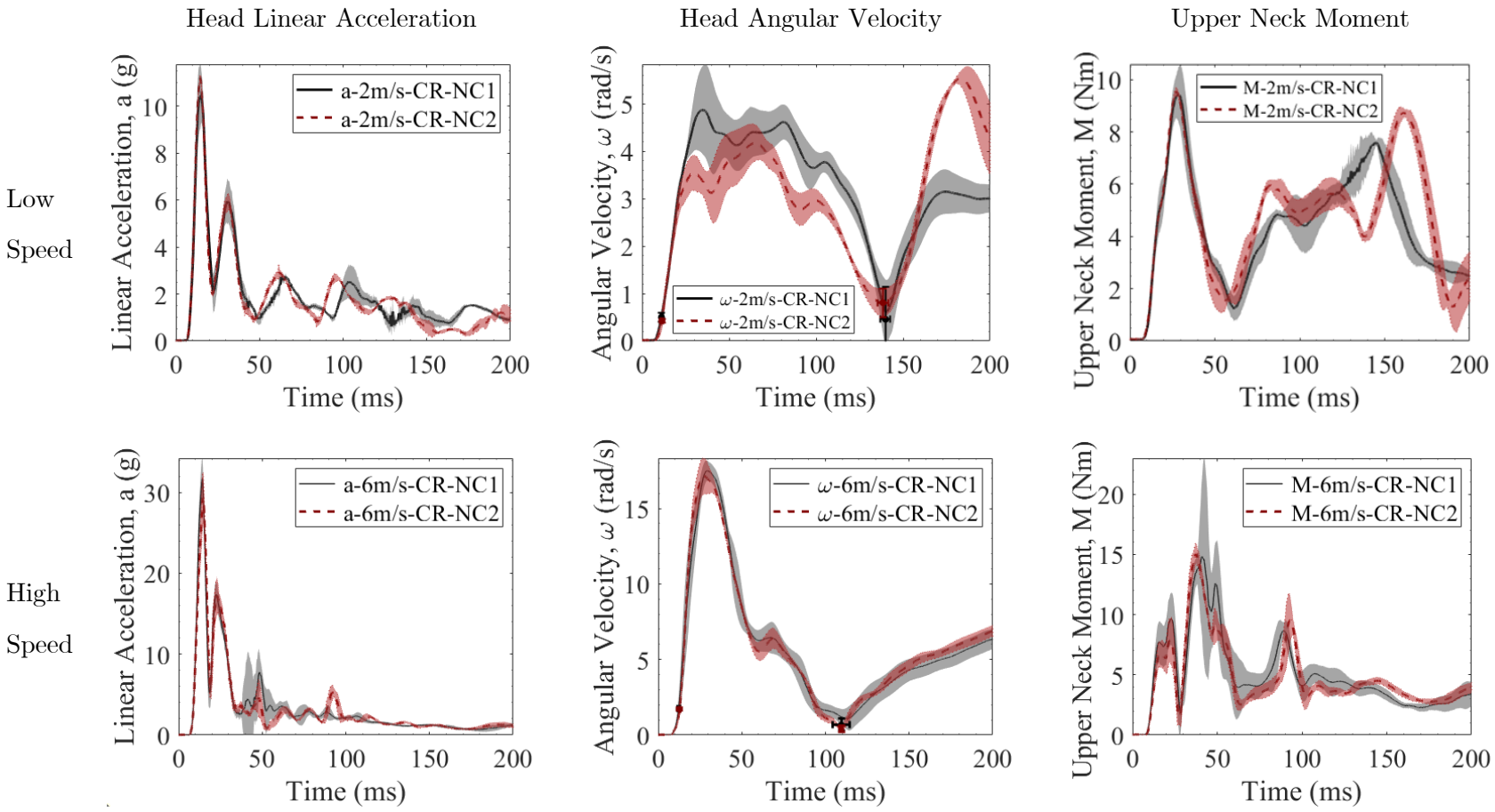

Figure 4.4: Crown impact with two NC case ensemble averages of linear acceleration, angular velocity, and upper neck moment (columns) from low and high speed (rows). Solid lines represent case repeat averages and shaded regions represent ± one SD. Angular velocity plots include duration markers with SD error bars.

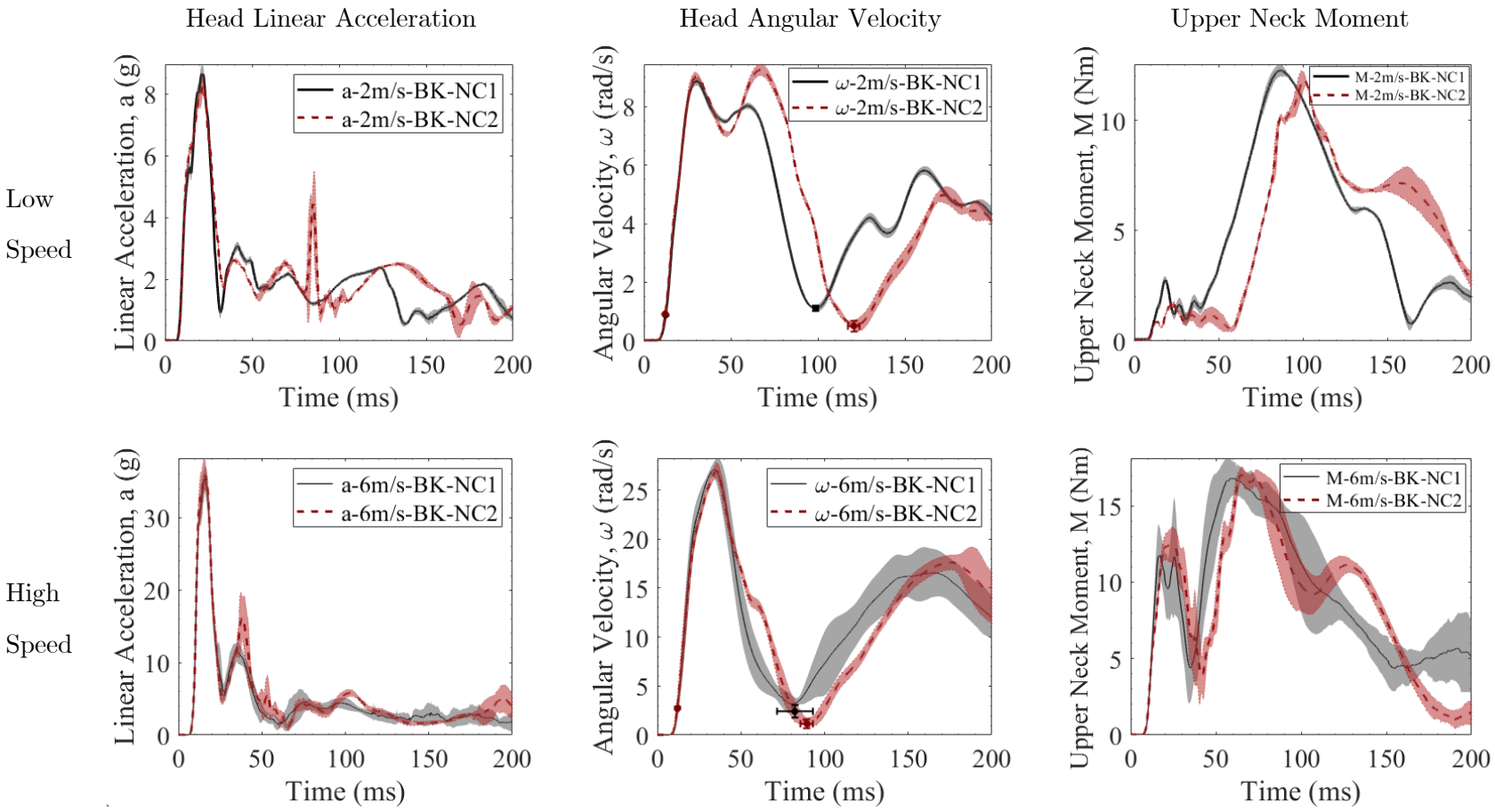

Figure 4.5: Back impact with two NC case ensemble averages of linear acceleration, angular velocity, and upper neck moment (columns) from low and high-speeds (rows). Solid lines represent case repeat averages and shaded regions represent ± one SD. Angular velocity plots include duration markers with SD error bars.

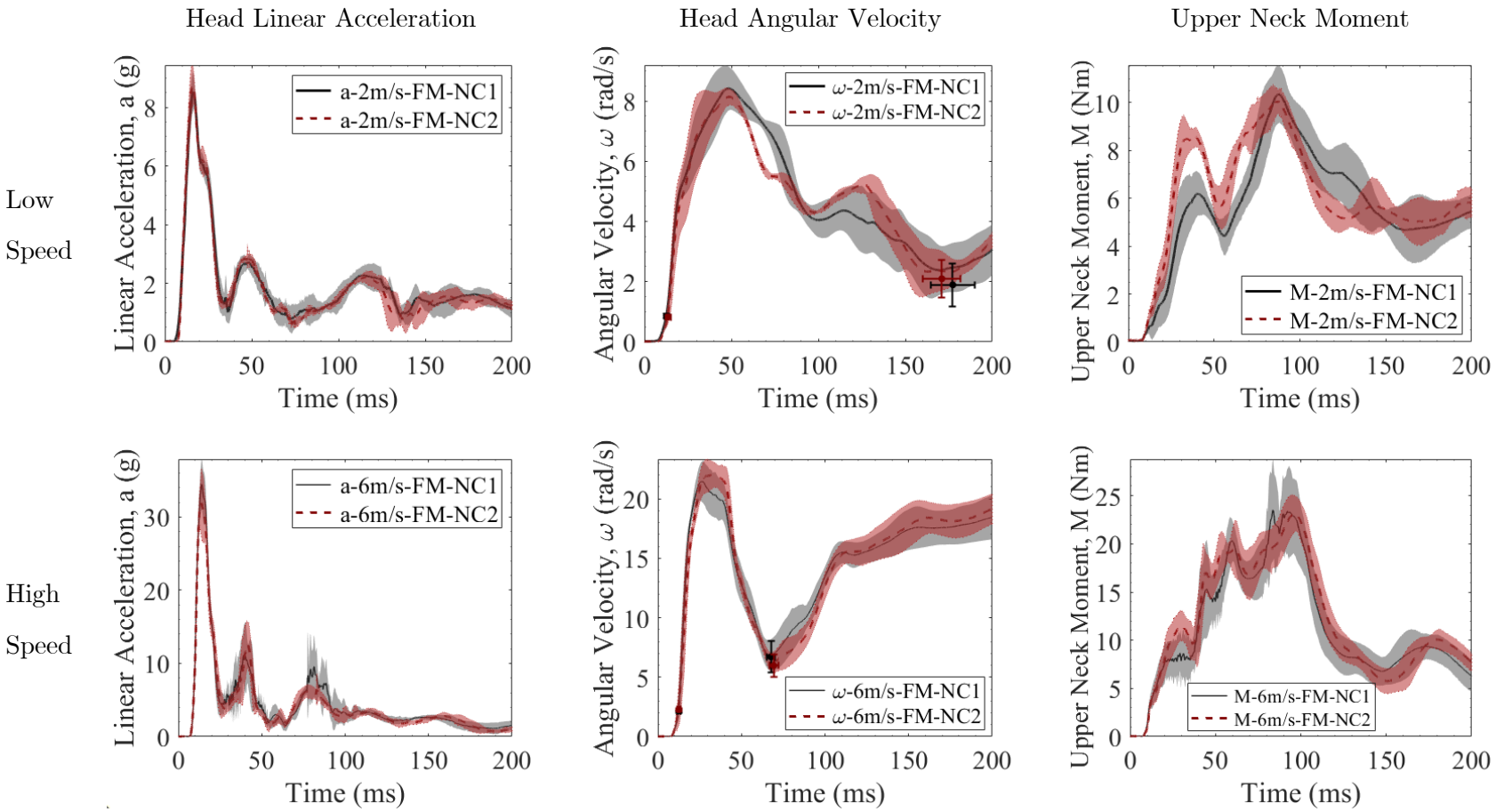

Figure 4.6: Facemask impact with two NC case ensemble averages of linear acceleration, angular velocity, and upper neck moment (columns) from low and high-speeds (rows). Solid lines represent case repeat averages and shaded regions represent ± one SD. Angular velocity plots include duration markers with SD error bars.

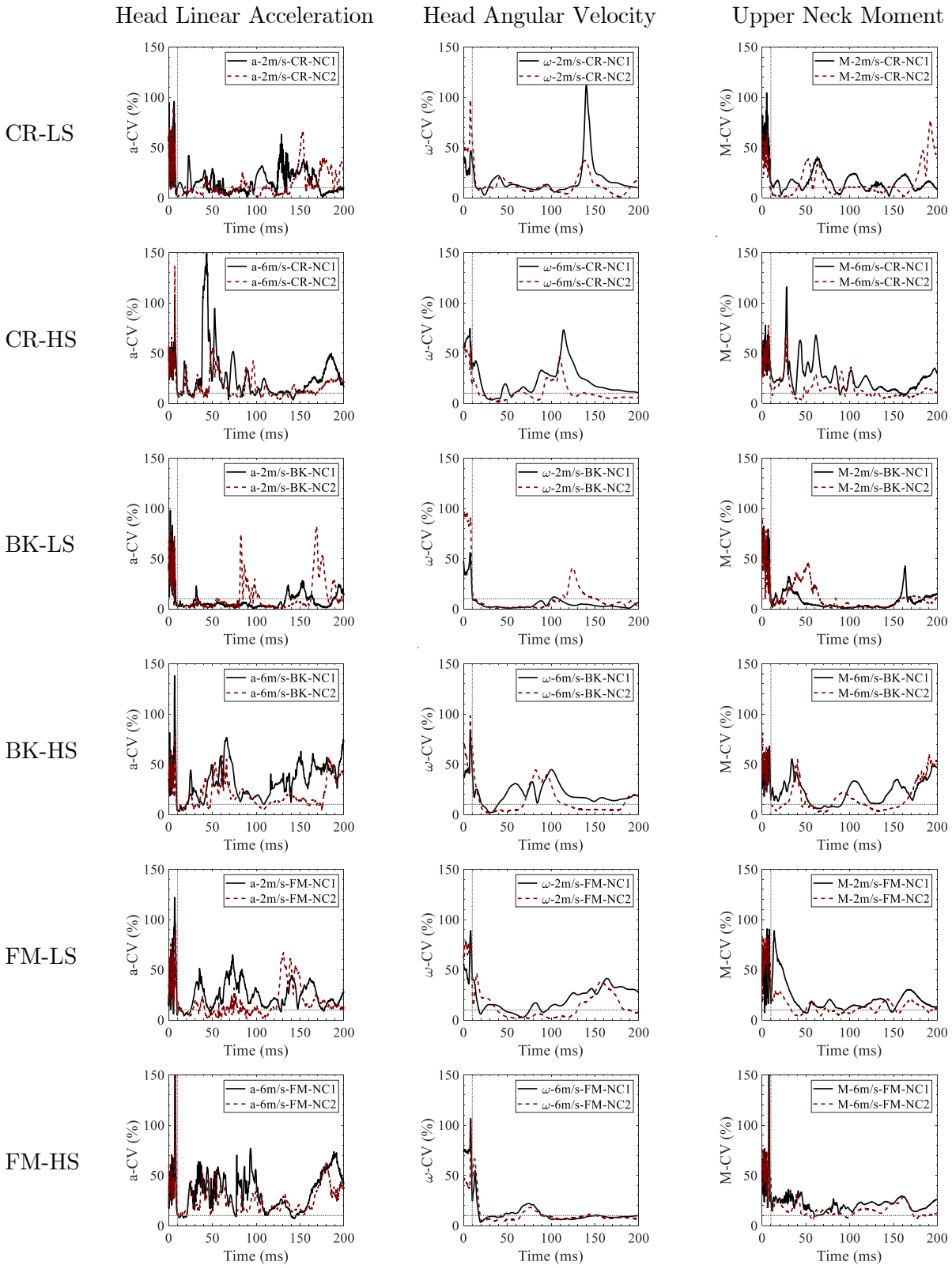

Figure 4.7: Percent CVs for each NC case linear acceleration, angular velocity, and upper neck moment from all impact conditions (low - LS and high speed - HS).

4.3 Tunability

Differences between NC case impact metrics were investigated to determine PII neck tunability. Overall, head kinematics and upper neck kinetics demonstrated excellent tunability from back impacts and promising potential for tunability for crown and facemask locations.

4.3.1 Tunability of Discrete Impact Metrics

For each impact condition, differences between discrete impact metrics were evaluated using a nonparametric Mann Whitney U-test ($p < 0.05$). Table 4.2 summarizes the median values of each metric and indicates the significantly different NC case pairs. Plots of case medians with individual repeats for impact speed and discrete impact metrics are shown in Appendix B.

Table 4.2: Median values of discrete impact metrics from case repeats.

		*NC	v (m/s) *median*	Peak a (g) *median*	Peak α (rad/s²) *median*	Peak ω (rad/s) *median*	Δt_ω (ms) *median*	Peak F (N) *median*	Peak M (Nm) *median*	Impact F (N) *median*	Impact M (Nm) *median*
Low speed n=5	CR	1	2.1	10.8	374.8	4.5	129.6	445.2	9.7	121.0	4.8
		2	2.1	11.2	363.5	4.2	126.0	481.9	9.5	139.7	5.1
	BK	1	2.3	8.5	792.1	8.8	86.3	268.8	12.3	194.3	2.0
		2	2.3	8.3	807.4	9.3	108.1	332.4	11.7	157.8	0.6
	FM	1	2.3	8.6	802.8	8.3	165.8	170.4	11.1	49.1	0.7
		2	2.3	8.8	759.3	8.1	163.4	157.1	10.0	48.1	1.7
High speed n=10	CR	1	6.0	32.6	2105.0	17.6	97.5	943.2	16.1	411.1	6.3
		2	6.1	29.6	2287.6	17.0	96.4	973.1	15.1	429.4	6.9
	BK	1	6.1	36.4	2576.6	27.4	67.1	561.5	17.6	453.2	10.7
		2	6.1	36.5	2339.1	26.9	77.1	816.8	17.5	296.5	8.6
	FM	1	6.0	35.8	3315.3	22.1	55.0	725.0	28.1	174.2	4.3
		2	6.0	31.1	3083.7	22.8	56.7	678.7	24.2	174.7	4.9

**NC forces: $F_{NC1} = 63$ N, $F_{NC2} = 163$ N*
Shaded cells indicate a significant difference ($p < 0.05$) for NC1 results compared to the respective NC2 results (Mann-Whitney U test).

Statistically significant differences between NC1 and NC2 impact metrics were observed from low and high-speed back impacts for angular velocity duration, peak upper neck force, and impact upper neck force and moment. One metric during low-speed crown impacts and two metrics during high-speed facemask impacts were different between NC cases; however, no low-speed facemask nor high-speed crown cases produced statistically different case medians. For all conditions, no differences between median NC case peak linear acceleration values were observed, while peak upper neck force produced the highest number of NC case differences.

4.3.2 Tunability of Time Series Impact Metrics

Time series differences between NC case metrics were visually investigated for time-dependent patterns of residuals plotted respect to time. The time series residual plots included two vertical lines, which indicated times of initial linear acceleration pulse peak and pulse minimum. The initial impact time region refers to the time before the linear acceleration pulse minimum. Residuals were small during the initial impact time region and were more substantial with increasing time. This behaviour was most evident from back impact (Figure 4.8) head angular velocity and upper neck moments. Low-speed crown and facemask angular velocity residuals were, again, small within the initial impact region and larger with increasing time (Appendix B). This residual pattern was more evident in low-speed impact metrics compared to high-speed, and most evident for angular velocity metrics.

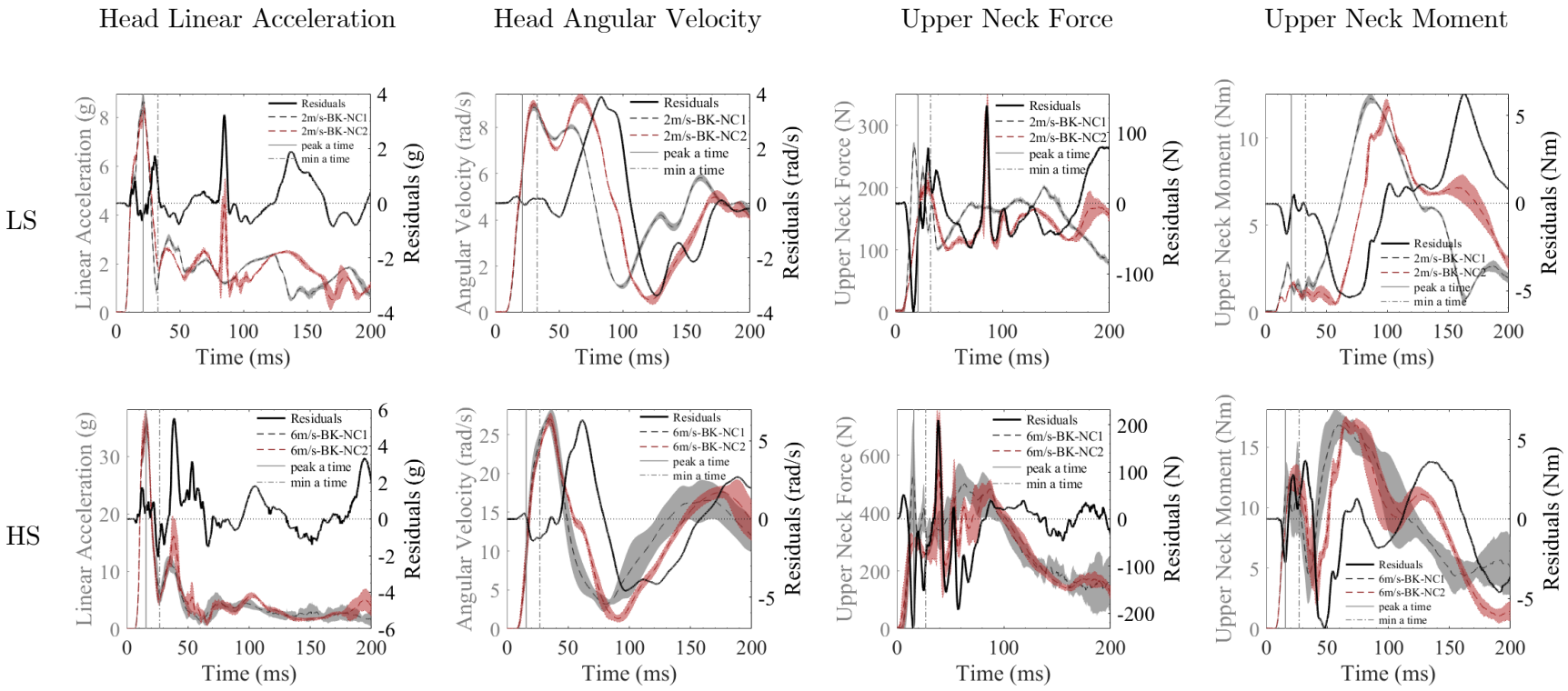

Figure 4.8: Time series response residuals between NC cases and NC case responses for linear acceleration, angular velocity, upper neck force, and upper neck moment from low (LS) and high-speed (HS) back impacts.

4.4 Durability – Long-Term Repeatability

Consistency of impact metrics was investigated from 50 consecutive facemask impacts in NC2 as a measure of long-term repeatability. Overall, excellent long-term repeatability was exhibited by head kinematics during the entire sampled time and upper neck kinetics during the first 60 ms after impact.

4.4.1 Durability of Discrete Impact Metrics

A linear regression model was used to determine the slope and slope significance ($p < 0.05$) of discrete metrics plotted against impact repeat number (Figure 4.9). Table 4.3 summarized slope results from the linear regression fit. Impact velocity plotted against impact repeat number is shown in Appendix C.

Table 4.3: Slope coefficient and slope p-value from the linear regression model of discrete metrics against impact repeat number.

High Speed (6 m/s), Facemask Impact, NC2 (163 N), n = 50									
	v (m/s)	Peak a (g)	Peak α (rad/s^2)	Peak ω (rad/s)	Δt_ω (ms)	Peak F (N)	Peak M (Nm)	Impact F (N)	Impact M (Nm)
slope	0.002	0.042	6.970	-0.001	0.078	2.894	0.271	-0.251	0.011
p-value	0.023	0.241	0.032	0.969	0.181	0.000	0.000	0.453	0.655

P-values of 0.000 reflect a significance level lower than the shown level of precision, not zero. Shaded cells indicate a slope significance of $p < 0.05$.

Although input speed systematically increased, determined from a statistically significant slope, speed did not likely affect the output mechanics as the variability and range were minimal for injury assessment applications, with a 1.6% CV and a minimum and maximum of 5.84 and 6.28 m/s. The majority of head kinematic slope coefficients were not statistically significant, which indicated consistent measures (Figure 4.9 a-d). The peak force and moment systematically increased, which was indicated by significant slope coefficients (Figure 4.9 e and f). Impact force and moment slope coefficients were not significant, which indicated consistent measures (Figure 4.9 g and h).

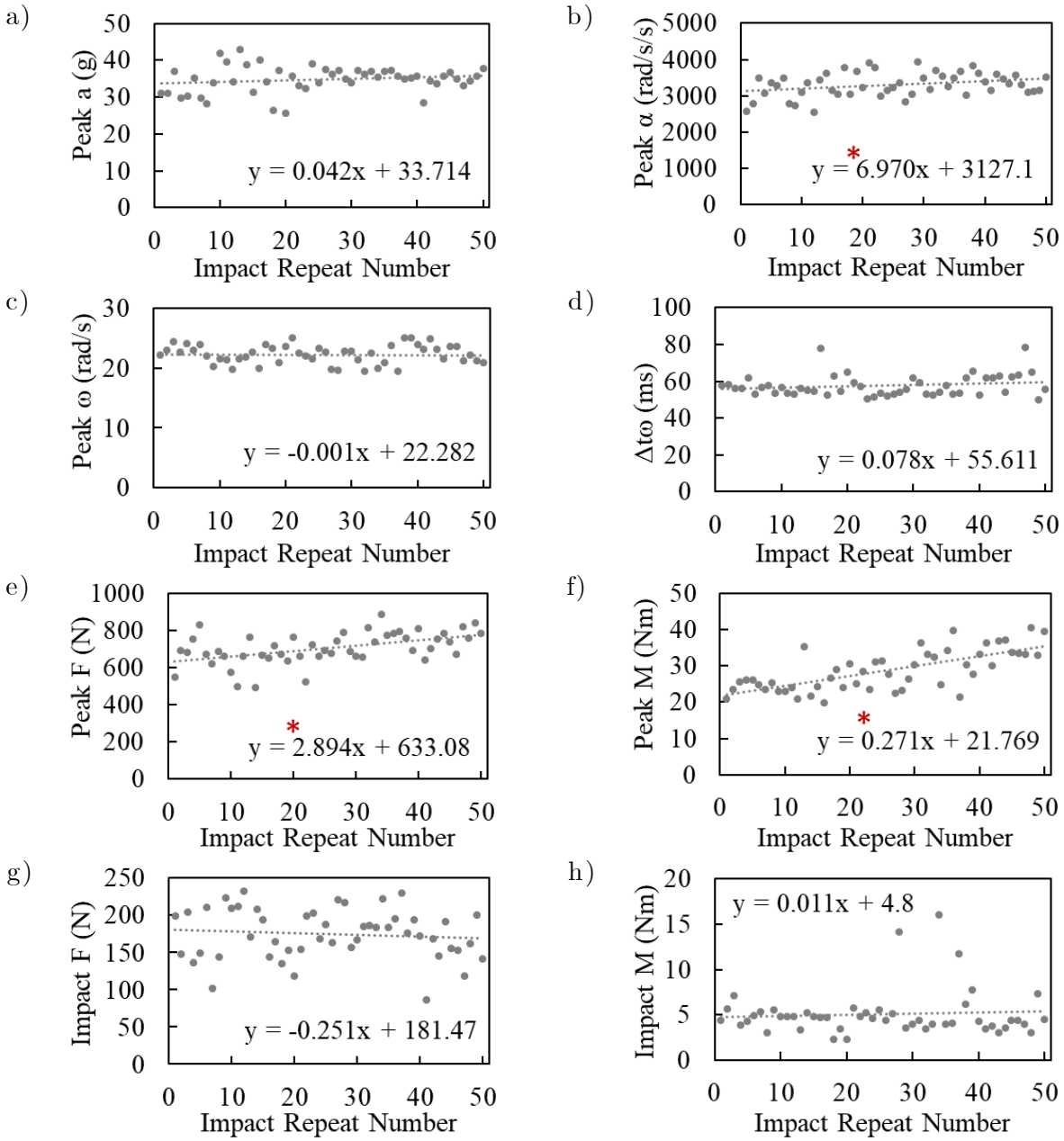

Figure 4.9: Discrete metrics against impact repeat number with the equation of the linear regression line, for a-d) head kinematics and e-h) upper neck kinetics. An asterisk indicates a slope significance with $p < 0.05$.

To determine if impact metric consistency was affected by increasing speed values, another slope significance analysis was conducted with transformed data. Discrete metrics were divided by the corresponding impact speed (transformed data) to reduce the effects of increasing speed values. The transformed data slope coefficient results were consistent

with the original data except for the transformed peak angular acceleration, which exhibited an insignificant slope (results are shown in Appendix C).

4.4.2 Durability of Time Series Impact Metrics

Time series mechanics were subject to a hierarchical clustering analysis (k = 2 clusters) using the Wards method [75] to calculate the distance between data subgroups through a Euclidean distance metric. Separate cluster analyses were conducted for different time ranges to investigate metric consistency during the initial impact time region (0 – 60 ms) without measures from the helmet-plate interaction and entire sampled time (0 – 200 ms).

Clustered time series upper neck kinetics are shown in Figure 4.10 and head kinematics are shown in Figure 4.11. These figures also delineate the makeup of each cluster in terms of impact repeat number. Dendrograms are shown in Appendix C.

Based on the cluster analysis from 0 – 200 ms (Figure 4.10 a and b), upper neck force and moment time series responses appeared to shift with increasing impact repeat number. However, the notable cluster differences occurred after the initial impact time region (0 – 60 ms) and may have represented measures during the helmet-plate interaction. Based on the cluster analysis from the initial impact time region (0 – 60 ms), the upper neck force and moment did not present an apparent pattern for cluster number against impact repeat number (Figure 4.10 c and d). The non-systematic cluster assignment indicated consistent time series upper neck kinetics during the initial impact time region and confirmed the discrete analysis trends.

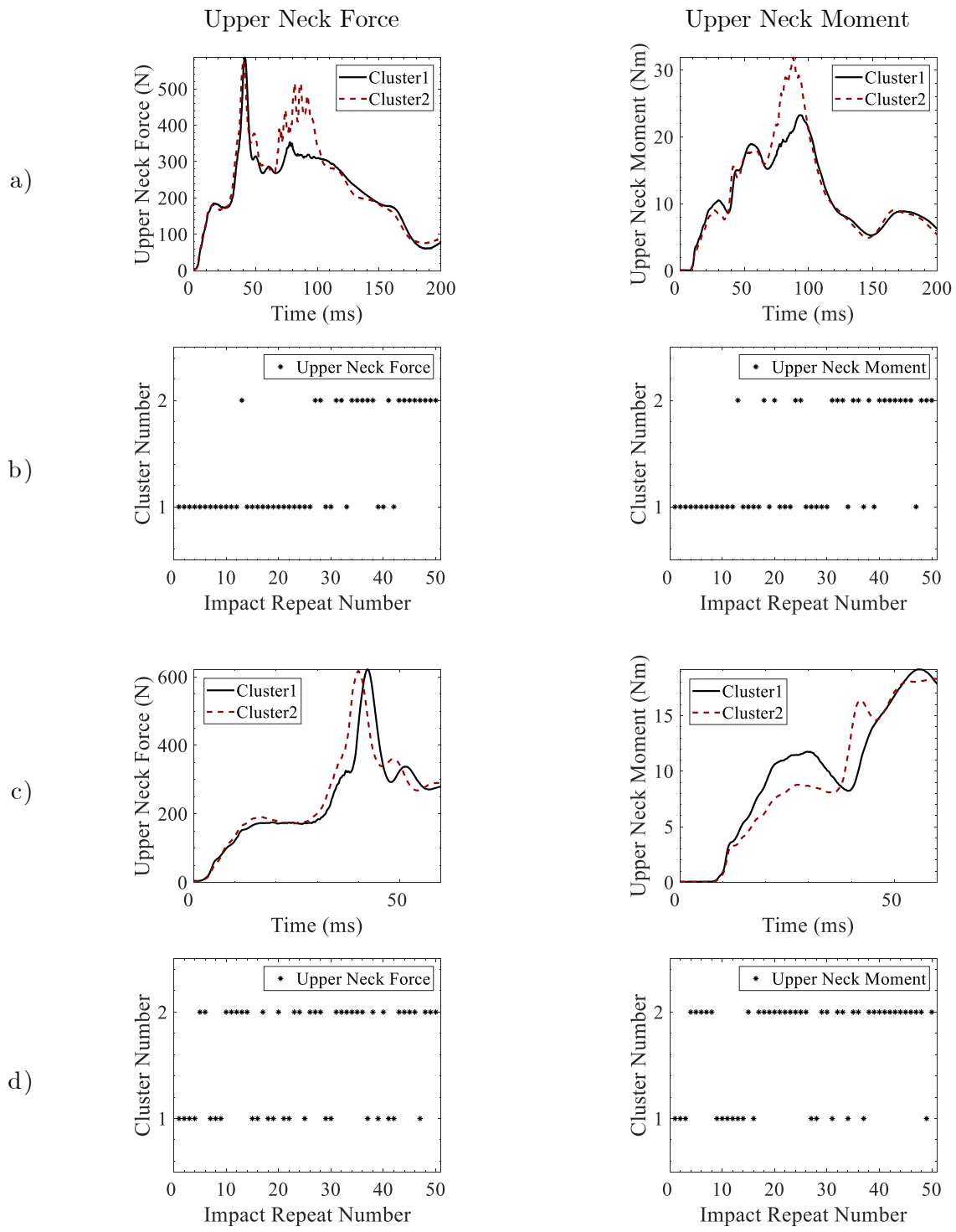

Figure 4.10: Upper neck kinetic cluster time series response [a) 0 – 200 and c) 0 – 60 ms] and cluster number against impact repeat number [b) 0 – 200 and d) 0 – 60 ms].

Head kinematic cluster time series and cluster number are shown in Figure 4.11 from the 0 – 200 ms and 0 – 60 ms analyses. From both time region analyses, head kinematics did not indicate an apparent pattern for cluster number against impact repeat number. The non-systematic time series kinematics were consistent with discrete slope results. Dendrograms are shown in Appendix C.

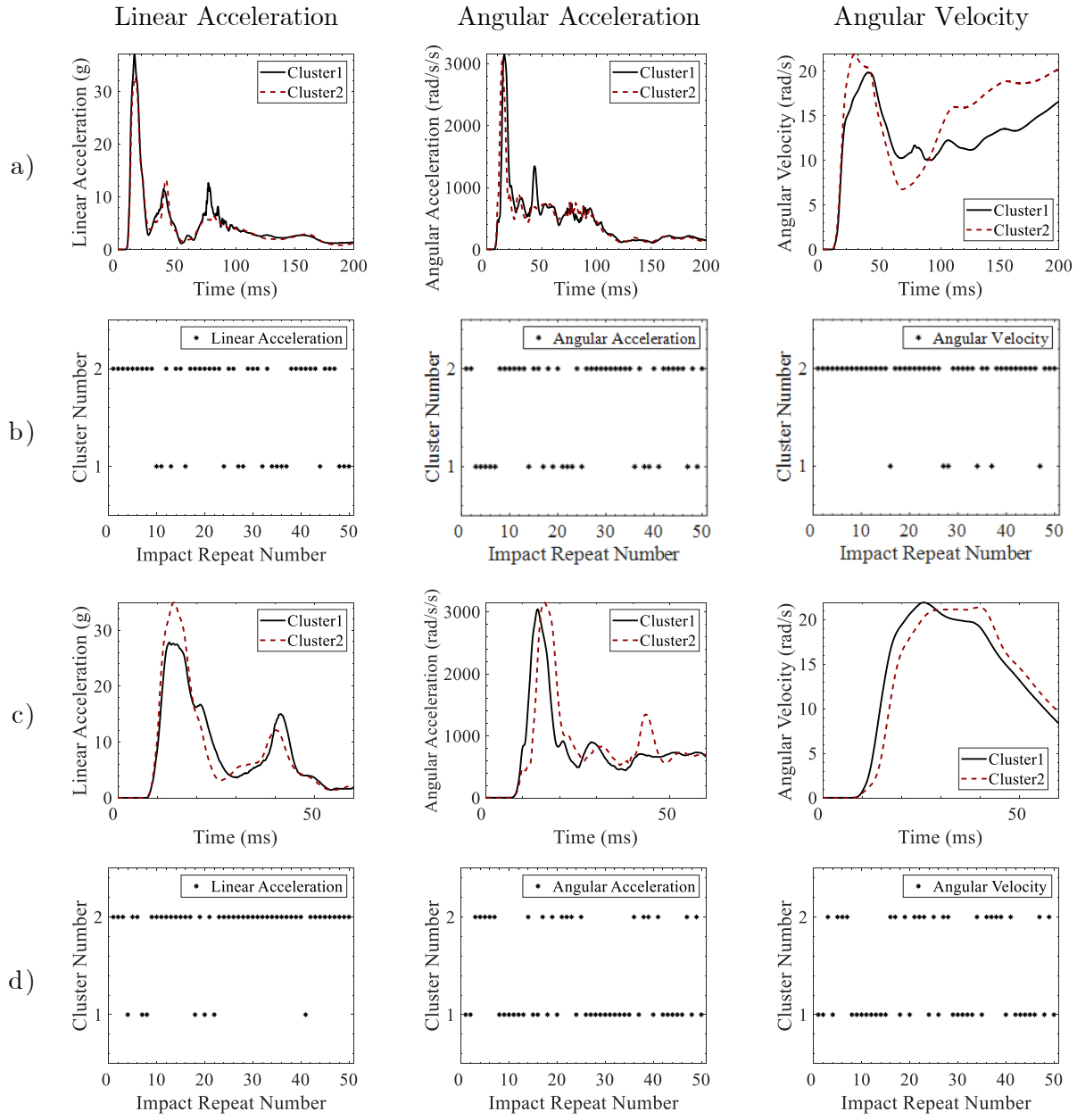

Figure 4.11: Head kinematic cluster time series response [a) 0 – 200 and c) 0 – 60 ms] and cluster number against impact repeat number [b) 0 – 200 and d) 0 – 60 ms].

4.4.3 Durability of High-Speed Video Observations

The PII neck impact responses were investigated visually using high-speed video for differences between the first, twenty-fifth, and fiftieth (last) impacts. Based on the observations (Figure 4.12), a response difference between the first and last impact was identified. During the last impact, the PII neck produced a more compliant response and reached a greater range of motion compared to the first impact. While the difference would indicate poor durability, the high-speed video observations were determined to be a poor measure due to the inconsistencies in impact locations and errors in identifying the moment of impact during video analysis.

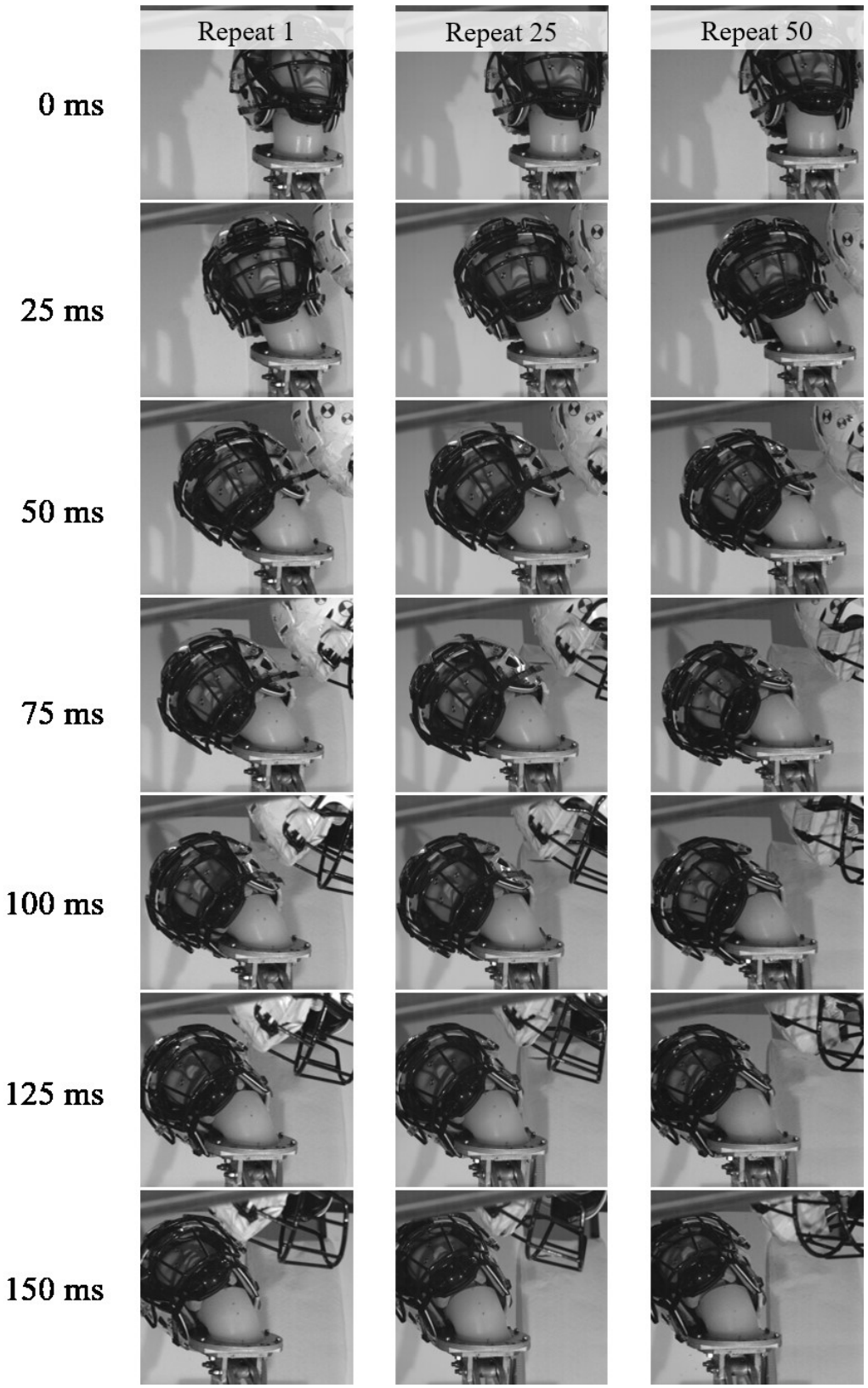

Figure 4.12: High-speed video images of PII neck response for repeats 1, 25, and 50 from the long-term repeatability study (n = 50).

4.5 Durability – Inspection of Mechanical Components

Based on component inspections, there was no evidence of damage or failure from the impact experiments. Silicone tears around the steel cables were observed on the Phase I neck after impact experiments [18]. No such silicone tears were observed on the PII neck (Figure 4.13). Based on CBCT imaging scans (Figure 4.14), the internal structures were not damaged as component spacing remained consistent with the pre-impact structure.

Figure 4.13: No observed damage after impact experiments on the PII neck base.

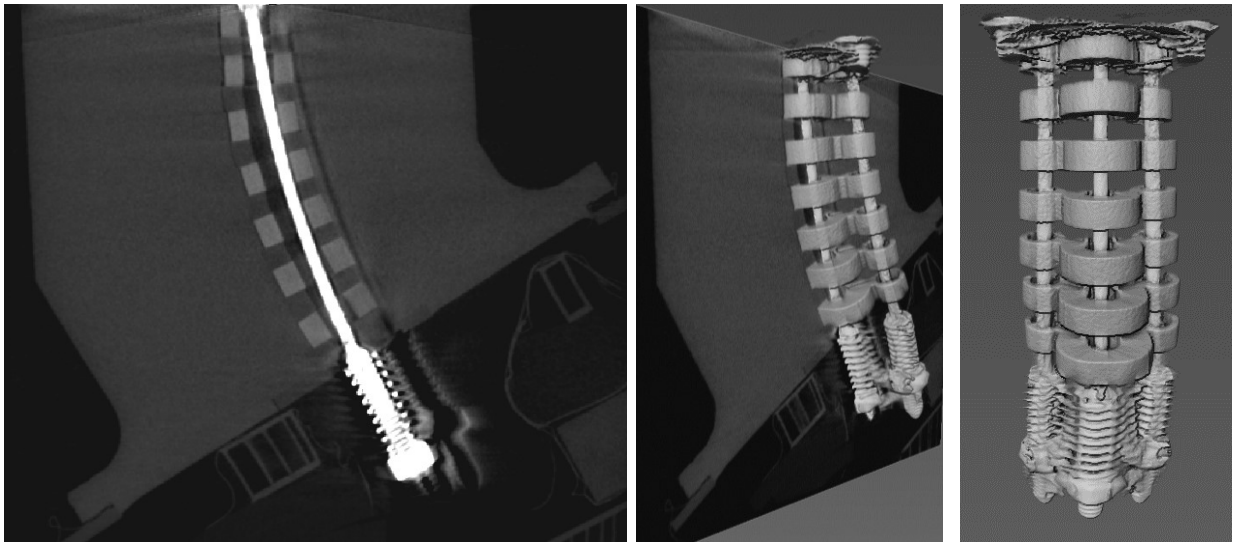

a) b) c)

Figure 4.14: Imaging scans of the PII neck, post experiments, presented as a sample raw image (a) and processed imagery (b and c). The rubber discs were not displayed in the processed images as the software could not distinguish them from the silicone.

4.6 Biofidelity – Volunteer Comparison

Biofidelity of head kinematics was investigated through a comparison against human volunteer head impact data [54]. Overall, head kinematics exhibited excellent biofidelity as they were similar to those of the human volunteers.

For the two NC cases, Figure 4.15 illustrated high-speed images of the PII neck response at six-time points during head impacts. The first column of every impact sequence displayed the moment of impact (time = 0 ms). The PII neck response was similar between NC cases, but the NC1 returned to the neutral, upright position before the NC2 case.

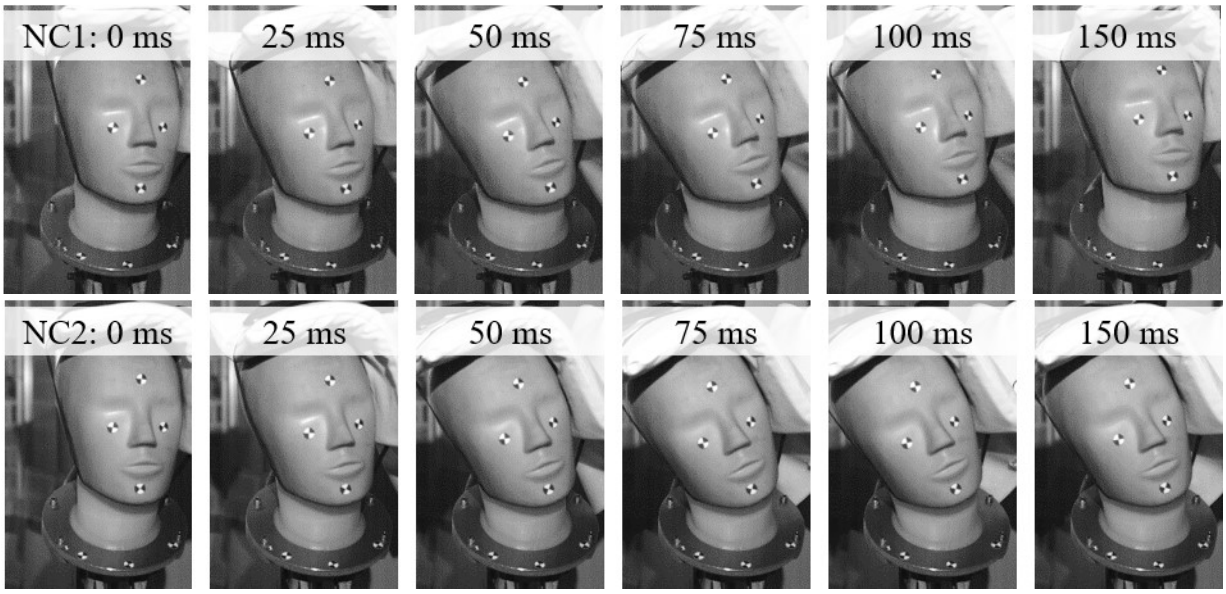

Figure 4.15: Example high-speed images of PII neck response, for both NC cases, from the low-speed volunteer comparison study.

Between NC1 and the unilateral volunteer condition, peak linear acceleration was statistically similar, but peak x-angular velocity was statistically different (Figure 4.16 a and c). NC2 peak linear acceleration was statistically similar to those produced by the passive and co-contracted conditions (Figure 4.16 a). Both NC cases produced peak x-angular accelerations similar to the co-contracted volunteer condition (Figure 4.16 b). For x-angular velocity duration measures, NC1 was between the passive and co-contracted conditions and NC2 was similar to the passive condition (Figure 4.16 d).

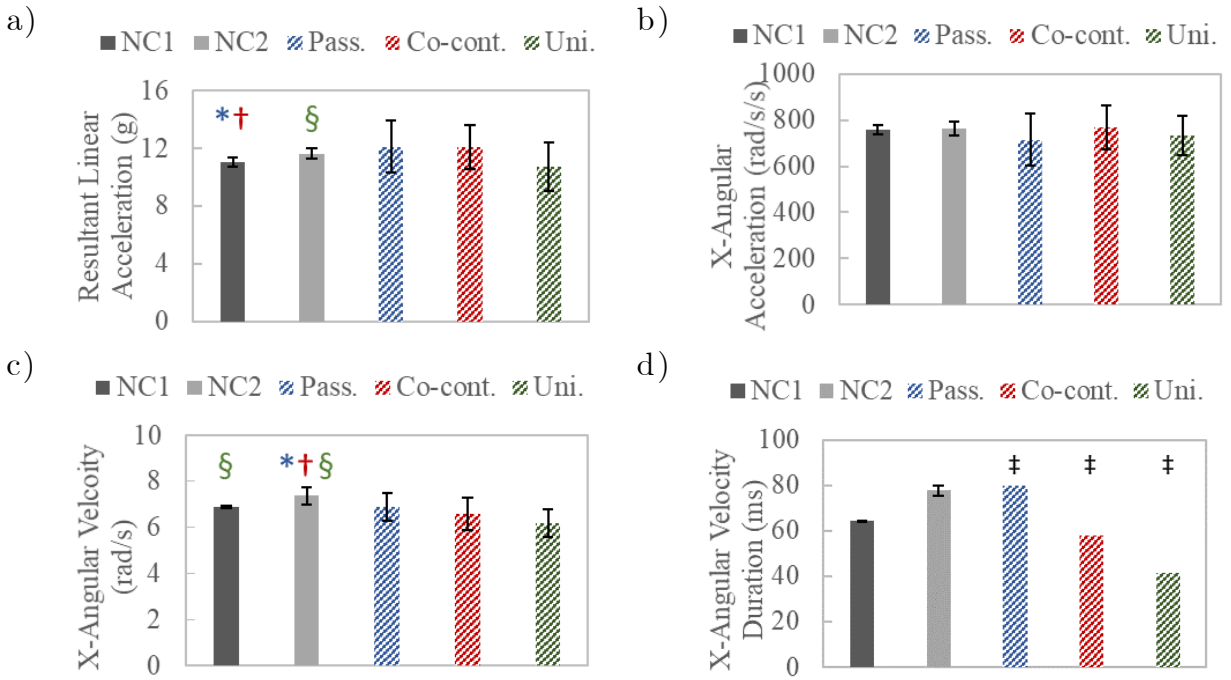

Figure 4.16: Peak head a) resultant linear acceleration, b) x-angular acceleration, c) x-angular velocity, and d) x-angular velocity duration for each PII NC case and human volunteer neck-muscle activation condition [54]. Displayed volunteer x-angular kinematics are the opposite sign from the published data [54]. Volunteer angular velocity durations were manually calculated (‡). Significance of $p < 0.05$ when compared to volunteer passive (*), co-contracted (†), and unilateral (§).

From time series resultant linear acceleration and x-angular velocity (Figure 4.17 a and c), NC1 followed the co-contracted condition and NC2 followed the passive condition, explicitly identified by the narrow and wide x-angular velocity peak responses. From time series x-angular acceleration (Figure 4.17 b), both NC cases displayed higher peaks compared to all-volunteer conditions. However, during the pulse completion sections (20 – 40 ms), responses are again similar between the NC1 and co-contracted cases, as well as between the NC2 and passive condition cases. The PII neck curves displayed a more sudden toe region (0 – 10 ms) compared to volunteer responses, most prominent from resultant linear acceleration and x-angular acceleration curves (Figure 4.17 a and b). The sudden toe region resulted in a shifted response between the PII neck and volunteer conditions; however, curve slopes during rising time regions appeared to be similar.

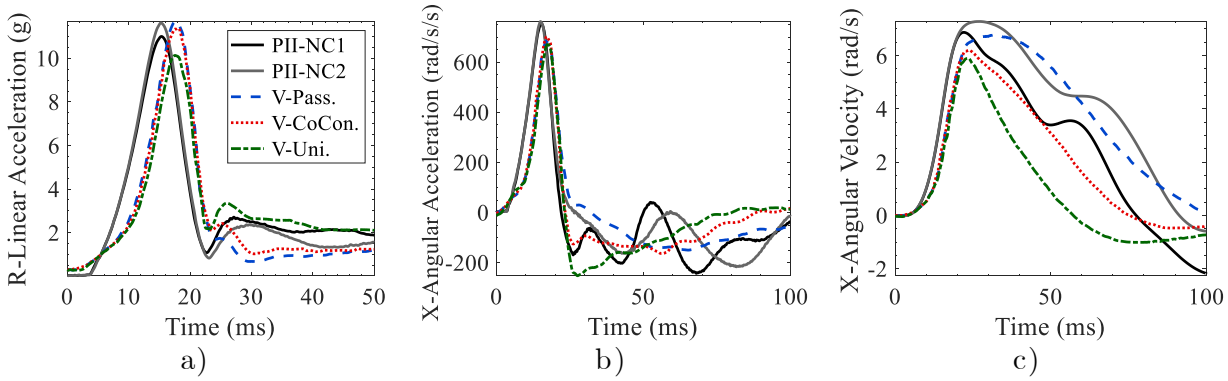

Figure 4.17: Mean head a) resultant linear acceleration, b) x-angular acceleration, and c) x-angular velocity for each PII NC case and volunteer neck-muscle activation condition. Volunteer data was digitized from literature [54], with the authors permission, and reproduced (inversed sign and synchronized) for comparison.

Separate CORAplus analyses were conducted for each comparison using the volunteer responses as the reference curve and the PII neck responses as the comparison curve. The CORAplus ratings, displayed in Figure 4.18, represent the average rating from all three response curves (resultant linear acceleration, x-angular acceleration, and x-angular velocity). Based on time series CORAplus ratings, the PII neck responses correlated best between the NC1 and co-contracted volunteer (0.75), and the NC2 and passive volunteer (0.76) (Figure 4.18). When evaluating multiple curves, a CORAplus rating greater than 0.7 is considered a good correlation [78].

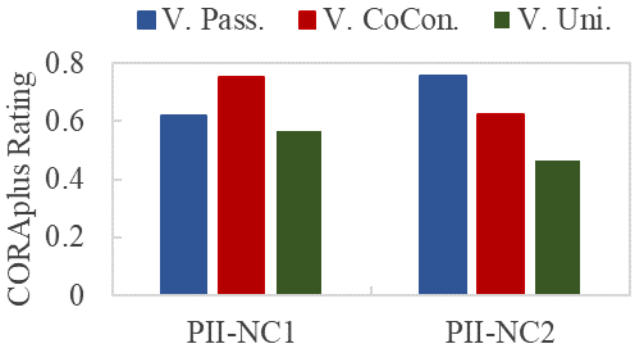

Figure 4.18: Overall CORAplus rating from PII neck comparison with volunteer conditions. CORAplus rating is an average rating from curve comparisons for resultant linear acceleration, x-angular acceleration, and x-angular velocity.

5 Discussion

This chapter explores how the thesis objectives, to refine and assess the biomechanical response of a mechanical surrogate neck model for use in direct head impacts, were supported. Limitations of the PII neck design and response were explored.

5.1 PII Neck Response Characteristics

The objectives of this thesis were to refine the Phase I neck design and characterize the PII neck response in dynamic impact experiments to assess design improvements and performance requirements including repeatability, tunability, durability, and biofidelity. This section discusses the design and experimental results used to achieve the objectives.

5.1.1 PII Neck Design Refinements

Overall, design refinements were successful in advancing the Phase I neck to prevent neck hyperextension, reduce cable tension variation, improve upright position stability, and introduce the ability to tune impact mechanics. This section discusses the effects of design refinements on observable neck responses.

The silicone base redesign and additional clamping plates successfully prevented silicone separation during all impact experiments except for high-speed back impacts with NC2, where a posterior section of silicone shifted out of the clamping plates. As the clamping

plates were bolted along the lateral sides, the silicone separation likely resulted from weak compression force along the posterior section. Even in the impacts where silicone shifted out of the clamping plates, there was no observable neck hyperextension, an improvement over the Phase I neck that exhibited consistent hyperextension in drop impacts. A considerable advancement in neck neutral position stability was achieved by using silicone with higher shore hardness. The PII neck was able to support an upright helmeted ATD headform and return to the neutral position after an impact, unlike its predecessor.

The PII neck locknut system achieved a reduction in cable tension variation as, between repeats, similar responses were observed with high-speed video. The variation reduction in impact mechanics will be discussed in Section 5.1.2. To provide the ability to tune impact mechanics, springs were added at the base of the cervical cables to create a passive neck compression force and adjust neck bending stiffness. Based on the gross neck response, the two NC case responses did not substantially differ, but quantitative measures of tunability will be discussed in Section 5.1.3.

5.1.2 PII Neck Repeatability

Overall, this work was an advancement for repeatability of impact mechanics compared to the Phase 1 neck, as CVs were 11% on average, with the majority below 10%.

An objective of this thesis was to assess the repeatability of impact mechanics, as it is required of ATD necks in injury assessment studies and helmet performance assessments. Repeatability of discrete and time series response metrics was quantitatively evaluated using a percent CV. Discrete metric repeatability was categorized as acceptable or unacceptable based on a 10% threshold [11]. Time series response metrics were assessed with qualitative SD corridors and percent CV values.

Repeatable neck response was indicated by acceptable CVs in 62 of the 96 measures across all impact conditions. Furthermore, some of the unacceptable CVs occurred because of

anomaly impacts with inconsistent impact vectors and not because of PII neck response. Based on post hoc high-speed video observation, the inconsistent impact vectors resulted in undesired head motion and outlier data. For example, during low-speed CR-NC1 impacts, one repeat with an off-centre impact caused large undesired axial head rotation and produced outlier head kinematics, which resulted in unacceptable repeatability measures (11%, 14% and 19% peak CVs for linear acceleration, angular acceleration, and angular velocity, respectively). By removing the outlier set, acceptable head kinematic repeatability was observed (3%, 4% and 5% peak CVs for linear acceleration, angular acceleration, and angular velocity, respectively). Off-centre impacts and outlier data also occurred for other impact cases. Outlier data was not removed from the results presented because of small sample sizes; however, when evaluating overall PII neck repeatability, outliers were noted and excluded. It is hypothesized that experiments with consistent impact vectors will decrease the number of unacceptable repeatability cases. Further study with greater sample sizes and consistent impact vectors is recommended.

The majority of discrete head kinematic CVs were less than 10%, which indicated repeatable responses. The few unacceptable cases were still within ranges customary of biomechanical testing with ATDs [14]. Head angular velocity CVs exhibited the most repeatable measures with all discrete CVs less than 10%, except for one. As head motion can be well described by angular velocity, the excellent repeatability results indicated an overall repeatable PII neck response. The few unacceptable linear and angular acceleration repeatability cases were likely due to the high-frequency signal, which may be more susceptible to small differences in the input impact vector.

For discrete upper neck kinetics, most peak-CVs were acceptable but most impact-CVs were unacceptable. The unacceptable impact-kinetic CVs likely resulted from the time-dependent method used to determine impact kinetics. In many cases, impact force and moment occurred at a time where their response curve was sharply rising. Therefore, small variations in the peak acceleration time produced variable impact force and moments.

Comparing results across impact conditions, repeatability was found to be acceptable for a majority of measures in all conditions but high-speed facemask impacts. Low-speed impacts exhibited more repeatable mechanics compared to high-speed impacts. Inconsistent impact vectors may have had less of an effect on the mechanics from lower energy impacts, which resulted in greater repeatability. Facemask impacts exhibited a high amount of unacceptable repeatability. As facemask impacts caused axial, lateral, and sagittal head-neck rotations, they were expected to produce more variation compared to crown and back impact locations. Between NC cases, NC2 exhibited a greater amount of acceptable repeatability mechanics. The higher neck compression force may have caused a more regulated PII neck response.

Through a qualitative time series assessment, mechanics during the initial impact time were more repeatable compared to later in the time series. This was hypothesized to result from a shift in the response governing mechanism. The initial, more repeatable responses resulted from high and consistent impact energy governing the system. Later in the time series, neck properties began to govern the response, resulting in less repeatable responses.

Impact mechanic repeatability exhibited an advancement with the PII neck, compared to the Phase I neck. By disregarding outlier data and impact kinetics, PII neck repeatability assessment produced maximum discrete CVs of approximately 18% and 19% for head kinematics and upper neck kinetics, respectively. Phase I neck repeatability assessment resulted in maximum CVs of approximately 38% and 32% for head kinematics and upper neck kinetics, respectively [18]. The improvement was likely attributed to the redesigned cable tension-locknut system.

Repeatability results supported PII neck efficacy as a standardized model for direct head impact applications. Acceptable CVs for Hybrid III neck repeatability, specified by the CFR [14], were 23% and 50% in flexion and extension, respectively. PII neck CVs from crown (extension) and back (flexion) impacts were within the CFR acceptability range.

5.1.3 PII Neck Tunability

As the Phase I neck was not capable of tuning impact mechanics, this work was an advancement for tunability as it introduced and demonstrated a capacity to tune head mechanics in back impact locations.

An objective of this work was to introduce the capacity to tune impact mechanics through design modifications. With the capacity to tune head mechanics, the neck model could be adjusted to match living human impact responses. To provide tunability, interchangeable springs were incorporated at the cervical cable base to contribute passive neck compression force across the column base. It was hypothesized that with different amounts of passive compression force, the neck bending stiffness would be modified, and the impact response altered accordingly. The ability to tune head mechanics was evaluated using the difference between two NC cases achieved using two different sets of compression springs. Based on the assessment, head mechanics were tunable for back impacts and displayed promising tunability for crown and facemask impacts.

The time series angular velocity tunability results indicated an overall tunable PII neck response as head motion can be well described by angular velocity, which showed substantial differences between NC cases. The lack of linear acceleration tunability did not discredit PII neck tunability as linear head mechanics are less governed by neck properties [10], [79] and more governed by impact energy.

Back impacts exhibited statistically different head angular velocities and upper neck kinetics between NC cases, and with greater differences in applied compressive forces, greater differences in mechanics would likely be observed. From the NC cases used, the difference between impact mechanics in terms of practical clinical significance for injury assessment may not have been great enough. For low-speed back impacts, peak angular velocity and angular velocity durations were statistically different, with 8.8 rad/s and 86.3 ms for NC1, and 9.3 rad/s and 108.1 ms for NC2. Practically, angular velocity durations

were different, but peak angular velocities were similar. Although some mechanics were not practically different, the study demonstrated an ability to achieve different responses. As compressive force can be easily customized, mechanics can be tuned to match human impact responses.

Through a qualitative time series assessment, mechanics later in the time series exhibited greater tunability compared to those in the initial impact time region. The time-dependent tunability likely resulted from a shift in the response governing mechanism. Small response differences were observed during the initial linear acceleration pulse time when impact energy was governing the response system. Later in the time series, when neck properties were governing the system, larger response differences were observed between NC cases.

Time series response curves displayed differences in the curve duration between NC cases, indicating PII neck tunability. This time series response difference was observed even though some discrete values did not produce a statistical difference. Upper neck moment for low-speed back impacts and head angular velocity for high-speed back impacts exhibited time series differences but lacked discrete metric differences. Time series response duration shift was observed in volunteer head impact studies, where different neck muscle activation cases produced similar peak head kinematics but angular velocity durations differed [54]. The lack of statistical difference between discrete values does not discredit PII tunability as time series responses were observed to differ.

PII neck tunability was more prominent during back impacts than during crown and facemask impacts. Tunability during back impacts can be explained by the design and placement of the cervical cables and compression springs. One cervical cable was positioned along the central axis of the neck, and two cervical cables were positioned posterior-laterally to the central axis of the neck. As a result, the springs were also positioned along the central axis and posterior-laterally to the central axis. During head-neck flexion (back impact), the cervical cables were tensioned, which actively compressed

the springs (Figure 5.1). During the head-neck extension (crown and facemask impacts), the posterior-lateral cervical cables were not tensioned, and the springs were not activated (Figure 5.1). Although the different compression spring cases were implemented to cause a variation in the passive neck compression, the springs contributed an active compression force during back impacts. The different passive compression forces were not able to tune head mechanics during crown and facemask impacts, but different active compression forces produced during back impacts were able to tune head response. A refinement of the PII neck design, to incorporate additional cervical cables and compression springs anterior-lateral to the central axis of the neck, will likely produce PII neck tunability during crown and facemask impacts.

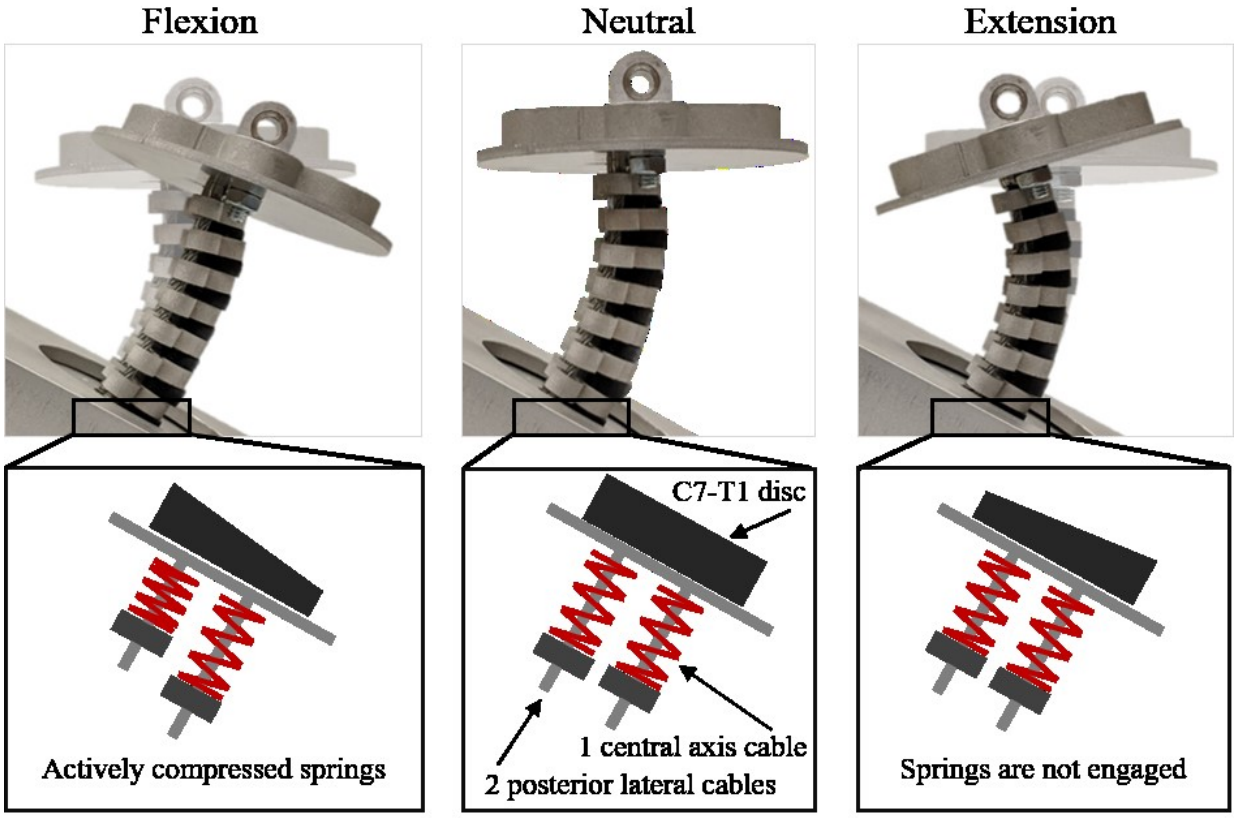

Figure 5.1: Exaggerated schematic of spring activation during head-neck flexion and extension compared to its neutral position.

5.1.4 PII Neck Durability

Overall, this work was an advancement for the durability of impact mechanics and mechanical components compared to the Phase 1 neck, as mechanics were on average consistent over 50 repeats and no structural damage was observed.

An objective of this work was to assess PII neck durability in dynamic head impacts, as mechanical component durability is required of ATD necks in injury assessment studies and helmet performance assessments. PII neck durability was quantitatively evaluated by characterizing the impact metric consistency and qualitatively evaluated through an inspection of the mechanical components. Impact mechanic consistency was assessed for systematic trends or patterns in the discrete and time series measures. Overall, the results indicated consistent and durable PII neck responses to head impact experiments.

Discrete and time series upper neck kinetics were consistent during the initial impact time region (0 – 60 ms); however, kinetics systematically trended upwards during the entire sample time (0 – 200 ms). The entire sampled time (0 – 200 ms) was chosen to include the initial impact response period, the maximum range of motion response, and the recovery period (return to the upright neutral position). During high-speed facemask impacts, the helmet on the headform would strike the neck base plate at approximately 70 ms. As response metrics after 60 ms may represent helmet-plate interaction measures, they were not considered for the durability evaluation and did not discredit PII neck durability. Therefore, upper neck kinetics indicated acceptable PII neck durability.

Head kinematics were consistent during all evaluated time regions and indicated a durable PII neck response. Consistent results during each evaluated time region were likely attributed to the high-energy impact event, which dominated head kinematics throughout the response. Therefore, the effects of the helmet-plate interaction were not great enough to alter the head kinematics.

The few systematically increasing measures that indicated poor durability were likely influenced by impact location inconsistencies and not PII neck durability. During the long-term repeatability study there were challenges with achieving a consistent impact location because of shifting equipment. If the study was repeated with a consistent pendulum system, more consistent mechanics would likely be observed.

Although post hoc high-speed video observations identified a response difference between the first and last impact during the long-term repeatability study, the analysis was limited and was not used to conclude PII neck durability. Although the last impact seemed to produce a more compliant and extensive response, the image difference likely resulted from slight impact location variation or human error in the high-speed video analysis. The impacted equipment occasionally shifted due to the high impact energy, which introduced potential alignment errors from minor adjustments. The moment of impact was manually identified for each impact using high-speed video. Further investigation with consistent impact locations and post hoc impact identification are required before a durability conclusion can be made based on the observable difference.

Based on the inspections, no damage to the PII neck components was observed after 100 impacts at 6 m/s. PII neck durability was an improvement to the Phase I neck. Phase I neck durability began to falter during dynamic drop experiments at impact speeds higher than 5.0 m/s; small silicone tears were observed around the steel cables [18]. The improved durability was likely attributed to silicone with greater shore hardness and a welded steel cable assembly. However, it is recommended to conduct dynamic drop experiments to further assess PII neck durability against the Phase I neck.

The PII neck was deemed highly durable after 100 impacts at 6 m/s with no component damage. Standardized ATD component durability, as specified by the CFR, is assessed qualitatively after a minimum of ten impacts at conditions 150% of the highest standard use levels [11]. In head injury studies, ATD neck models may experience impact speeds

up to 10 m/s [80]. However, with the available pendulum impactor, the maximum achievable speed was 6 m/s. It is recommended to test the PII neck against ten repeat impacts at 150% of 10 m/s to satisfy standardized ATD durability requirements [11].

Overall, this study indicated improved durability over the Phase I neck, and recommended further investigation of high-speed video differences and against CFR specifications [11].

5.1.5 PII Neck Biofidelity

This work was an advancement as PII head impact mechanics indicated excellent biofidelity compared against living human volunteer data, based on CORAplus ratings greater than 0.7.

An objective of this work was to evaluate PII neck biofidelity (ability to simulate humanlike responses) in head impact conditions. PII neck biofidelity was evaluated through comparison against published head kinematic data from human volunteers [54]. The PII head kinematics exhibited excellent correlation to human volunteer data and indicated PII neck biofidelity. Each NC case correlated best to a different volunteer neck-muscle activation condition, which further demonstrated PII neck tunability.

The results of the initial comparison against human-volunteer head kinematics in head impact experiments produced CORAplus ratings of 0.75 for NC1 and 0.76 for NC2. From multiple curve evaluations, ratings greater than 0.7 indicate highly correlated responses [78], and while achieving higher ratings would be possible through design iterations, these ratings are considered to indicate excellent biofidelity for an early stage mechanical surrogate prototype. CORAplus has mainly been used to validate finite element models, where ratings greater than 0.7 have been achieved after model optimization [81].

While CORAplus ratings exhibited excellent biofidelity, a consistent phase shift between PII and human neck response was observed. CORAplus ratings would likely increase if responses were more in phase. Angular velocity was the most in phase curve and produced

CORAplus ratings of 0.80 for NC1 compared to the co-contracted human volunteer and 0.85 for NC2 compared to the passive human volunteer. The phase-shifted curves resulted from a sudden rise in the toe region, which likely resulted because of a lack of a neutral zone response by the PII neck. The neutral zone is the motion region where intervertebral discs offer little resistance, often observed in displacement and load experiments with the osteoligamentous cervical spine [82]. Comparisons between the Phase I neck and PMHS data [18] observed the lack of a neutral zone motion region from quasi-static bending experiments. To further improve PII neck biofidelity, future prototype iterations should introduce a neutral zone response mechanism.

There was potential for errors between the recreated and published input impact mechanics as the experiments were recreated with different equipment. The study was limited to low-speed lateral impacts and the CORAplus analysis was limited to default settings.

5.2 Limitations

Study limitations included impact location inconsistencies, small sample sizes, and helmet-plate interference. Anomaly impacts with inconsistent impact locations resulted in outlier response measures. During high-speed impacts, there was greater potential for alignment errors because the impacted equipment occasionally shifted between repeats. Human error during the manual raise and release of the pendulum impactor could have also contributed to the outlier responses. Because of small sample sizes for low-speed experiments, outlier data was not removed from the presented results. The removal of outlier data improved PII neck repeatability, but it is not understood how outlier data affected PII neck tunability and durability results. Helmet-plate interactions may have caused misrepresentations of the PII neck response as demonstrated through the durability analysis. The effects of these interactions were eliminated in the durability analysis; however, it is unclear how they affected repeatability and tunability results.

For future PII neck evaluations, it is recommended to conduct experiments with more consistent impact vectors and larger sample sizes. It is recommended to automate the pendulum raise and release process, and to better secure the impacted equipment to decrease impact location variation. To prevent helmet-plate interference, it is recommended to decrease neck plate diameter and perform experiments with helmet models without a cheek section or with bare headforms.

A limitation of the PII neck response was silicone separation from the top plate (Figure 5.2). The silicone-top plate separation resulted in head motion independent of the silicone. During high-speed facemask impacts, Hybrid III headform axial rotations continued beyond the silicone rotation capabilities (Figure 5.2). The head and neck longitudinal axes should be aligned if the silicone and top plate did not separate. Independent head and silicone responses may have resulted in measures that misrepresent the PII neck response as the head mechanics were controlled only by the steel cables and not the silicone.

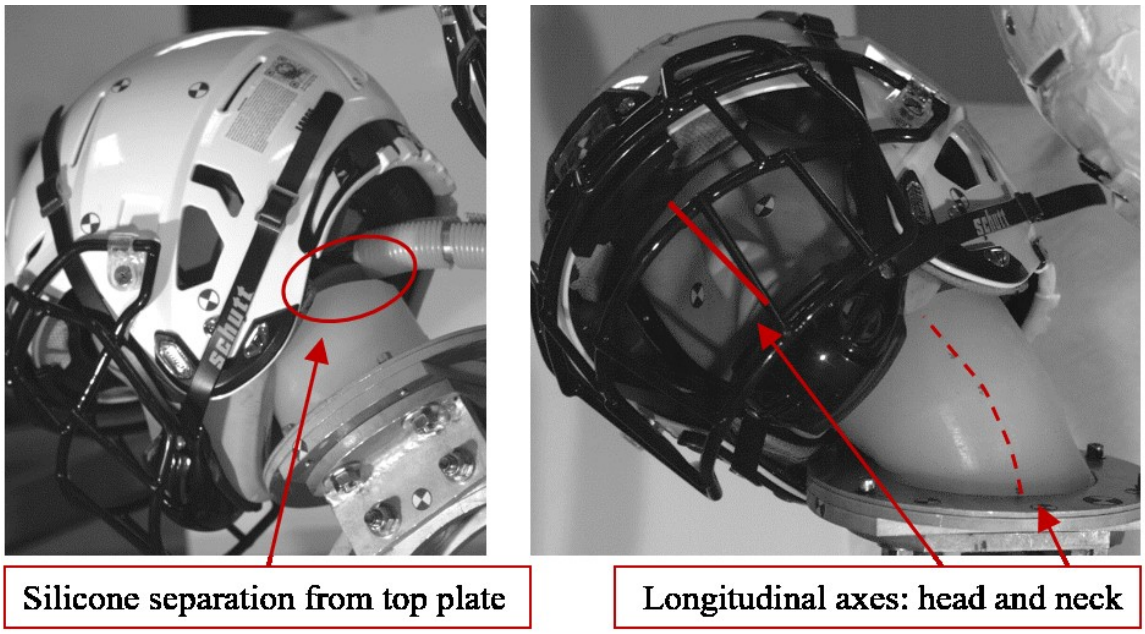

Figure 5.2: Silicone separation from the top plate resulting in misalignment of the head and neck longitudinal axes.

6 Conclusion

This chapter provides a review of the thesis objectives, contributions, and future work recommendations.

With the overarching goal of developing a mechanical neck model that can produce humanlike response during head impacts, the primary objective of this work was to develop a refined mechanical surrogate neck prototype, based on the Phase I neck [18], and characterize its response during head impact experiments. Current head injury research and helmet certifications utilize mechanical surrogate neck models to acquire injury mechanics. Many current neck models are too stiff in bending and produce responses that do not accurately represent human head-neck behaviour during direct head impacts. Because of the continuous occurrence of diffuse brain injuries from head impact events, a mechanical surrogate neck model that offers realistic humanlike head impact response is necessary. This study designed and built a refined neck model, and the methods effectively improved model performance during head impacts. The PII neck model demonstrated, through head impact experiments, repeatable, tunable, durable, and biofidelic mechanics.

6.1 Contributions

Current neck models, used in head impact injury assessment, were not designed or validated for direct head impacts, and produce inaccurate human responses when used in

this fashion. This work presents a refined novel neck prototype and a detailed evaluation of its response characteristics during head impacts. The contributions of this work include:

(1) Design refinement contributions:

- A redesigned silicone base and the addition of aluminum plates to prevent silicone-base plate separation and neck hyperextension in impacts.
- New silicone material to allow for the full support of an upright helmeted ATD headform while maintaining flexible responses.
- A threaded rod and locknut system at the steel cable base to better secure the internal structural steel cables to reduce tension variation.
- Introduction of compression springs to contribute passive neck compression force, which can be customized to tune head impact mechanics.

(2) Response characterization contributions:

- PII neck repeatability of head mechanics was improved compared to the Phase I neck as CVs were 11% on average and satisfied requirements for standardized ATD necks as maximum CVs from extension and flexion impacts were less than 20%.
- PII neck tunability of head mechanics was introduced for impact conditions that engaged the compression springs. This demonstrated the potential to introduce tunability for all impact locations with a minor design iteration.
- PII neck durability was improved compared to the Phase I neck as consistent head mechanics over successive impact experiments was demonstrated and no structural damage to the prototype was observed after all experiments.
- PII neck biofidelity of head mechanics was confirmed from a preliminary comparison to human volunteer head impact head-kinematics as CORAplus (curve correlation) ratings were greater than 0.7.

Overall, this work was an advancement towards an accurate head impact surrogate neck.

6.2 Future Work and Recommendations

At this stage of developing a novel surrogate neck model for head impact applications, a proof of concept prototype (Phase I neck [18]) and a refined prototype (PII neck) have been produced. The refined prototype was developed to address the limitations of the concept prototype and assess standard performance characteristics. The next steps to develop a realistic head impact neck model are to address PII neck limitations through further design refinement, to conduct a comprehensive analysis of humanlike head impact response accuracy (biofidelity), and to assess model reproducibility. Before implementing the model into standardized applications, final refinements to the novel neck model will be required.

Future design suggestions include: adapting the interior aluminum elements to add two cables anterior-lateral to the central axis, decreasing the silicone-compression plate diameter, redesigning the silicone and top-plate connection to prevent separation, and introducing a neutral zone response mechanism. The addition of cables and compression springs located anterior-laterally to the central axis would achieve neck tunability for all impact directions. Smaller diameter silicone-compression plates would prevent helmet-plate interactions, therefore impact measures that do not represent neck response. A secure connection between the silicone and top-plate would prevent independent head motion, which does not accurately represent neck response. Introducing a neutral zone response mechanism would improve the biofidelity of head impact mechanics.

Future experimental investigations include: further impact experiments with a consistent impact vector and greater NC force differences, a comprehensive biofidelity and reproducibility assessment, drop impact experiments, and quasi-static bending tests. Further experimental tests with consistent input mechanics can be used to confirm repeatability and durability mechanics. To achieve greater response differences between NC cases, different compression springs can be used during experimental impacts. Further

assessment of model durability and relevance can be accomplished from drop impact experiments, as this type of impact is done in many surrogate model head impact applications. Quasi-static bending tests with and without the silicone are required to quantify bending stiffness contribution between the compression springs and silicone. By fully characterizing the contribution of the compression springs to the bending stiffness, the impact mechanics can be more accurately tuned. An assessment of model reproducibility is required for standardization to ensure similar results between different models built by different individuals. A comprehensive biofidelity study against other data sets of live human head impact response is required to validate the neck before it can be implemented into head impact injury assessment research and helmet certification methods.

References

[1] Centers for Disease Control and Prevention, 'Surveillance Report of Traumatic Brain Injury-related Emergency Department Visits, Hospitalizations, and Deaths—United States, 2014', Centers for Disease Control and Prevention, U.S. Department of Health and Human Services, 2019.

[2] T. Kay, D. E. Harrington, R. Adams, T. Anderson, S. Berrol, K. Cicerone, C. Dahlberg, D. Gerber, R. Goka, P. Harley, J. Hilt, L. Horn, D. Lehmkuhl, and J. Malec, 'Definition of mild traumatic brain injury', *J. Head Trauma Rehabil.*, vol. 8, no. 3, pp. 86–87, 1993.

[3] D. C. Viano, A. I. King, J. W. Melvin, and K. Weber, 'Injury biomechanics research: An essential element in the prevention of trauma', *J. Biomech.*, vol. 22, no. 5, pp. 403–417, Jan. 1989, doi: 10.1016/0021-9290(89)90201-7.

[4] J. R. Crandall, D. Bose, J. Forman, C. D. Untaroiu, C. Arregui-Dalmases, C. G. Shaw, and J. R. Kerrigan, 'Human surrogates for injury biomechanics research', *Clin. Anat. N. Y. N*, vol. 24, no. 3, pp. 362–371, Apr. 2011, doi: 10.1002/ca.21152.

[5] E. G. Takhounts, M. J. Craig, K. Moorhouse, J. McFadden, and V. Hasija, 'Development of brain injury criteria (BrIC)', *Stapp Car Crash J.*, vol. 57, pp. 243–266, Nov. 2013.

[6] J. W. Melvin and J. W. Lighthall, 'Brain-Injury Biomechanics', in *Accidental Injury: Biomechanics and Prevention*, A. M. Nahum and J. W. Melvin, Eds. New York, NY: Springer, 2002, pp. 277–302.

[7] E. S. Gurdjian, V. L. Roberts, and L. M. Thomas, 'Tolerance curves of acceleration and intracranial pressure and protective index in experimental head injury', *J. Trauma*, vol. 6, no. 5, pp. 600–604, Sep. 1966, doi: 10.1097/00005373-196609000-00005.

[8] P. Yarnell and A. K. Ommaya, 'Experimental cerebral concussion in the rhesus monkey.', *Bull. N. Y. Acad. Med.*, vol. 45, no. 1, pp. 39–45, Jan. 1969.

[9] T. A. Gennarelli, L. E. Thibault, and A. K. Ommaya, 'Pathophysiologic Responses to Rotational and Translational Accelerations of the Head', SAE International, Warrendale, PA, SAE Technical Paper 720970, Feb. 1972. doi: 10.4271/720970.

[10] C. P. Eckersley, R. W. Nightingale, J. F. Luck, and C. R. Bass, 'The role of cervical muscles in mitigating concussion', *J. Sci. Med. Sport*, vol. 22, no. 6, pp. 667–671, Jun. 2019, doi: 10.1016/j.jsams.2019.01.009.

[11] 'ISO 15830-1:2013(en), Road vehicles — Design and performance specifications for the WorldSID 50th percentile male side-impact dummy — Part 1: Terminology and rationale', ISO Standard 2, 2013. Accessed: May 15, 2019. [Online]. Available: https://www.iso.org/obp/ui/#iso:std:iso:15830:-1:ed-2:v1:en.

[12] H. J. Mertz, R. F. Neathery, and C. C. Culver, 'Performance Requirements and Characteristics of Mechanical Necks', in *Human Impact Response: Measurement and Simulation*, W. F. King and H. J. Mertz, Eds. Boston, MA: Springer US, 1973, pp. 263–288.

[13] J. G. M. Thunnissen, J. S. H. M. Wismans, C. L. Ewing, and D. J. Thomas, 'Human Volunteer Head-Neck Response in Frontal Flexion: A New Analysis', *SAE Trans.*, vol. 104, pp. 3065–3086, 1995.

[14] '49 Code of Federal Regulations (CFR) Part 572 - Anthropomorphic Test Devices', National Highway Traffic Safety Administration, Department of Transportation, 2011.

[15] N. Yoganandan, A. Sances, and F. Pintar, 'Biomechanical Evaluation of the Axial Compressive Responses of the Human Cadaveric and Manikin Necks', *J. Biomech. Eng.*, vol. 111, no. 3, pp. 250–255, Aug. 1989, doi: 10.1115/1.3168374.

[16] A. Sances, 'Dynamic Comparison of the Hybrid III and Human Neck', in *N. Yoganandan et al. (Eds.) Frontiers in Head and Neck Trauma: Clinical and Biomechanical*, Amsterdam: IOS Press, 1998.

[17] D. Parent, M. Craig, and K. Moorhouse, 'Biofidelity Evaluation of the THOR and Hybrid III 50th Percentile Male Frontal Impact Anthropomorphic Test Devices', *Stapp Car Crash J.*, vol. 61, pp. 227–276, Nov. 2017.

[18] M. K. Ogle, 'Development and Characterization of a Mechanical Surrogate Neck Prototype for Use in Helmet Certification Applications', Master of Science, University of Alberta, Department of Mechanical Engineering, Edmonton AB Canada, 2018.

[19] M. Beusenberg, J. Wismans, E. Faerber, R. Lowne, D. Cesari, F. Bermond, C. Nilsson, M. Koch, P.-L. Ardoino, and E. Fossat, 'EEVC Recommended requirements for the development and design of an advanced frontal impact dummy', EEVC-Report, Sep. 1996.

[20] F. H. Martini, J. L. Nath, and E. F. Bartholomew, *Fundamentals of Anatomy & Physiology (10th Edition)*, 10th ed. San Francisco, California: Pearson Education, Inc., 2015.

[21] H. J. Mertz and A. L. Irwin, 'Anthropomorphic Test Devices and Injury Risk Assessments', in *Accidental Injury: Biomechanics and Prevention*, N. Yoganandan, A. M. Nahum, and J. W. Melvin, Eds. New York, NY: Springer, 2015, pp. 83–112.

[22] H. J. Mertz, 'Anthropomorphic models', in *Nahum AM, Melvin JW (eds) The biomechanics of trauma*, Appleton, Norwalk, 1985, pp. 31–60.

[23] J. K. Foster, J. O. Kortge, and M. J. Wolanin, 'Hybrid III-A Biomechanically-Based Crash Test Dummy', presented at the Proc Stapp Car Crash, Feb. 1977, vol. 21, pp. 975–1014, doi: 10.4271/770938.

[24] H. J. Mertz and L. M. Patrick, 'Strength and Response of the Human Neck', *SAE Trans.*, vol. 80, pp. 2903–2928, 1971.

[25] B. Rowson, S. Rowson, and S. M. Duma, 'Hockey STAR: A Methodology for Assessing the Biomechanical Performance of Hockey Helmets', *Ann. Biomed. Eng.*, vol. 43, no. 10, pp. 2429–2443, Oct. 2015, doi: 10.1007/s10439-015-1278-7.

[26] B. M. Knowles and C. R. Dennison, 'Predicting Cumulative and Maximum Brain Strain Measures From HybridIII Head Kinematics: A Combined Laboratory Study and Post-Hoc Regression Analysis', *Ann. Biomed. Eng.*, vol. 45, no. 9, pp. 2146–2158, Sep. 2017, doi: 10.1007/s10439-017-1848-y.

[27] H. Y. Yu and C. Dennison, 'A laboratory study on effects of cycling helmet fit on biomechanical measures associated with head and neck injury and dynamic helmet retention', *J. Biomech. Eng.*, Jul. 2018, doi: 10.1115/1.4040944.

[28] J. A. Newman, M. C. Beusenberg, N. Shewchenko, C. Withnall, and E. Fournier, 'Verification of biomechanical methods employed in a comprehensive study of mild traumatic brain injury and the effectiveness of American football helmets', *J. Biomech.*, vol. 38, no. 7, pp. 1469–1481, Jul. 2005, doi: 10.1016/j.jbiomech.2004.06.025.

[29] D. P. Parent, M. Craig, S. A. Ridella, and J. D. McFadden, 'Thoracic Biofidelity Assessment of the THOR Mod Kit ATD', presented at the 23rd International Technical Conference on the Enhanced Safety of Vehicles (ESV)National Highway Traffic Safety Administration, 2013.

[30] M. Haffner, R. H. Eppinger, N. Rangarajan, T. A. Shams, M. Artis, and D. Beach, 'Foundations and elements of the NHTSA THOR alpha ATD design', presented at the The 17th Int. Technical Condf. on the Enhanced Safety of Vehicles, 2001, pp. 1–12.

[31] L. Xu, J. Jensen, K. Byrnes, A. Kim, V. Agaram, K. L. Davis, R. W. Hultman, G. Kostyniuk, M. E. Marshall, H. Mertz, G. Nusholtz, S. Rouhana, and R. Scherer, 'Comparative Performance Evaluation of THOR and Hybrid III', *SAE Trans.*, vol. 109, pp. 284–308, 2000.

[32] Z. J. Wang, 'THOR neck moment calculation at atlanto-occipital joint', *SAE Tech. Pap.*, vol. 2019-April, no. April, 2019, doi: 10.4271/2019-01-1037.

[33] 'NHTSA/GESAC, Inc., THOR NT User's Manual - 50% Male Frontal Dummy', U.S. Department of Transportation, Boonsboro, MD, GESAC-05-02.

[34] 'GESAC, Inc. (2005b) THOR Certification Manual, Revision 2005.2', U.S. Department of Transportation, Washington, DC, GESAC-05-04.
[35] 'GESAC, Inc. (2005a) Biomechanical Response Requirements of the THOR NHTSA Advanced Frontal Dummy, Revision 2005.1', U.S. Department of Transportation, Washington, DC, GESAC-05-03.
[36] D. L. Albert, S. M. Beeman, and A. R. Kemper, 'Evaluation of Hybrid III and THOR-M neck kinetics and injury risk under various restraint conditions during full-scale frontal sled tests', *Traffic Inj. Prev.*, vol. 19, no. sup2, pp. S40–S47, 2018, doi: 10.1080/15389588.2018.1524141.
[37] H. Rhule, B. Donnelly, K. Moorhouse, and Y. S. Kang, 'A Methodology for Generating Objective Targets for Quantitatively Assessing the Biofidelity of Crash Test Dummies', presented at the 23rd International Technical Conference on the Enhanced Safety of Vehicles (ESV)National Highway Traffic Safety Administration, 2013.
[38] C. G. Shaw, J. R. Crandall, and J. Butcher, 'Biofidelity Evaluation of the THOR Advanced Frontal Crash Test Dummy', presented at the IRCOBI Conference on the Biomechanics of Impact, Montpelier, France, 2000.
[39] 'The EUROSID-1', Technical information from the TNO Crash Safety Research Center, Delft, 1995.
[40] M. van Ratingen, 'Development and evaluation of the ES-2 side impact dummy', presented at the Proceedings of 17th International Technical Conference on the Enhanced Safety of Vehicles, Amsterdam, 2001.
[41] A. Sutterfield, K. Pecoraro, S. W. Rouhana, L. Xu, J. Abramczyk, J. Berliner, A. Irwin, J. Jensen, H. J. Mertz, G. Nusholtz, H. Pietsch, R. Scherer, and S. Tylko, 'Evaluation of the ES-2re Dummy in Biofidelity, Component, and Full Vehicle Crash Tests', *Stapp Car Crash J.*, vol. 49, pp. 481–508, Nov. 2005.
[42] 'EuroSID-2re Male Side Impact Dummy Parts Catalog', Humanetics Innovative Solutions, Inc., Farmington Hills, MI, 175-0000-H, 2017.
[43] M. S. Beebe, 'What is Biosid?', SAE International, Warrendale, PA, SAE Technical Paper 900377, Feb. 1990. doi: 10.4271/900377.
[44] M. R. Seemann, W. H. Muzzy, and L. S. Lustick, 'Comparison of Human and Hybrid III Head and Neck Dynamic Response', SAE International, Warrendale, PA, SAE Technical Paper 861892, Oct. 1986. doi: 10.4271/861892.
[45] R. Scherer, D. Cesari, T. Uchimura, G. Kostyniuk, M. Page, K. Asakawa, E. Hautmann, K. Bortenschlager, M. Sakurai, and T. Harigae, 'Design and evaluation of the WorldSID prototype dummy', presented at the Proceedings of 17th International Technical Conference on the Enhanced Safety of Vehicles, Amsterdam, 2001.
[46] B. Been, M. Philippens, R. De Lange, and M. Van Ratingen, 'WorldSID Dummy Head-Neck Biofidelity Response', *SAE Tech. Pap.*, vol. 2004-November, no. November, 2004, doi: 10.4271/2004-22-0019.

[47] A. Linder, M. Y. Svensson, J. Davidsson, A. Flogård, P. Lövsund, Y. Håland, L. Jakobsson, and K. Wiklund, 'Design and Validation of the Neck for a Rear Impact Dummy (BioRID I)', *Traffic Inj. Prev.*, vol. 3, no. 2, pp. 167–174, Jun. 2002, doi: 10.1080/15389580211995.

[48] 'ISO TC22/SC12/WG5 (2012) Adult dummies recommended by WG5', Document N1012, 2012.

[49] M. R. Maltese, R. H. Eppinger, H. H. Rhule, B. R. Donnelly, F. A. Pintar, and N. Yoganandan, 'Response corridors of human surrogates in lateral impacts', *Stapp Car Crash J.*, vol. 46, pp. 321–351, Nov. 2002.

[50] C. VanIngen-Dunn and I. Kaleps, 'A Pursuit for a More Biofidelic Manikin Neck', in *N. Yoganandan et al. (Eds.) Frontiers in Head and Neck Trauma: Clinical and Biomechanical*, Amsterdam: IOS Press, 1998, pp. 131–145.

[51] J. Wismans and C. H. Spenny, 'Performance requirements for mechanical necks in lateral flexion', *SAE Tech. Pap.*, 1983, doi: 10.4271/831613.

[52] L. C. Wu, V. Nangia, K. Bui, B. Hammoor, M. Kurt, F. Hernandez, C. Kuo, and D. B. Camarillo, 'In Vivo Evaluation of Wearable Head Impact Sensors', *Ann. Biomed. Eng.*, vol. 44, no. 4, pp. 1234–1245, Apr. 2016, doi: 10.1007/s10439-015-1423-3.

[53] F. Hernandez and D. B. Camarillo, 'Voluntary Head Rotational Velocity and Implications for Brain Injury Risk Metrics', *J. Neurotrauma*, vol. 36, no. 7, pp. 1125–1135, Apr. 2019, doi: 10.1089/neu.2016.4758.

[54] K. A. Reynier, A. Alshareef, D. F. Shedd, E. J. Sanchez, J. R. Funk, and M. B. Panzer, 'Comparison of the Hybrid III and Human Volunteer in Low-Severity Lateral Head Impacts', in *IRCOBI Conference Proceedings*, Florence, Italy, 2019.

[55] E. J. Pellman, D. C. Viano, A. M. Tucker, I. R. Casson, and J. F. Waeckerle, 'Concussion in professional football: reconstruction of game impacts and injuries', *Neurosurgery*, vol. 53, no. 4, pp. 799–812; discussion 812-814, Oct. 2003.

[56] 'Standard Linear Impactor Test Method and Equipment Used in Evaluating the Performance Characteristics of Protective Headgear and Faceguards', NOCSAE, U.S. Standard (ND) 081-18am19a, Nov. 2019.

[57] A. Rizzetti, D. Kallieris, P. J. Schiemann, and R. Mattern, 'Response and injury severity of the head-neck unit during a low velocity head impact', in *IRCOBI Conference Proceedings*, 1997.

[58] T. S. Nelson and P. A. Cripton, 'A New Biofidelic Sagittal Plane Surrogate Neck for Head-First Impacts', *Traffic Inj. Prev.*, vol. 11, no. 3, pp. 309–319, Jun. 2010, doi: 10.1080/15389581003614870.

[59] E. S. Walsh, M. Kendall, A. Post, A. Meehan, and T. B. Hoshizaki, 'Comparative analysis of Hybrid III neckform and an unbiased neckform', *Sports Eng.*, vol. 21, no. 4, pp. 479–485, Dec. 2018, doi: 10.1007/s12283-018-0286-x.

[60] A. N. Vasavada, J. Danaraj, and G. P. Siegmund, 'Head and neck anthropometry, vertebral geometry and neck strength in height-matched men and women', *J. Biomech.*, vol. 41, no. 1, pp. 114–121, 2008, doi: 10.1016/j.jbiomech.2007.07.007.

[61] McConville, 'John Anthropometric Relationships of Body and Body Segments Moments of Inertia Anthropology Research Project, Inc. A/F Aerospace Medical Res', NASA-STD-3000 275e AF AMRL-TR-180-119. Accessed: Apr. 22, 2020. [Online]. Available: https://msis.jsc.nasa.gov/sections/section03.htm.

[62] M. M. Panjabi, J. Duranceau, V. Goel, T. Oxland, and K. Takata, 'Cervical human vertebrae. Quantitative three-dimensional anatomy of the middle and lower regions', *Spine*, vol. 16, no. 8, pp. 861–869, Aug. 1991, doi: 10.1097/00007632-199108000-00001.

[63] P. H. F. Nicholson, X. G. Cheng, G. Lowet, S. Boonen, M. W. J. Davie, J. Dequeker, and G. Van der Perre, 'Structural and material mechanical properties of human vertebral cancellous bone', *Med. Eng. Phys.*, vol. 19, no. 8, pp. 729–737, Oct. 1997, doi: 10.1016/S1350-4533(97)00030-1.

[64] Rapoff, 'MER/BIO Soft Tissue Mechanics: Spine Biomechanics'. .

[65] S. Schleifenbaum, M. Schmidt, R. Möbius, T. Wolfskämpf, C. Schröder, R. Grunert, N. Hammer, and T. Prietzel, 'Load and failure behavior of human muscle samples in the context of proximal femur replacement', *BMC Musculoskelet. Disord.*, vol. 17, no. 1, p. 149, Apr. 2016, doi: 10.1186/s12891-016-0998-7.

[66] J. L. Sparks, N. A. Vavalle, K. E. Kasting, B. Long, M. L. Tanaka, P. A. Sanger, K. Schnell, and T. A. Conner-Kerr, 'Use of silicone materials to simulate tissue biomechanics as related to deep tissue injury', *Adv. Skin Wound Care*, vol. 28, no. 2, pp. 59–68, Feb. 2015, doi: 10.1097/01.ASW.0000460127.47415.6e.

[67] A. J. Padgaonkar, K. W. Krieger, and A. I. King, 'Measurement of Angular Acceleration of a Rigid Body Using Linear Accelerometers', *J. Appl. Mech.*, vol. 42, no. 3, pp. 552–556, Sep. 1975, doi: 10.1115/1.3423640.

[68] S. of A. Engineers, 'J211 - (R) Instrumentation for impact test - Part 1 - electronic instrumentation', Society of Automotive Engineers, 2003.

[69] N. R. Miller, R. Shapiro, and T. M. McLaughlin, 'A technique for obtaining spatial kinematic parameters of segments of biomechanical systems from cinematographic data', *J. Biomech.*, vol. 13, no. 7, pp. 535–547, Jan. 1980, doi: 10.1016/0021-9290(80)90054-8.

[70] H. Y. Yu, 'A Laboratory Study on the Effect of Helmet Fit on Biomechanical Measures of Head and Neck Injury in Simulated Impact', University of Alberta, Edmonton AB Canada, 2017.

[71] F08 Committee, 'Performance Specification for Ice Hockey Helmets', ASTM International. doi: 10.1520/F1045-16.

[72] R. Eppinger, E. Sun, F. Bandak, M. Haffner, N. Khaewpong, M. Maltese, S. Kuppa, T. Nguyen, E. Takhounts, R. Tannous, A. Zhang, and R. Saul, 'Development of Improved Injury Criteria for the Assessment of Advanced Automotive Restraint Systems - II', *NHTSA Docket*, p. 180, 1999.

[73] S. R. MacGillivray, J. P. Carey, and C. R. Dennison, 'Repeatability of a mechanical surrogate neck for low speed impact testing: a preliminary assessment', presented at

the Proceedings of the 2019 International IRCOBI Conference on the Biomechanics of Injury, 2019.

[74] H. B. Mann and D. R. Whitney, 'On a Test of Whether one of Two Random Variables is Stochastically Larger than the Other', *Ann. Math. Stat.*, vol. 18, no. 1, pp. 50–60, Mar. 1947, doi: 10.1214/aoms/1177730491.

[75] J. H. W. Jr, 'Hierarchical Grouping to Optimize an Objective Function', *J. Am. Stat. Assoc.*, vol. 58, no. 301, pp. 236–244, Mar. 1963, doi: 10.1080/01621459.1963.10500845.

[76] C. Thunert, 'CORAplus 4.0.4 User's Manual', Germany, May 2017.

[77] C. Gehre, H. Gades, and P. Wernicke, 'Objective Rating of Signals using test and simulation responses', in *Preceedings of the 21st International Technical Conference on the Enhanced Safety of Vehicles*, Stuttgart Germany, 2009.

[78] C. Gehre and S. Stahlschmidt, 'Assessment of Dummy Models by Using Objective Rating Methods', presented at the 22nd International Technical Conference on the Enhanced Safety of Vehicles (ESV)National Highway Traffic Safety Administration, 2011.

[79] C. P. Eckersley, R. W. Nightingale, J. F. Luck, and C. R. Bass, 'Effect of neck musculature on head kinematic response following blunt impact', presented at the Conference proceedings International Research Council on the Biomechanics of Injury, IRCOBI, 2017, vol. 2017-September, pp. 685–698.

[80] J. A. Newman, M. C. Beusenberg, N. Shewchenko, C. Withnall, and E. Fournier, 'Verification of biomechanical methods employed in a comprehensive study of mild traumatic brain injury and the effectiveness of American football helmets', *J. Biomech.*, vol. 38, no. 7, pp. 1469–1481, Jul. 2005, doi: 10.1016/j.jbiomech.2004.06.025.

[81] J. B. Putnam, J. T. Somers, and C. D. Untaroiu, 'Development, calibration, and validation of a head-neck complex of THOR mod kit finite element model', *Traffic Inj. Prev.*, vol. 15, no. 8, pp. 844–854, 2014, doi: 10.1080/15389588.2014.880886.

[82] M. M. Panjabi, J. J. Crisco, A. Vasavada, T. Oda, J. Cholewicki, K. Nibu, and E. Shin, 'Mechanical properties of the human cervical spine as shown by three-dimensional load-displacement curves', *Spine*, vol. 26, no. 24, pp. 2692–2700, Dec. 2001, doi: 10.1097/00007632-200112150-00012.

Appendix A: Repeatability

Percent CV values of discrete impact metrics were used to assess PII neck repeatability, as were time series ensemble average plots of resultant head angular acceleration and upper neck force.

Table A.1: Percent coefficient of variation (CV) values of resultant discrete impact mechanics from case repeats for all impact conditions.

			v	Peak a	Peak α	Peak ω	Δt_ω	Peak F	Peak M	Impact F	Impact M
		*NC	*CV*	*CV*	*CV*	*CV*	*CV*	*CV*	*CV*	*CV*	*CV*
Low speed, n=5	CR	1	1.8	11.1	13.6	18.7	2.6	4.7	9.7	50.1	25.0
		2	1.1	1.1	6.0	9.1	2.2	1.8	1.6	6.8	43.6
	BK	1	1.5	3.3	3.2	1.7	1.6	2.2	1.9	4.2	18.2
		2	1.5	3.8	2.5	2.1	2.8	8.3	3.9	4.0	4.0
	FM	1	1.7	6.5	9.3	8.7	7.6	5.2	12.4	8.6	60.3
		2	3.5	7.4	14.1	6.6	7.2	5.2	6.8	9.7	22.7
High speed, n=10	CR	1	1.9	8.4	17.6	3.7	4.8	3.7	40.2	13.2	93.0
		2	1.9	10.4	6.5	6.7	0.6	3.7	5.5	7.4	16.3
	BK	1	1.3	3.8	12.1	3.5	15.2	19.3	5.5	37.8	16.4
		2	1.4	5.0	7.6	2.7	4.8	11.7	2.5	5.5	25.7
	FM	1	2.4	10.5	10.2	6.5	4.2	9.2	11.7	19.5	24.9
		2	1.7	12.9	11.1	5.6	4.3	12.1	7.1	23.9	22.4

**NC forces: F_{NC1} = 63 N, F_{NC2} = 163 N; Shaded cells indicate CV values greater than 10%.*

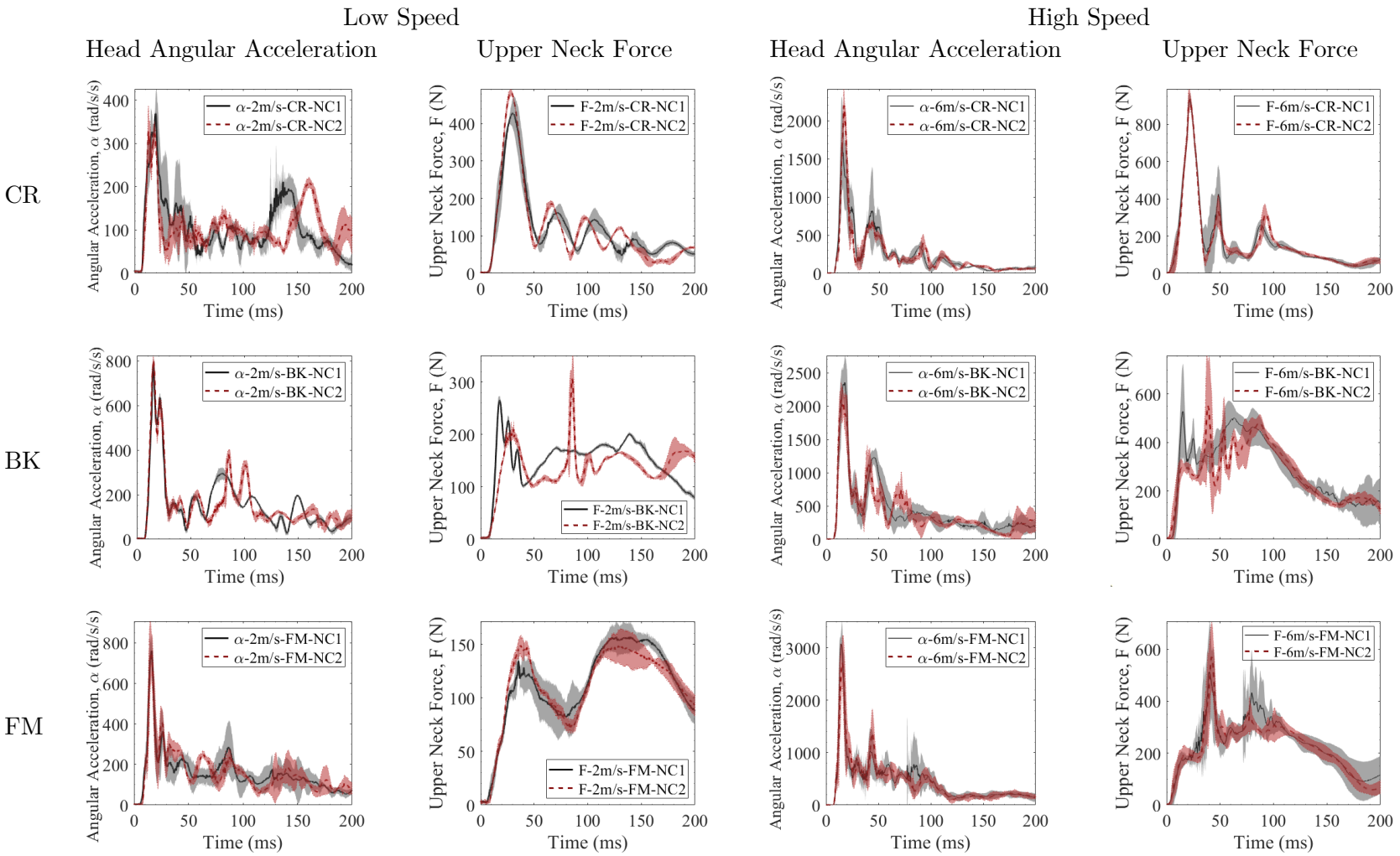

Figure A.1: Ensemble average plots with two NC cases of head angular acceleration and upper neck force from crown, back, and facemask impacts (rows), for low and high-speeds. Solid lines represent case repeat averages and shaded areas represent ± one SD.

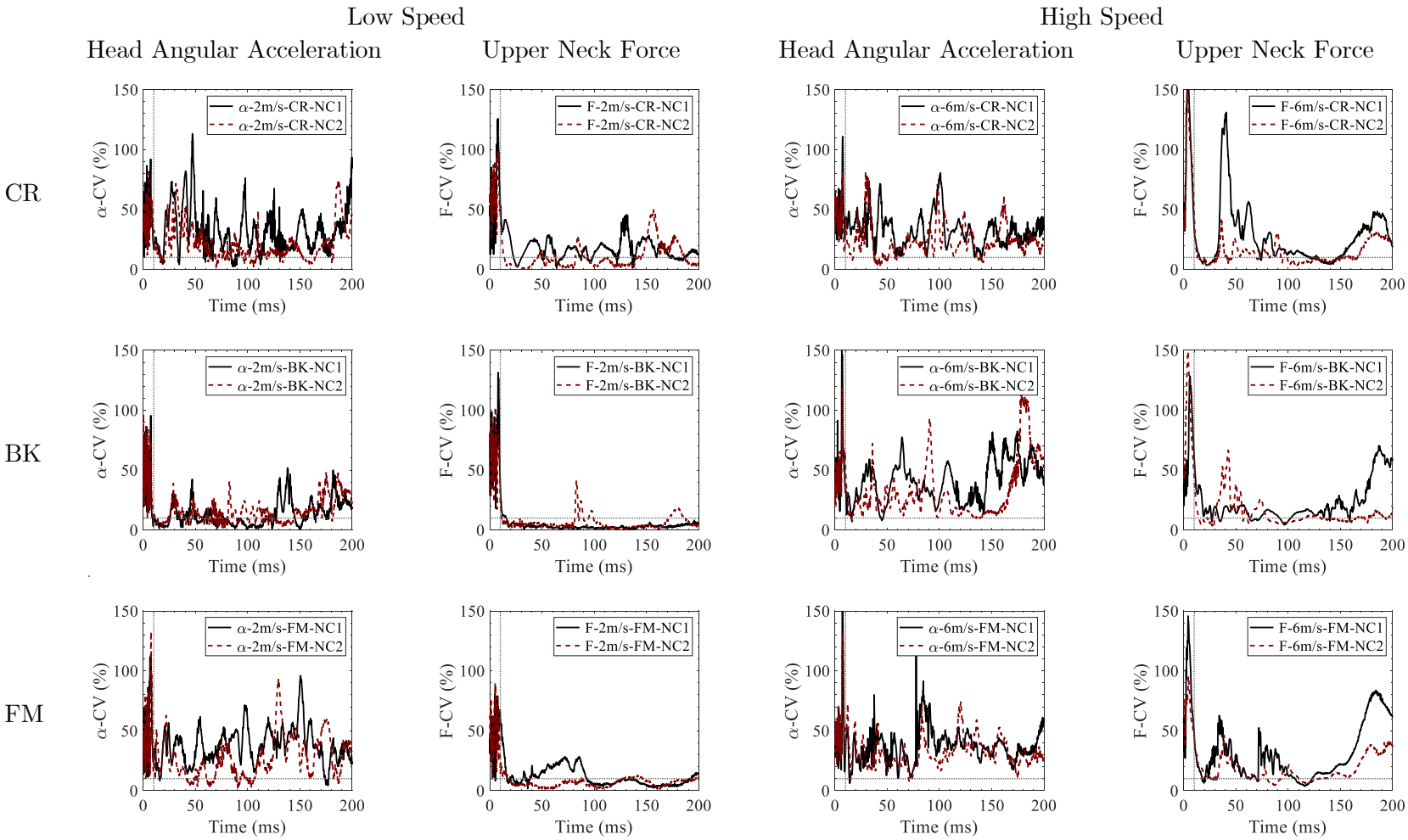

Figure A.2: Percent CVs for each NC case head angular acceleration and upper neck force from the crown, back, and facemask impacts (rows), for low and high-speeds.

Appendix B: Tunability

Impact speed was not considered a covariate because ranges were small.

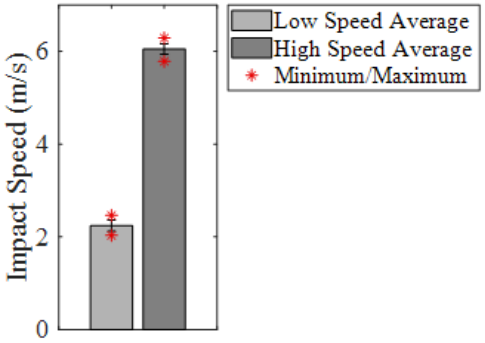

Figure B.1: Average impact speed values from all impact conditions with error bars (± one SD) and markers for minimum and maximum values.

NC case differences assessed PII neck tunability. Discrete values were plotted with case median lines and time series metrics were plotted with NC response residuals.

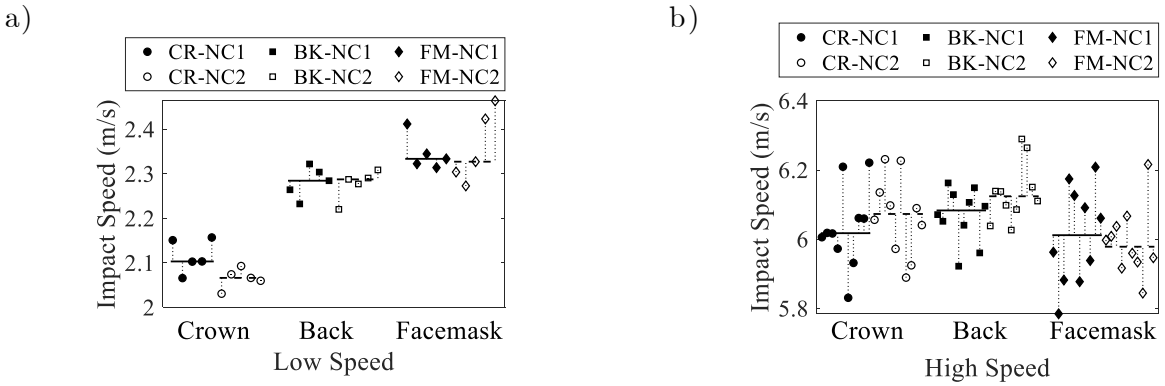

Figure B.2: Individual values and repeat median values of impact speed from a) low and b) high-speed experiments.

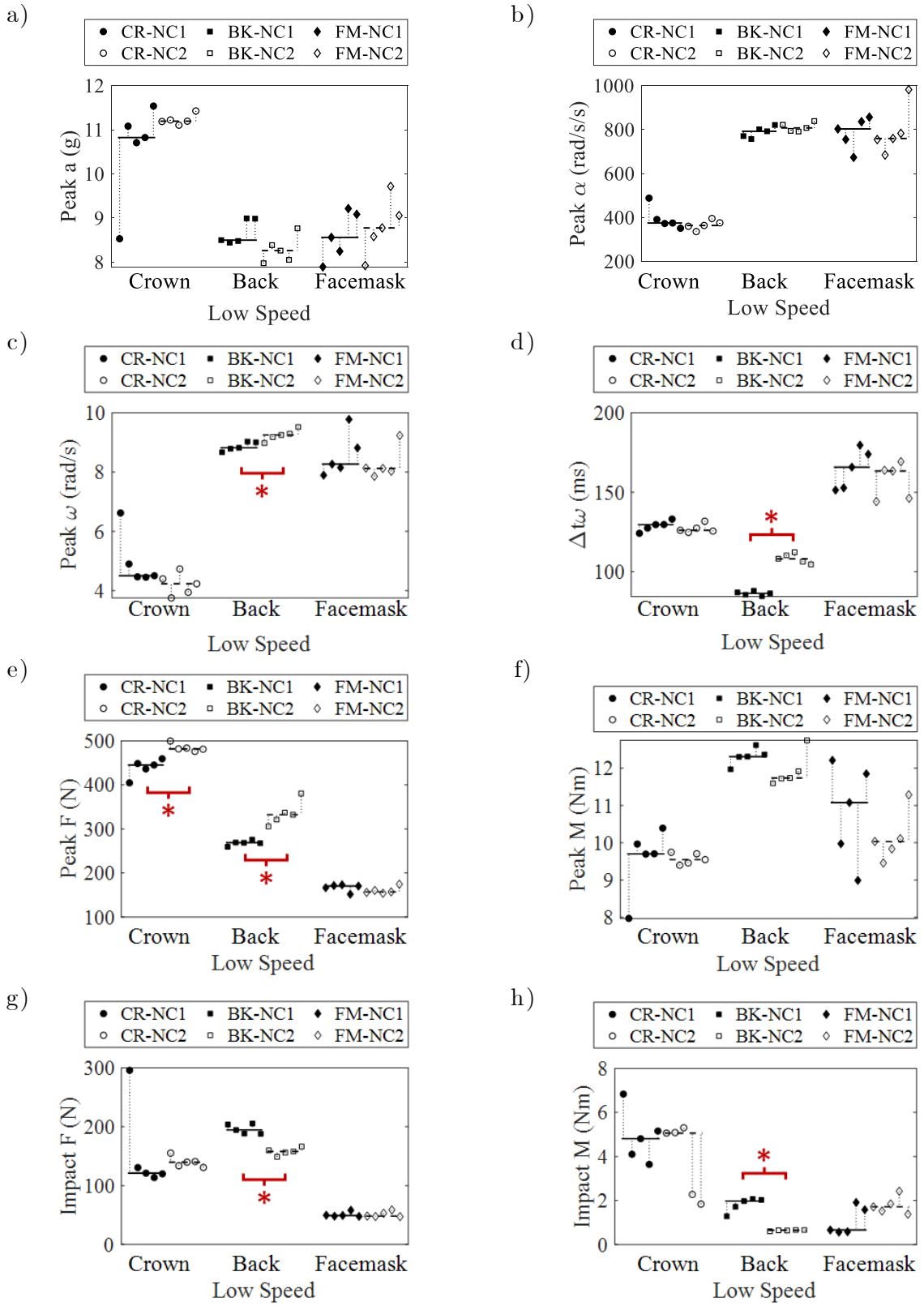

Figure B.3: Individual and repeat median values for discrete response metrics from low-speed conditions. Asterisks indicate $p < 0.05$ between NC case medians.

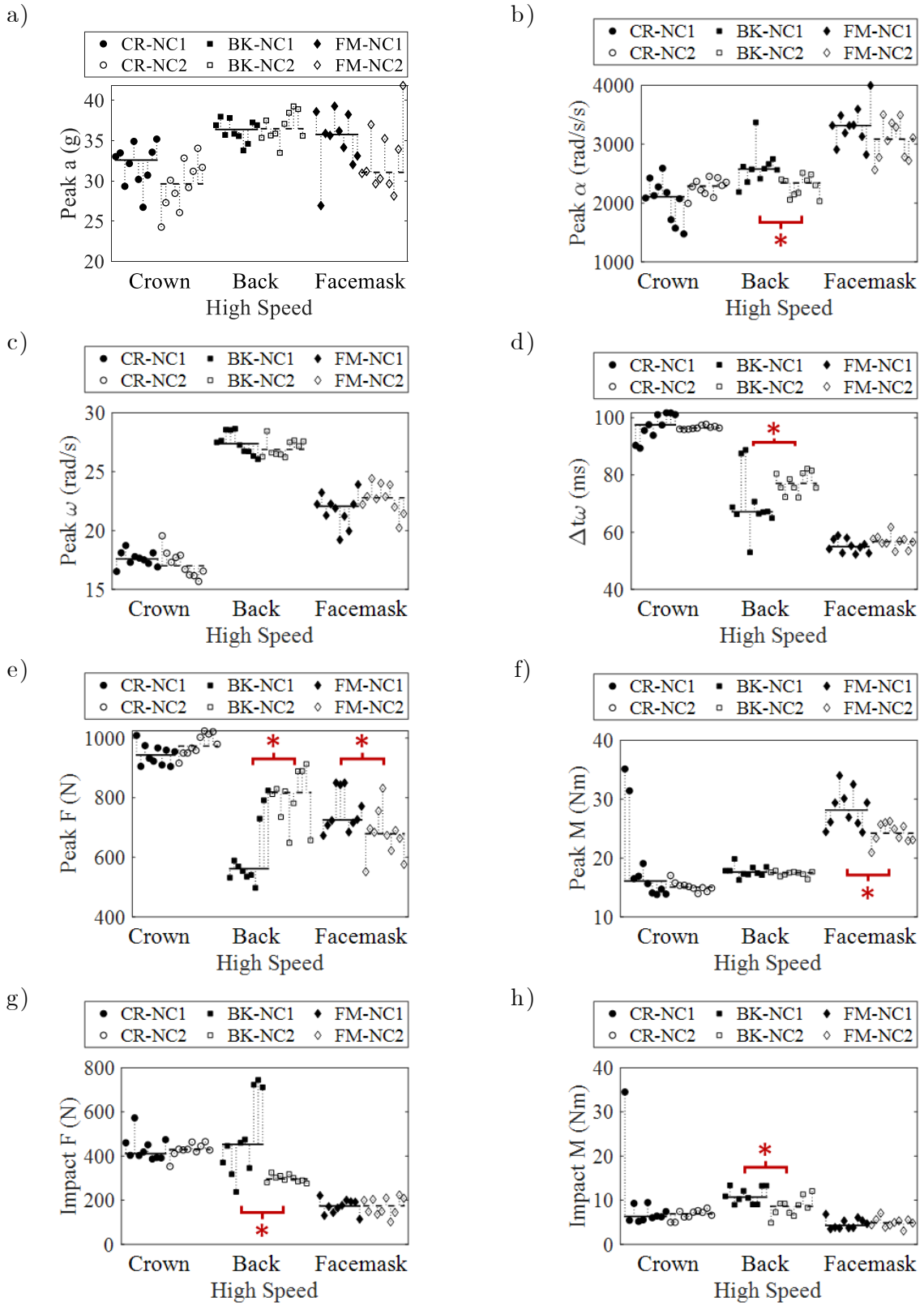

Figure B.4: Individual and repeat median values for discrete response metrics from high-speed conditions. Asterisks indicate $p < 0.05$ between NC case medians.

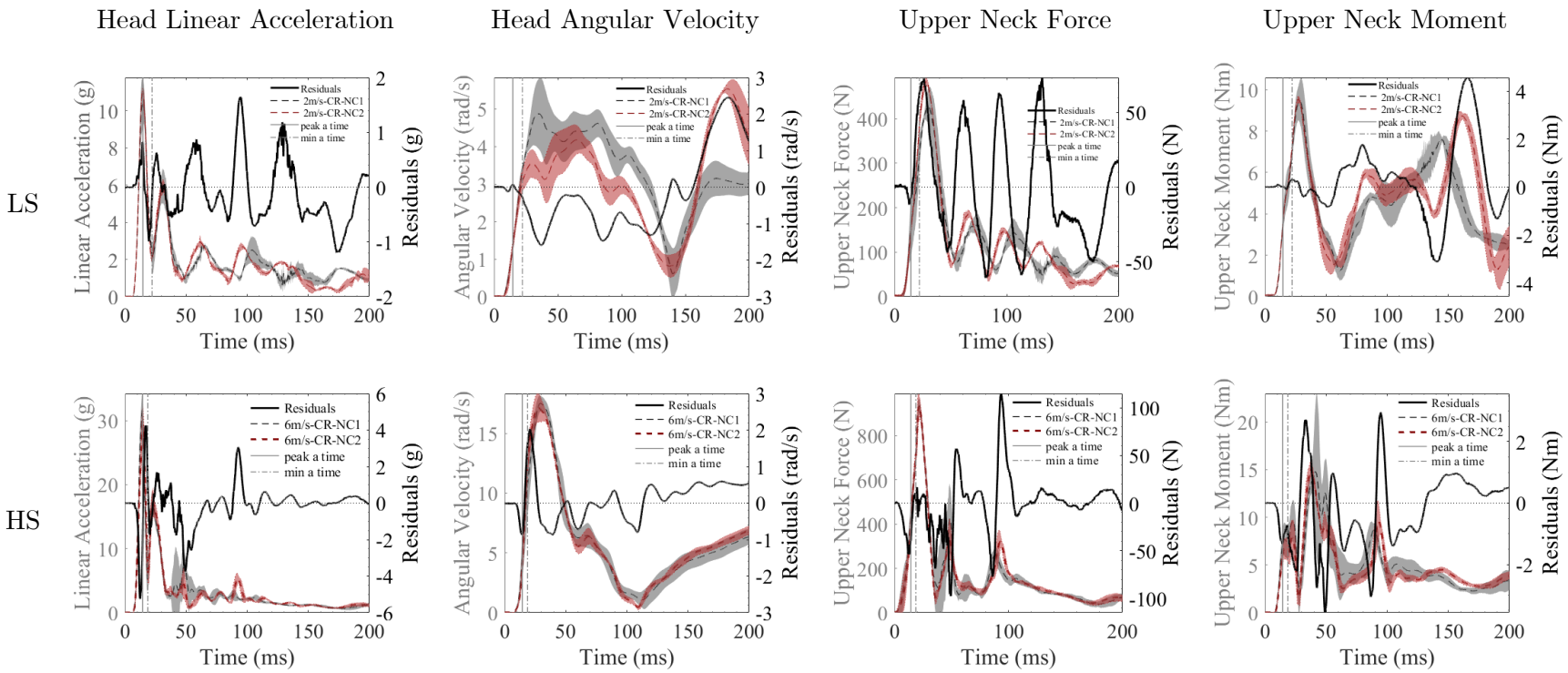

Figure B.5: Time series response residuals between NC cases and NC case responses for linear acceleration, angular velocity, upper neck force, and upper neck moment from low (LS) and high-speed (HS) crown impacts.

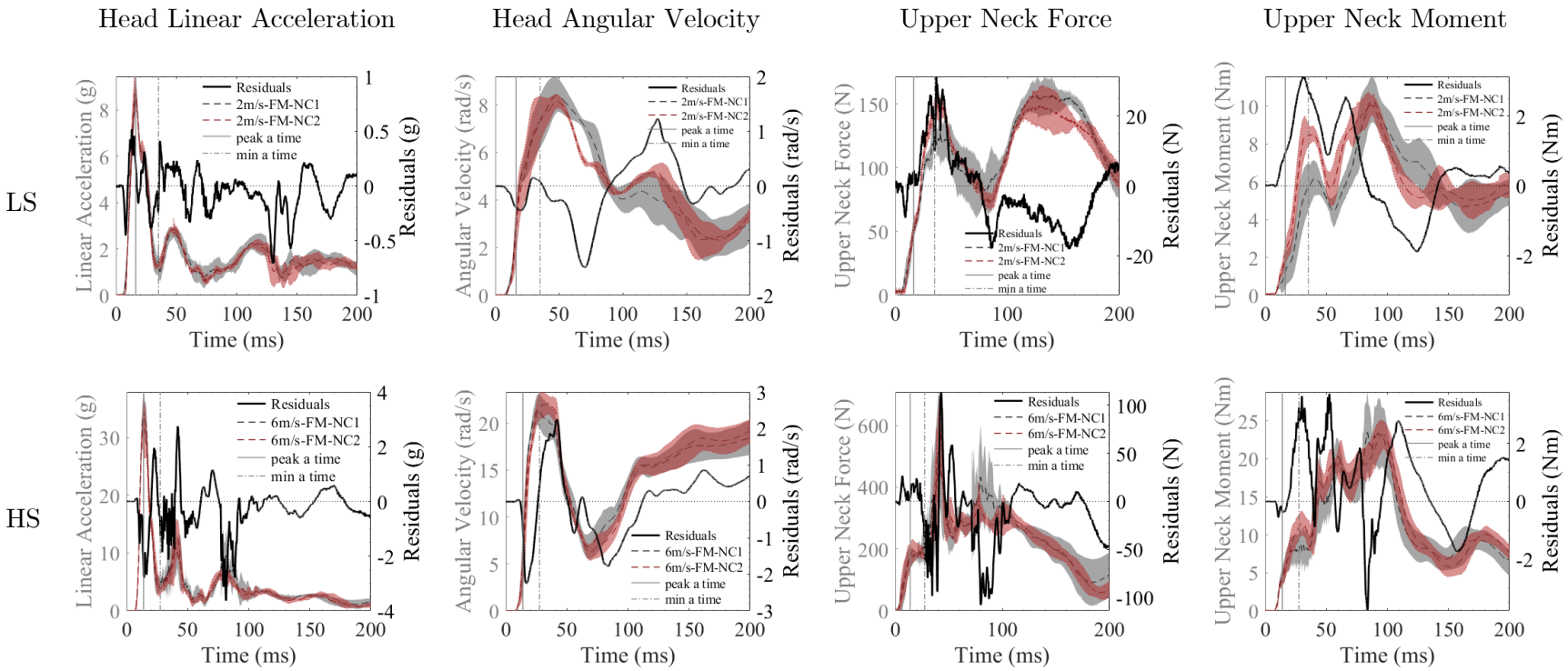

Figure B.6: Time series response residuals between NC cases and NC case responses for linear acceleration, angular velocity, upper neck force, and upper neck moment from low (LS) and high-speed (HS) facemask impacts.

Appendix C: Long-Term Repeatability

Shown below are additional results from the long-term repeatability analyses for peak (linear regression slope significance) and time series metrics (hierarchical clustering).

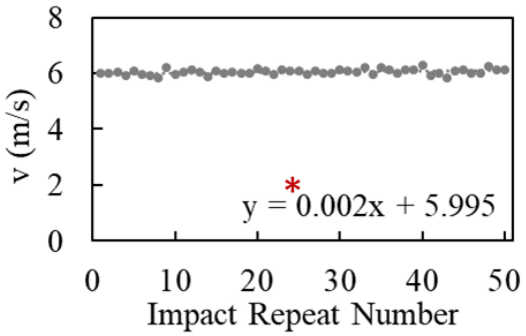

Figure C.1: Impact speed against repeat number with the equation of the regression line. An asterisk indicates a slope coefficient with $p < 0.05$.

Table C.1: Slope coefficient and slope p-value from the linear regression model of transformed discrete response metrics against impact repeat number.

High Speed (6 m/s), Facemask Impact, NC2 (163 N), n = 50									
	v	Peak a/v	Peak α/v	Peak ω/v	Δt_ω/v	Peak F/v	Peak M/v	Impact F/v	Impact M/v
slope	0.002	0.005	0.958	-0.001	0.010	0.438	0.043	-0.051	0.002
p-value	0.023	0.441	0.077	0.580	0.332	0.001	0.000	0.349	0.700

P-values of 0.000 reflect a significance level lower than the shown level of precision, not zero. Shaded cells indicate a slope significance of $p < 0.05$.

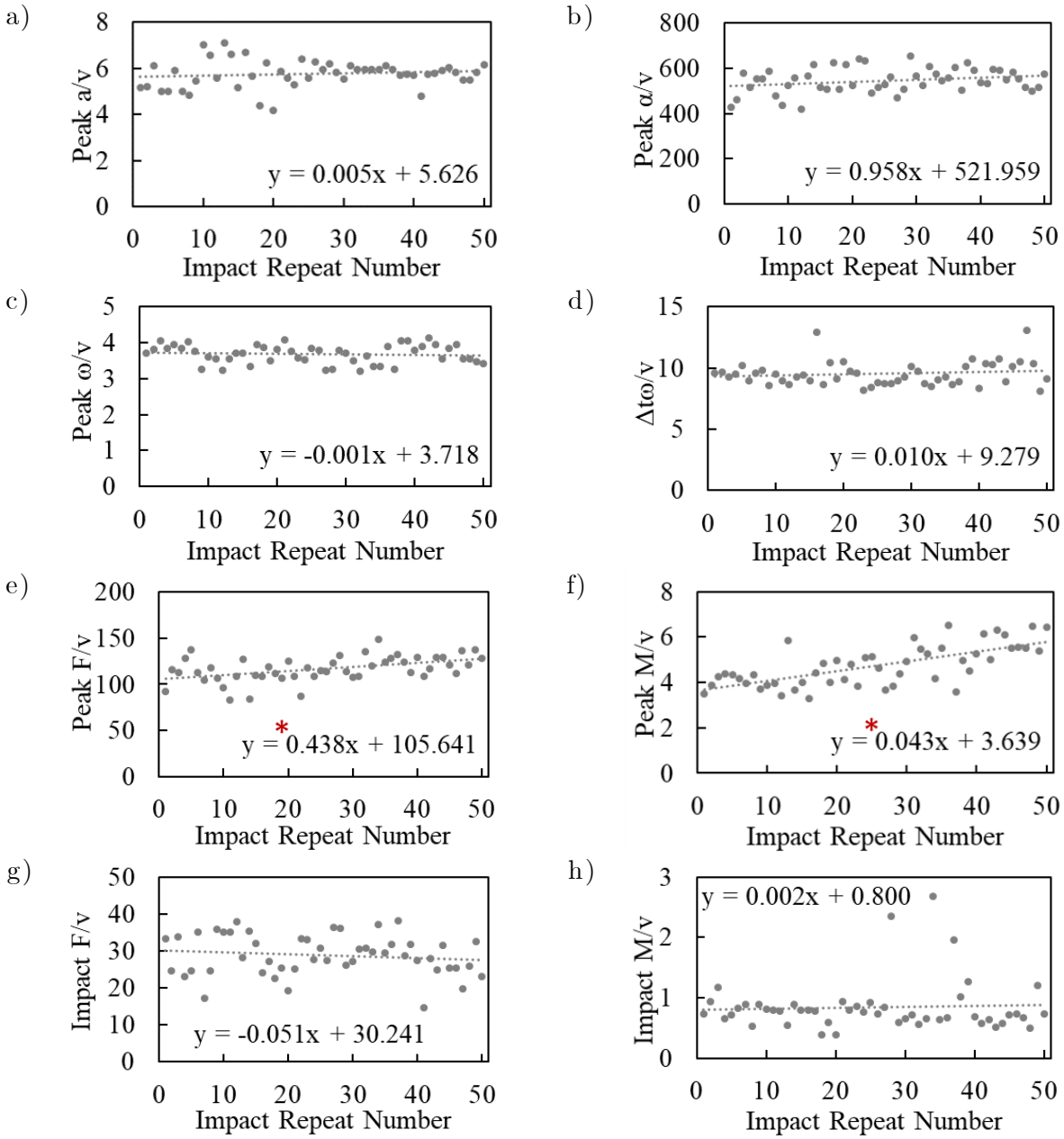

Figure C.2: Transformed discrete response metrics against impact repeat number with linear regression equation, for a-d) head kinematics and e-h) upper neck kinetics. An asterisk indicates a slope significance with $p < 0.05$.

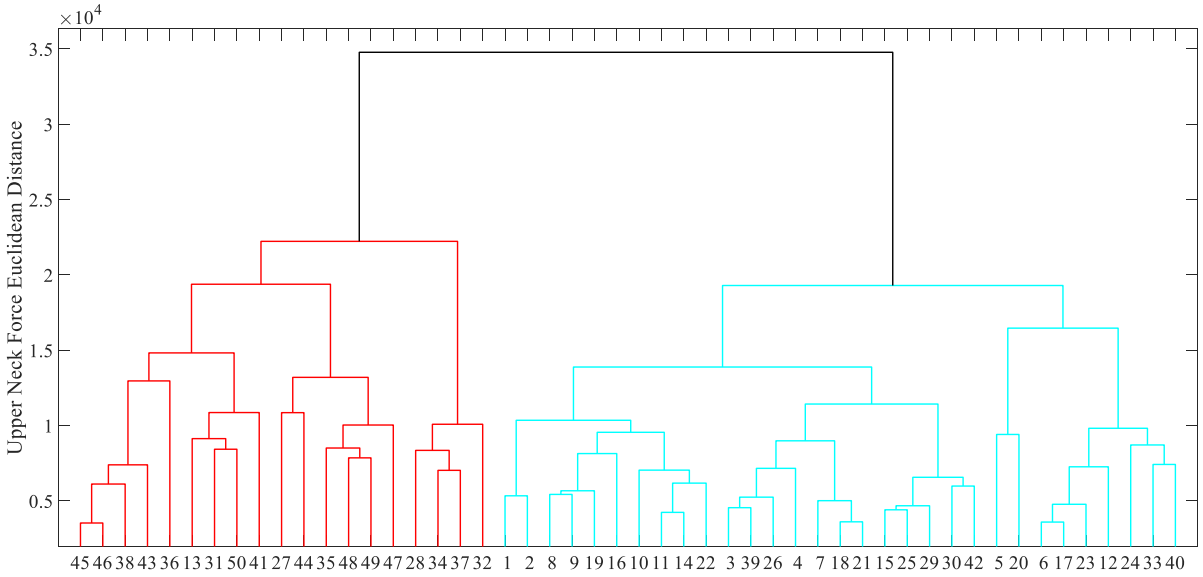

a)

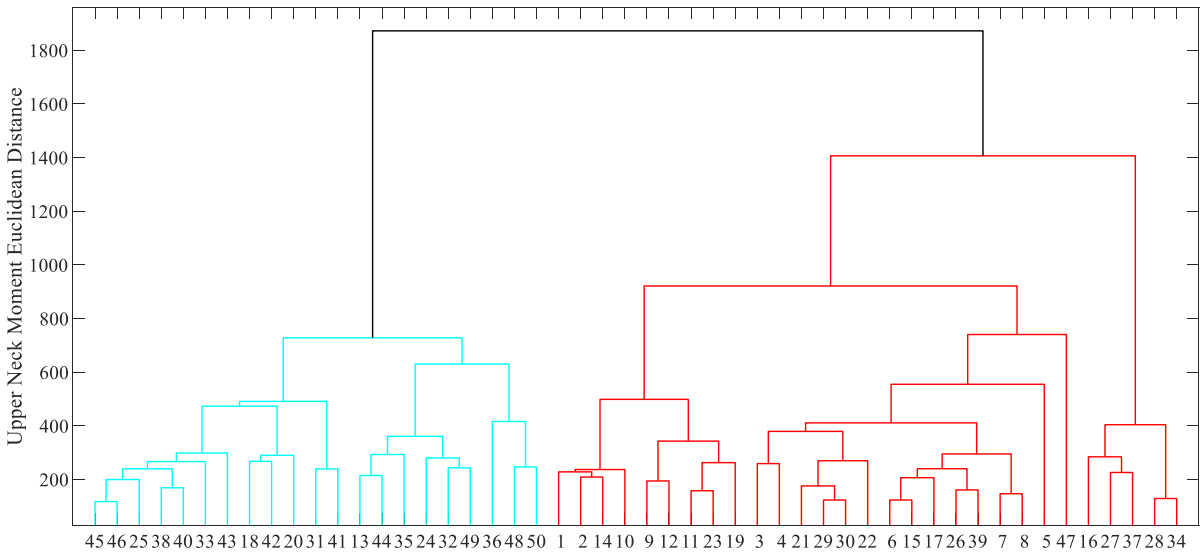

b)

Figure C.3: Dendrogram (0 – 200 ms time frame) showing cluster structure and Euclidean distances between clusters, for upper neck a) force and b) moment.

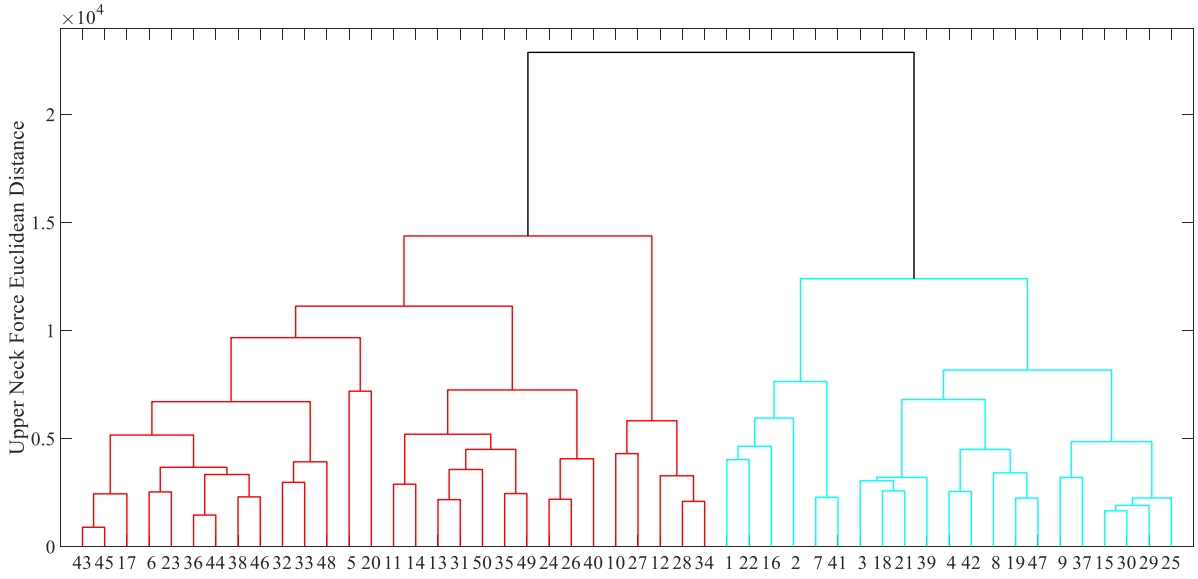

a)

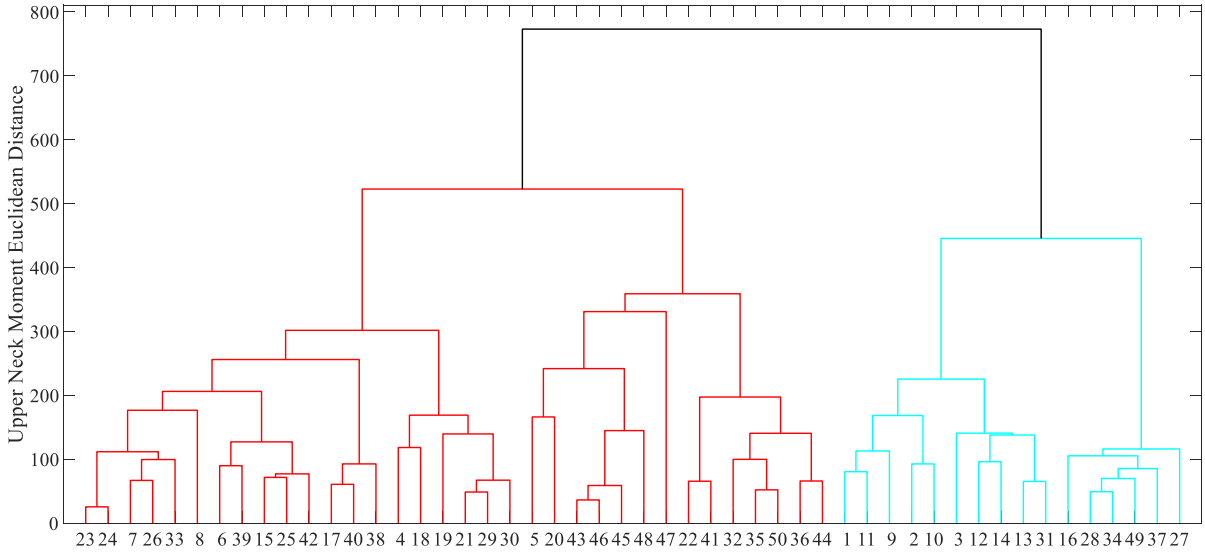

b)

Figure C.4: Dendrogram (0 – 60 ms time frame) showing cluster structure and Euclidean distances between clusters, for upper neck a) force and b) moment.

a)

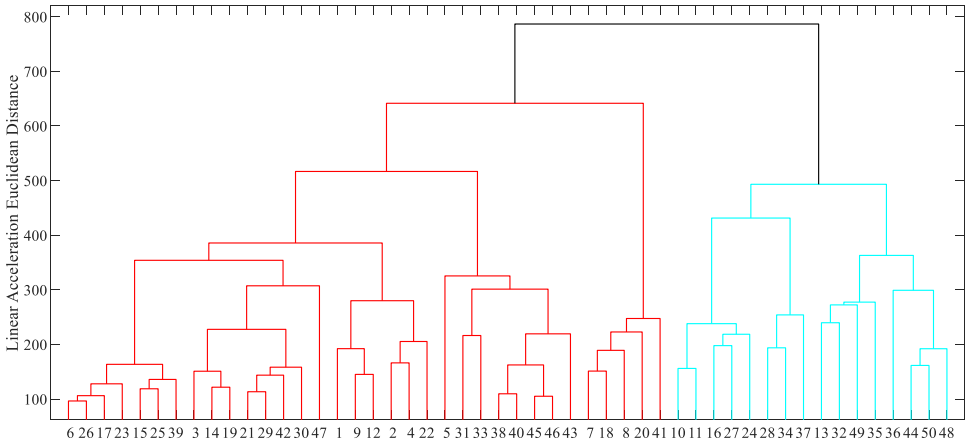

b)

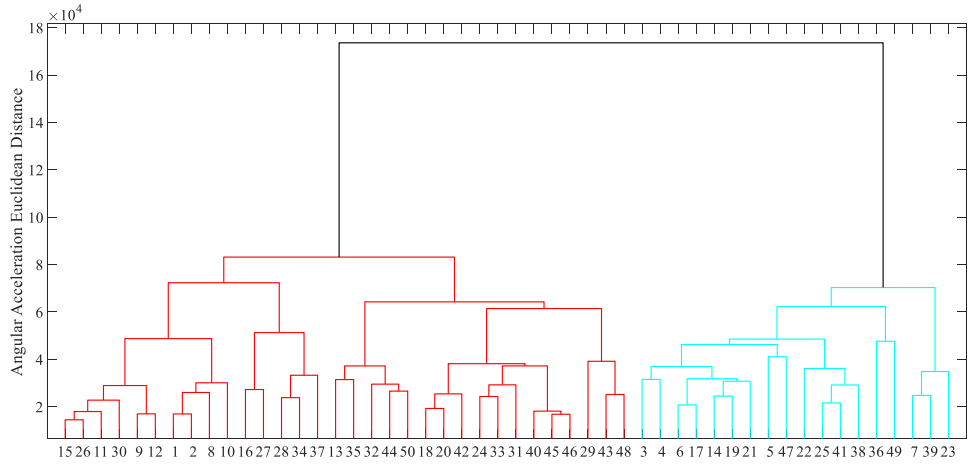

c)

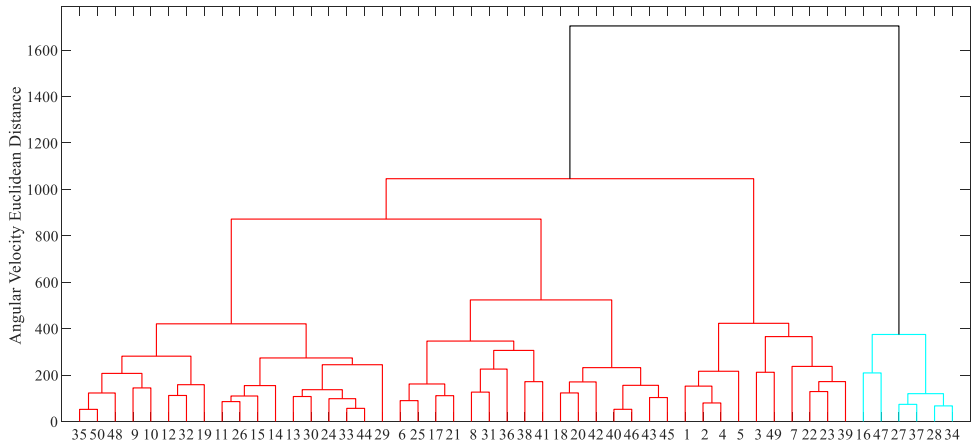

Figure C.5: Dendrogram (0 - 200 ms time frame) showing cluster structure and Euclidean distances between clusters, for head a) linear acceleration, b) angular acceleration, and c) angular velocity.

a)

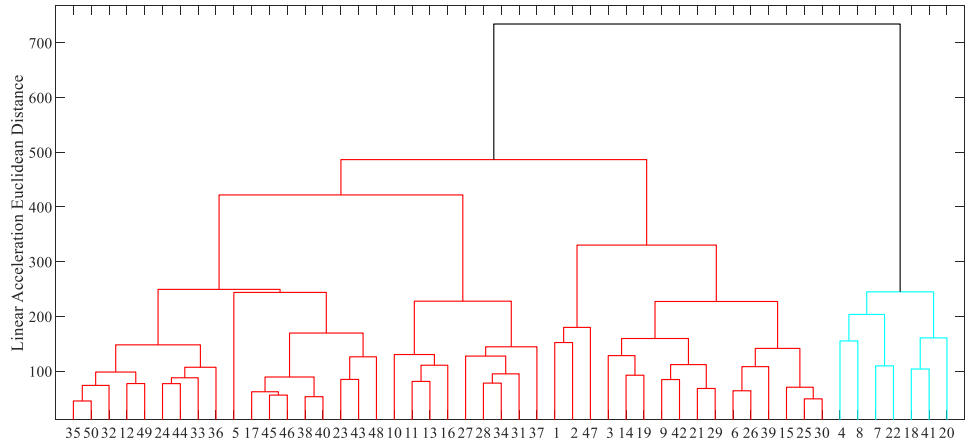

b)

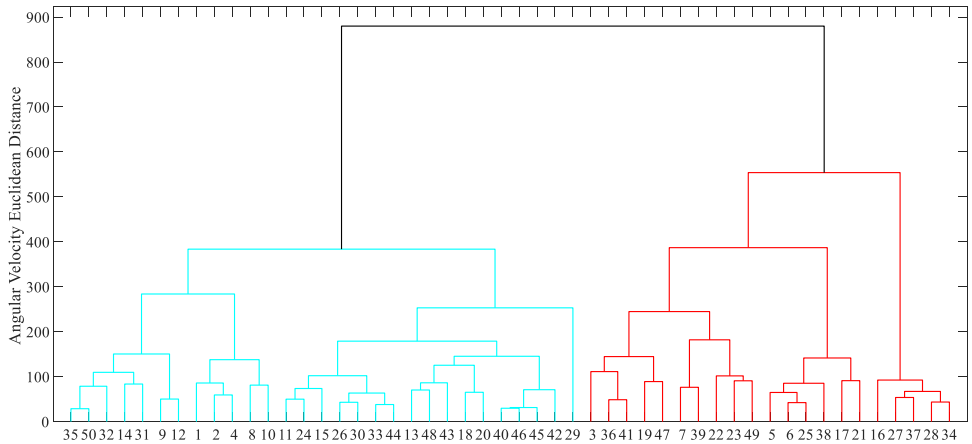

c)

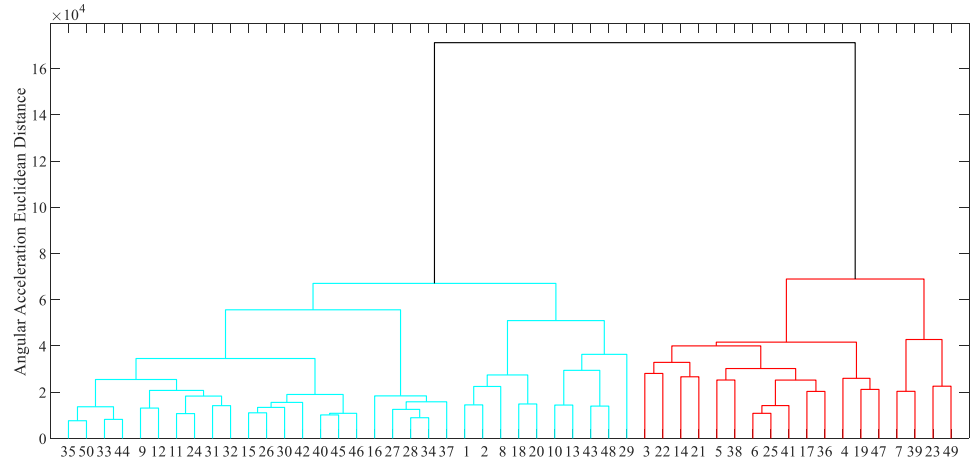

Figure C.6: Dendrogram (0 - 60 ms time frame) showing cluster structure and Euclidean distances between clusters, for head a) linear acceleration, b) angular acceleration, and c) angular velocity.